REPUBLIQUE ALGERIENNE DEMOCRATIQUE ET POPULAIRE
MINISTERE DE L'ENSEIGNEMENT SUPERIEUR ET DE LA RECHERCHE SCIENTIFIQUE

Université Ferhat ABBAS – Sétif-1-

THÈSE

Présentée à la Faculté de Technologie
Département de Génie des Procédés
pour l'obtention du diplôme de

DOCTORAT EN SCIENCES

Option : Génie des polymères

Par

Mohammed BOUCHAKOUR

Thème

Irradiation Polymerization of Polypropyleneglycoldiacrylates/Liquid Crystal E7 Systems

Soutenue le 28/11/2016 devant un Jury composé de:

Nacerddine. HADDAOUI	Professeur à l'université Ferhat Abbas, Sétif-1	Président
Farid. RIAHI	Professeur à l'université Ferhat Abbas, Sétif-1	Directeur de thèse
Ulrich MASCHKE	Directeur de Recherche, Université Lille 1	Co-directeur de thèse
Djafer. BENACHOUR	Professeur à l'université Ferhat Abbas, Sétif-1	Examinateur
Kamel CHAOUI	Professeur à l'université Badji Mokhtar, Annaba	Examinateur
Toufik BOUCHAOUR	Professeur à l'université Abou Bekr Belkaid Tlemcen	Examinateur
Mohamed BAKAR	Professeur à Polytechnika Radomska, Poland	Examinateur

Dedication

I would like to dedicate the present work to my father and mother, my sisters and brothers.

To the memory of my father in law, to my mothers in law, my sisters and brothers in law

I wish also to dedicate this work to my wife Wahiba, my sons Anes Attia, Moadh Tayeb and Mohammed Farid, and…

Aknowledgments

I would like to thank deeply my two advisors, Pr. Farid RIAHI and Dr. Ulrich MASCHKE , for all their patience, instructions, moral support and encouragement.

During the years of 2011 to 2013, I got a PROFAS scholarship from the Algerian ministry of higher education and scientific reasurch to accomplish a deep PhD reasurch about Liquid crystals and Polymer dispersed liquid crytals PDLC's at the Unité Materiaux et Transformations "UMET" of the University of Sciences and Technology of Lille1. I would like to express my gratitude to all of them.

I would like to thank some Scientific Staff of UMET for their considerable help and freindship.

My gratitude are expressed to the members of the jury mamely Pr. N. Haddaoui, Pr. Dj. Benachour, Pr. K. Chaoui, Pr. T. Bouchaour and Pr. M. Bakar who accepted to judge this work.

I received a lot of help from Dr. Christophe BEYENS, Dr. Mohammed Makhloufia, Dr. Yazid Derouiche, Dr. Ammar Elqidrea, Dr. Guy Joel, Dr. K. Bouraa, Dr. Nouria Bouchikhi, Ahmed Touati, Sofiane Bedjaoui, I would like to thank all of them for their assistance and helpful discussions.

Special gratitude to my family, especially my parents, for their long-term support and encouragement. I would like to use my dissertation as a special gift to my lovely sons.

Abstract:

This contribution focuses on a detailed investigation of the relationship between the methods of polymerization/cross-linking, such as slow and rapid UV radiation, and high voltage accelerated electron beam (EB), and the resulting physical properties including phase diagrams, polymerization and phase separation kinetics, morphologies, thermal properties and electro-optical responses of polypropyleneglycoldiacrylate (PPGDA800) and tripropyleneglycoldiacrylate (TPGDA) monomers, in the presence of the nematic liquid crystal E7, used to prepare a polymer dispersed liquid crystal (PDLC). Based on the phase diagrams obtained by polarized optical microscopy, 60wt.% E7 was found to be the limit of solubility of the LC in PPGDA800. The longer the spacing between the double bonds in PPGDA800, the more rapid was the photopolymerization under both UV systems; nevertheless, the opposite was proved under EB. More homogenous and regular morphologies were obtained under the more homogeneous EB curing; whereas, irregular ones resulted under the heterogeneous photopolymerization.

The electro-optical responses of various polymer dispersed liquid crystals (PDLCs) systems exhibited remarkable differences between the UV-cured samples and those cured by the EB technique. It was found that the threshold and saturation voltages considerably increased in the case of the UV-cured systems. Other results involving the contrast ratio, which is higher for EB-cured systems, confirm their higher quality, although the rapid photopolymerization UV source was employed, which slightly improved the electro-optical responses. Moreover, EB curing leads to high enough conversions without a photoinitiator, which may act as an impurity that might have a strong impact on the electro-optical performance and also lead to the discoloration of the obtained PDLCs.

Keywords: PDLC; polypropyleneglycoldiacrylate; E7; liquid crystal; photopolymerization; electron beam; electro-optical response

Contents:

Dedication……..
Aknowlegments ……
Abstract …….
Table of contents…… i
List of tables……... iv
List of figures…… v
Introduction…… 2
References…… 4

Chapter 1. Liquid crystals..... 8
1. Historical Aspect of LC's..... 8
2. Definition of Liquid Crystals..... 10
3. Classification of Liquid Crystals..... 10
3.1. Nematic..... 10
3.2. Smectic..... 10
3.3. Cholesteric..... 10
4. Types of Liquid Crystals..... 11
4.1. Thermotropic Liquid Crystals..... 11
4.2. Lyotropic Liquid Crystals..... 13
5. Eutectic Mixtures of Liquid Crystals..... 14
6. Properties of Liquid Crystals..... 16
6.1. Order Parameter..... 16
6.2. Optical Anisotropy or Birefringence..... 17
6.3. Dielectric Anisotropy..... 19
6.4. Elasticity..... 20
7. Phase Diagrams of Liquid Crystal/Monomer blends..... 21
References…….. 24

Chapter 2. **Polymer dispersed liquid crystals**……... 27
1. PDLC Preparation Techniques…… 27
1.1. Emulsion Technique……... 27
1.2. Phase Separation Technique..... 28
1.2.1. Solvent-induced Phase Separation..... 28
1.2.2. Temperature-induced Phase Separation..... 28
1.2.3. Polymerization-induced Phase Separation..... 28
1.2.3.1. Photopolymerization..... 29
a. Steady State Kinetics of Linear Photopolymerization..... 31
b. Kinetics of Crosslinking Photopolymerization..... 33
1.2.3.2. Polymerization by Accelerated Electron Beams..... 35
1.2.3.3. Comparison between EB and UV curing..... 36
2. Properties of PDLC's..... 37
2.1. Electro-optical Properties of PDLC's..... 37
3. Applications of PDLC's…… 42
3.1. Smart Windows..... 42
Conclusion..... 43
References…….. 43

Chapter 3. Experimental work..... 47
1. Raw Materials..... 47
2. Sample Preparation..... 48
2.1. Elaboration Techniques..... 48
2.1.1. UV Curing..... 48
2.1.2. EB Curing..... 50
3. Characterization Methods..... 51
3.1. Optical Methods..... 51
3.1.1. Polarised Optical Microscopy..... 51
3.1.2. Scanning Electron Microscopy..... 51
3.2. Spectroscopic Methods..... 52
3.2.1. Fourier Transform Infrared Spectroscopy..... 52
3.2.2. Nuclear Magnetic Resonance Spectroscopy..... 54
3.3. Thermal Methods..... 54
3.3.1. Thermo Gravimetric Analysis..... 54
3.3.2. Differential Scanning Calorimetry..... 54
3.4. Electro-optical Measurements..... 56
References..... 57

Chapter 4. Results and discussion..... 59
1. Analysis of Raw Materials..... 59
1.1. Spectroscopic Methods..... 59
1.1.1. FTIR Analysis..... 59
1.1.2. NMR Spectroscopy..... 62
1.2. Thermal Methods..... 65
1.2.1. Thermo Gravimetric Analysis TGA..... 65
2. Analysis of Monomers/LC E7 Mixtures..... 68
2.1. Phase Diagrams 68
3. Analysis of PDLC Systems..... 70
3.1. Infrared Spectroscopy..... 70
3.2. Morphologies..... 74
3.2.1. Morphology by POM..... 74
3.2.2. Morphology by SEM..... 76
3.3. Thermal Properties by DSC..... 77
3.4. Electro-optical Responses..... 82
References…….. 85
General Conclusions…….. 88
Recommendations……. 91

List of tables

1-1: Transition temperatures of the alkylcynobiphenyls nCB..... 13

4-1: IR band designations for TPGDA andPPGDA800..... 61

4-2: IR band designation of the LCE7..... 62

4-3: ^{1}H NMR results of PPGDA800..... 64

4-4:^{1}H NMR results of TPGDA..... 65

4-5: Transition temperatures in the neat, photopolymerized TPGDA and PPGDA800 with or without 60wt.%E7..... 81

List of figures:

1-1: Schematic description of (a) crystal, (b) liquid crystal and (c) liquid.....8
1-2:The chemical composition of 4'-n-heptyl-4-cyano-biphenyl known as 7CB.....9
1-3: Phase sequence of three organic substances; (a) n-heptane, (b) 4-cyanobiphenyl, (c) 7CB (4'-n-heptyl-4-cyano-biphenyl).....9
1-4: An example of cholestric molecule: 3-methyl 4'-hexyl 4-cyanobiphenyl.....11
I-5: Schematic description of mesogenic phases: (a) nematic, (b) smectic A, (c) smectic C, (d) cholestric.....11
1-6: Polymorphisms of the corresponding series nCB and nOCB.....13
1-7: Examples of some amphiphilic phospholipid molecules.....15
1-8: Theoretical phase diagram for the 5CB/7CB blend computed from the Schroder-van Laar law.....17
1-9: Definition of θ used in equation (5).....17
1-10: Variation of the order parameter S with temperature T.....18
1-11: A graphical illustration of optical anisotropy or birefringence.....18
1-12: a) Experimental evidence for nematic phase birefringence; two rays linearly polarized with a 90° difference exit the prism; b) measuring the angle of least deviation; c) photograph of the experimental setup.....19
1-13: A graphical illustration of (a) positive and (b) negative dielectric anisotropy.....21
1-14: Splay, twist, and bend elastic constants.....21
1-15: Phase diagram for uncured E7/NOA65 mixtures.....24
1-16: Measured and calculated mixing temperatures for uncured E7/NOA65 system. Points are Tmix values from Figure 1-15. Solid line is FH binodal curves; dashed line is corresponding spinodal curve. C, D: parameters of Eq. (3), m1, m2: number of sites occupied by LC and polymer segment (in Eq. (2), respectively, r1 and r2).....25
2-1: The decomposition of 2-hydroxy-2-methyl-1-phenyl-propane- 1-one (Darocur 1173), X is an OH group.....30
2-2: Photoinitiated crosslinking polymerisation of a diacrylate monomer. PI is an abbreviation for the photoinitiator.....31
2-3: Conversion Vs exposure time (solid line) and Rp Vs exposure time (dashed line) recorded by RTIR upon UV curing of a polyurethane acrylate at light intensity: 30 mW/ cm^2.....38

2-4: Schematic representation of a PDLC light shutter in the OFF-state (left) and when a low frequency electric field is applied across it (ON-state, right). Double arrows are a schematic representation of the droplet director.....39
2-5: a typical PDLC film: a) at the OFF-state, b) at the ON-state, c) when electric field is removed.....39
2-6: Typical behaviour of the light intensity transmitted by a PDLC film.....40
2.7: Common nematic director configurations: (a) bipolar, (b) radial, (c) toroidal, (d) axial.....42
3-1: Chemical structures of (a) polypropyleneglycoldiacrylate (PPGDA) monomers, (b) nematic LC E7 mixture and (c) photoinitiator: 2-hydroxy-2-methyl-1-phenyl-propane-1-one (Darocur 1173).....49
3-2: The UV light source TL08 used.....49
3-3: the lamp Philips TL08 spectrum.....50
3-4: Photo of the dosimeter used.....50
3-5: The Dr. Hönle UV lamp (UVH medium-pressure mercury arc lamp).....51
3-6: Scheme of Electron Beam EB process.....51
3-7: The Olympus BX-41 model; polarizing optical microscope POM.....52
3-8: Schematic diagram of a scanning electron microscope.....53
3-9: Sample preparation for the polymerization.....53
3-10: Double bond absorbance, before and after polymerization.....53
3-11: (a): NMR Bruker AC300, (b): NMR tube.....54
3-12: An electro-optical bench.....56
3-13: The manner of applying the voltage.....57
4-1: FTIR spectrum of TPGDA.....59
4-2: FTIR spectra of TPGDA and PPGDA800.....60
4-3: FTIR spectrum of LC E7.....61
4-4: The chemical structures of TPGDA (n=3) and PPGDA800 (n=12).....62
4-5: ^{1}H NMR spectrum of PPGDA800 (n=12).....63
4-6: ^{1}H NMR spectrum of TPGDA (n=3).....64
4-7: TGA thermograms of TPGDA and PPGDA800.....66
4-8: TGA thermograms of TPGDA and PPGDA800 from 450 to 600°C.....66
4-9: TGA thermograms of neat TPGDA and that of photopolymerized TPGDA (under UV-TL08 for about 10min).....67

4-10: Phase diagrams of the monomeric mixtures: PPGDA800/E7 (squared symbols) and TPGDA /E7 (triangular symbols).....68
4-11: Morphologies of monomeric PPGDA800/E7 mixtures obtained from POM at T = 20°C: (a) 60 wt %, (b) 70 wt % and (c) 80 wt % E7.....69
4-12: Variation of acrylic double bonds Conversion for TPGDA and PPGDA800, TPGDA/60 wt % E7 and PPGDA800/60 wt % E7as a function of exposure time, prepared by (a) UV-TL08, (b) UV-Dr. Hönle system and (c) EB curing.....73
4-13: Micrographs obtained by POM; UV-TL08: (a) PPGDA800/60 wt % E7; (b) TPGDA/60 wt % E7. UV-Dr. Hönle system: (c) PPGDA800/60 wt % E7; (d) TPGDA/60 wt % E7; and EB curing: (**e**) PPGDA800/60 wt % E7; (**f**) TPGDA/60 wt % E7.....75
4-14: SEM microphotographs of a: PPGDA800/60 wt. % E7 and b: TPGDA/60 wt. % E7....76
4-15: DSC thermograms of the photopolymerized samples under UV-TL08 a:TPGDA for about 10min, b: TPGDA/60 wt.% E7 for about 05min.....77
4-16: DSC thermograms of photopolymerized films under UV-TL08 of PPGDA800 for about 02min (blue line), PPGDA800/60 wt.% E7 for about 05min (black line).....78
4-17: DSC thermogram of LC E7.....79
4-18: Electro-optical responses of 17µm thick TPGDA/60wt.%E7 and PPGDA800/60wt.%E7 prepared by (a) UV-TL08; (b) UV-Dr Hönle system; and (c) EB curing.....83
4-19: The electro-optical responses of 17-µm-thick samples elaborated by UV-Dr. Hönle system and UVTL08; (a) TPGDA/60 wt % E7 and (b) PPGDA800/60 wt % E7…….....84

Introduction

Introduction:

Most people have been trained, since their first years at school, that there are only three states of matter: solid, liquid and gas. In reality, a solid matter can be either crystalline or amorphous and the most important property which distinguishes liquids from solids is their ability to flow. Although the early investigators of the 19th century, among whom O. Lehmann, discovered other phases which did not necessarily fall into these categories, he called these substances flowing crystals and later on the term "liquid crystals" (LC) was coined by G. Freidel [1,2]. LC's were once considered as a rare state of matter, but up to now several thousands of liquid crystalline compounds have been actually synthesized. [3]

Liquid crystals are intermediate phases; their properties such as partial or no positional order, partial orientational order are intermediate between those of anisotropic liquids which do not have positional nor orientational order and those of crystals which exhibit both positional and orientational order. A liquid crystal is a material that couples most of the mechanical properties of a liquid including its high fluidity and inability to support shear with some electromagnetic properties such as a high electrical, magnetic and optical anisotropies of a crystal [4]. LC's were known since the end of the 19th century but their first applications in electro-optic devices appeared in the mid of the 20th century. In such applications, the most attractive properties concern the possibility of controlling the LC optical anisotropy by means of an electric or magnetic field but the liquid behavior remains an undesired characteristic. To find more useful materials some authors have used LC's in compound materials such as droplets of a nematic material floating in an isotropic liquid or nematic LC confined in micrometer-sized cavities within a solid. Fergason in 1984 [5-6] and Doane et. al. [7-8] a few years later introduced a new class of composite materials constituted by small droplets of LC embedded in a polymeric film. The most current term used to describe these materials is PDLC which stands for "polymer dispersed liquid crystal". The introduction of PDLC's allowed to combine the peculiar mechanical properties of a polymeric film with the electro-optical properties of LC's, permitting hence the realization of many new applications such as flexible displays, smart windows, projection displays, sensors, etc [4,9] .

The preparation of these films is mainly based on phase separation induced by either polymerization (PIPS: polymerization induced phase separation), solvent evaporation (SIPS: solvent induced phase separation) or temperature reduction (TIPS: temperature induced phase separation) processes. The PIPS is the most widely used process through the use of either Electron Beams (EB), UV light or heat. The EB curing leads to high enough conversions

without a photoinitiator which may act as an impurity that might have a strong negative impact on the electro-optical performance of the obtained PDLC's [10-11].

In the PIPS process, thiol-enes, epoxy, styrene, mono-, di-, and multifunctional acrylates and methacrylates are the basic monomers and prepolymers used to prepare PDLC's. During the polymerization reaction, the liquid crystal becomes less miscible with the growing polymer, and finally, the mixture will separate into two phases; the polymer matrix presents the major phase and the droplets of confined liquid crystal molecules present the minor phase. A proper control of the phase separation phenomena of the polymer/liquid crystal composite system is necessary to obtain different morphologies, depending essentially on the polymerization conditions [12].

E. Andrzejewska [13], C. Decker et al.[14,15], T. Scherzer et al.[16], and K. S. Ansceth et al.[17] studied extensively the photopolymerization of multifunctional monomers. They found that it is a complicated process, especially with respect to reaction kinetics. The kinetics of network formation involve phenomena not observed in linear polymerizations, especially the immediate onset of autoacceleration and radical trapping at early stages as well as the dominance of reaction-diffusion as the means of migration of propagating radicals. In the later stages of polymerization, auto deceleration, or incomplete functional group conversion takes place because of the extremely low mobility of the propagating species in the crosslinked network.

B. Defoort et al. [18], C. Patacz et al.[19,20] U. Mashke et al.[21], W. Knolle et al.[22], have deeply studied the polymerization of Tripropyleneglycoldiacrylate (TPGDA) under accelerated electron beams. They found that EB-induced free radical polymerization of such acrylic monomer is considered to follow the same reaction scheme as for UV-induced polymerization. The main difference between the two initiation processes lies in the energy deposition and the pathway for free radical generation. EB networks are usually uniformly cured due to the fulldepth penetration of the electrons. Meanwhile, their UV counterparts tend to be less cured due to the photoinitiators which absorb more of the UV irradiation at the surface rather than in the core, resulting in the non-uniform polymer networks, especially for thick parts.

Motivation and organization of the thesis

The electro-optical properties of PDLC films have been the subject of several PhD and master theses at the laboratory of Ingénierie des Systèmes Polymères of UMET (Unité Matériaux Et Transformation) at the university of Lille 1 (France) and some studies did elsewhere in the world [23-31]. It was found that such properties are controlled by several factors including

the type of LC and monomers or prepolymers, the method of preparation, film thickness, droplet morphology, configuration and surface anchoring.

Therefore and, for the sake of completeness, it is still important to continue the exploration of the relationship between the methods of polymerization, the polymerization and phase separation kinetics, the morphologies and the electro-optical responses of some systems which were previously performed at UMETof [25-27]. On the other hand, since no attempt has been made to compare between rapid UV and rapid EB radiations the objective of this study was to use two diacrylates of polypropyleneglycol based monomers; namely: tripropyleneglycoldiacrylate (TPGDA) and polypropyleneglycoldiacrylate (PPGDA800) having molecular weights of 300 and 800g/mole respectively in the presence of the E7 liquid crystal .These were cured via PIPS process by slow and rapid UV and EB radiations; the aim behind the use of very rapid UV process (UV-Dr. Hönle) was to check whether the steep electro-optical responses had been previously seen, at the laboratory "ingénierie des systèmes polymères" of UMET, in EB samples that could be obtained.

This thesis is composed of four chapters; the first two chapters present the theoretical background of liquid crystals, methods of preparation of polymer dispersed liquid crystals and their properties and applications. The third chapter concerns the materials used and presents the experimental sample preparation methods as well as the different testing procedures. Chapter four discusses the results of the phase diagrams, polymerization kinetics, thermal properties, morphologies and electro-optical properties.

It is hoped that this contribution would provide useful information and a comprehensive material of interest to both scientists and technologists.

References

[1] S. Singh, Liquid crystals fundamentals, World Scientific, Singapore, **2002**.

[2] P. Oswald and P. Pieranski, Nematic and cholesteric liquid crystals concepts and physical properties, transl. by D. Constantin**,** Taylor & Francis CRC Press, New York, **2005**.

[3] G. P. Crawford and S. J. Woltman, Liquid crystals: A unique phase of matter, Chapter 1 in, liquid crystals frontiers in biomedical applications, edit. by S. J. Woltman, G. P. Crawford and G. D. Jay, World Scientific, Singapore, **2007**.

[4] F Bloisi and L Vicari, Polymer-dispersed liquid crystals, chapter 4 in , Optical applications of liquid crystals, Edit. by L Vicari, Institute of Physics Publishing, Bristol, UK: 185-210, **2003**.

[5] J. L. Fergason, Encapculated liquid crystal and methods, US Patent 4 435 047, **1984**.

[6] J. L. Fergason, Polymer encapsulated liquid crystals for display and light control applications, Tech. Digest. SID Int. Symp.;85: 68-70, **1985**.

[7] J. W. Doane, N. A. Vaz, B. G. Wu and S. Zumer, Field controlled light scattering from nematic microdroplets, Appl. Phys. Lett.; 48: 269-71, **1986**.

[8] J. W. Doane, G. Chidichimo and N. A. Vaz, US Patent 4 688 900, **1987**.

[9] J.P.F. Lagerwall, and G. Scalia, A new era for liquid crystal research: applications of liquid crystals in soft matter nano-, bio- and microtechnology. Curr. Appl. Phys.;12: 1387–12, **2012**.

[10] M. Mucha, Polymer as an important component of blends and composites with liquid crystals, Progr. Polym. Sci.; 28: 837–73, **2003**.

[11] Y. J. Jeon, Y. Bingzhu, J. T. Rhee, D. L. Cheung, and M. Jamil, Application and new developments in polymer-dispersed liquid crystal simulation studies, Macromol. Theory Simul.; 16: 643–59, **2007**.

[12] P. S. Drzaik, Liquid crystal dispersion, Series on liquid crystals, World scientific, Singapore, **1995**.

[13] E. Andrzejewska. Photopolymerization kinetics of multifunctional monomers. Prog Polym Sci.; 26: 605–65, **2001**.

[14] C. Decker, Photoinitiated crosslinking polymerisation. Prog. Polym. Sci.; 21: 593–50, **1996**.

[15] C. Decker, and B. Elzaouk, Photopolymérisation de monomères multifonctionnels—VII. Evaluation des constantes de vitesse de propagation et de terminaison. Eur. Polym. J.; 31: 1155–63, **1995**.

[16] T. Scherzer, and U. Decker, The effect of temperature on the kinetics of diacrylate photopolymerizations studied by real-time FTIR spectroscopy, Polymer, vol. 41, pp. 7681–7690, **2000**.

[17] K. S. Anseth, C. M. Wang, and C. N. Bowman, Kinetic evidence of reaction-diffusion during the polymerization of multi(meth)acrylate monomers, Macromolecules; 27: 650–55, **1994**.

[18] B. Defoort, D. Defoort, and X. Coqueret, Electron-beam initiated polymerization of acrylate compositions, 2. Simulation of thermal effects in thin films, Macromol. Theory Simul.; 9: 725–34, **2000**.

[19] C. Patacz, B. Defoort, and X. Coqueret, Electron-beam initiated polymerization of acrylate compositions 1: FTIR monitoring of incremental irradiation, Rad. Phys. Chem.; 59: 329–37, **2000**.

[20] C. Patacz, X. Coqueret, and C. Decker. Electron-beam initiated polymerization of acrylate compositions 3: compared reactivity of hexanediol and tripropyleneglycol diacrylates under UV or EB initiation. Rad. Phys. Chem.; 62: 403–10. **2001**.

[21] U. Maschke, X. Coqueret, and C. Loucheux, Electron beam processing for polymerization induced phase separation: preparation of polymer dispersed liquid crystal films. Nucl. Instr. Meth. Phys. Res. Sec. B: Beam Interact with Mater Atoms; 105: 262–66, **1995**.

[22] W. Knolle, and R. Mehnert, Primary reactions in the electron-induced polymerization of acrylates, Nucl. Instr. Meth. Phys. Res. Sec. B: Beam Interact. Mater. Atoms; 105: 154–58, **1995**.

[23] U. Maschke, N. Gogibus, A. Traisnel, and X. Coqueret, Preliminary communication. Electron beam cured liquid crystal-polymer composite materials: electrooptical enhancement effect, Liq. Cryst.; 23: 457–61, **1997**.

[24] U. Maschke, A. Traisnel, J. D. Turgis, and X. Coqueret, Influence of liquid crystal concentration on the electro-optical behavior of polymer dispersed liquid crystal films prepared by electron beam processing, Mol. Cryst. Liq. Cryst. Sci. Tech. Sec. A Mol. Cryst. Liq. Cryst.; 299: 371- 78, **1997**.

[25] F. Z. Abdoune, L. Benkhaled, L. Méchernène, and U. Maschke, Investigation of the electro-optical behavior of UV cured polymer/liquid crystal systems. Phys. Procedia; 2: 643–48, **2009**.

[26] M. Kashima, H. Cao, Q. Meng, H. Liu, D. Wang, F. Li, and H. Yang, The influence of crosslinking agents on the morphology and electro-optical performances of PDLC films, J. Appl. Polym. Sci.; 117: 3434–40, **2010**.

[27] Z. Yang, D. Li, C. Pan, and Y. Wang, Effects of hyperbranched prepolymers prepared from butyl acrylate and butyl methacrylate on the electro-optical properties of polymer dispersed liquid crystal, Polym. Adv. Technol.; 23: 1321–27, **2012**.

[28] J. He, B. Yan, B. Yu, S. Wang, Y. Zeng, and Y. Wang, The effect of molecular weight of polymer matrix on properties of polymer-dispersed liquid crystals, Eur. Polym. J.; 43: 2745–49, **2007**.

[29] J. H. Ryu, S. G. Lee, J. B. Nam, and K. D. Suh, Influence of SMA content on the electro-optical properties of polymer-dispersed liquid crystal prepared by monodisperse poly(MMA-co-SMA)/LC microcapsules, Eur. Polym. J.; 43: 2127–2134, **2007**.

[30] M. M. Dzhons, S. A. Bulgakova, I. A. Pantyukhina, and I. A. Kazantzeva. Effects of chemical structure and composition of the polymer matrix on the morphology and electro-optical performance of polymer-dispersed liquid crystal films. Liq. Cryst.; 38: 1263–68, **2011**.

[31] P. Malik, and K. K. Raina, Droplet orientation and optical properties of polymer dispersed liquid crystal composite films, Opt. Mat.; 27: 613–17, **2004**.

Chapter 1. Liquid Crystals

1. Historical Aspect of LC's

The origin of liquid crystals can be traced back to 1888 when an Austrian botanist F. Reinitzer was investigating some esters of cholesterol. He observed two melting points: at 145.5°C cholesteryl benzoate melted from a solid to a cloudy liquid and at 178.5°C, it turned into a clear liquid. Some unusual color behavior was also observed upon cooling: first, a pale blue color appeared as the clear liquid turned cloudy and then a bright blue-violet color as the cloudy liquid crystallized. Reinitzer sent the samples of this substance to a German Physicist O. Lehmann who was studying the crystallization properties of various substances. Lehmann observed the sample under his polarizing optical microscope and noted its similarity with some of his own samples. He observed that they flow like liquids and exhibit optical properties like those of a crystal. The subsequent studies established that these observed intermediate phases represent a new thermodynamic state of matter that is quite distinct from the isotropic liquid. The mechanical properties of these phases are intermediate between those of a crystalline solid and an isotropic liquid. Lehmann first referred to them as flowing crystals and, later on, G. Freidel coined the term "liquid crystals" in the twenties of the last century [1].

2. Definition of Liquid Crystals:

Liquid crystals are mesophases between crystalline solids and isotropic liquids. They are usually formed of elongated molecules in which their properties (partial or no positional order, partial orientational order) are intermediate between those of anisotropic liquid (neither positional nor orientational order) and those of a crystal (both positional and orientational order) as illustrated in figure 1-1 [2].

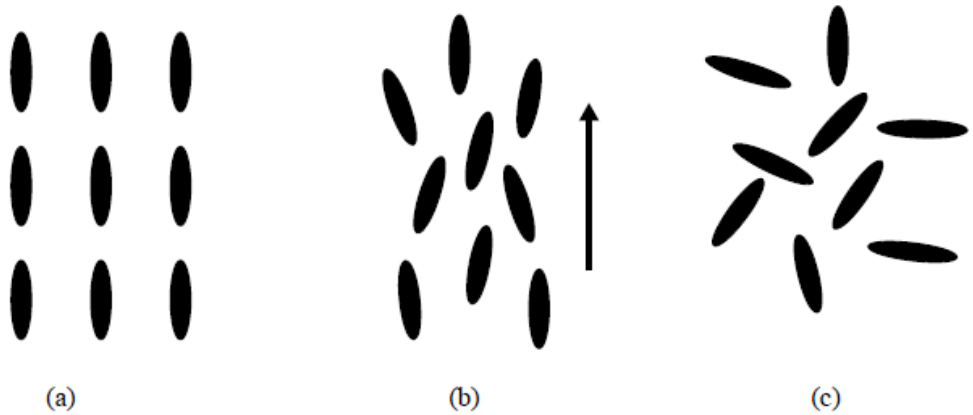

Figure 1-1 Schematic description of (a) crystal, (b) liquid crystal and (c) liquid.

Figure 1-2 shows a typical calamitic rod-like liquid crystal molecule. Its chemical name is 4'-n-heptyl-4-cyano-biphenyl and is abbreviated as 7CB. It consists of a cyanobiphenyl, which is the rigid core and a hydrocarbon chain, which is the flexible tail. If the molecule is completely flexible, it will not have orientational order. If it is completely rigid, it will transform directly from the isotropic liquid phase at high temperature to the crystalline solid phase at low temperature. The rigid part favors both orientational and positional order while the flexible part does not. With balanced rigid and flexible parts, the molecule exhibits liquid crystal phases as clearly indicated in figure 1-3 [3].

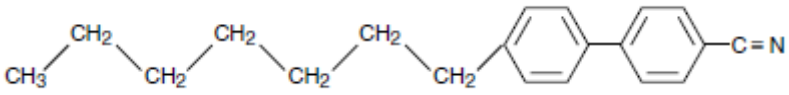

Figure 1-2: The chemical composition of 4'-n-heptyl-4-cyano-biphenyl known as 7CB

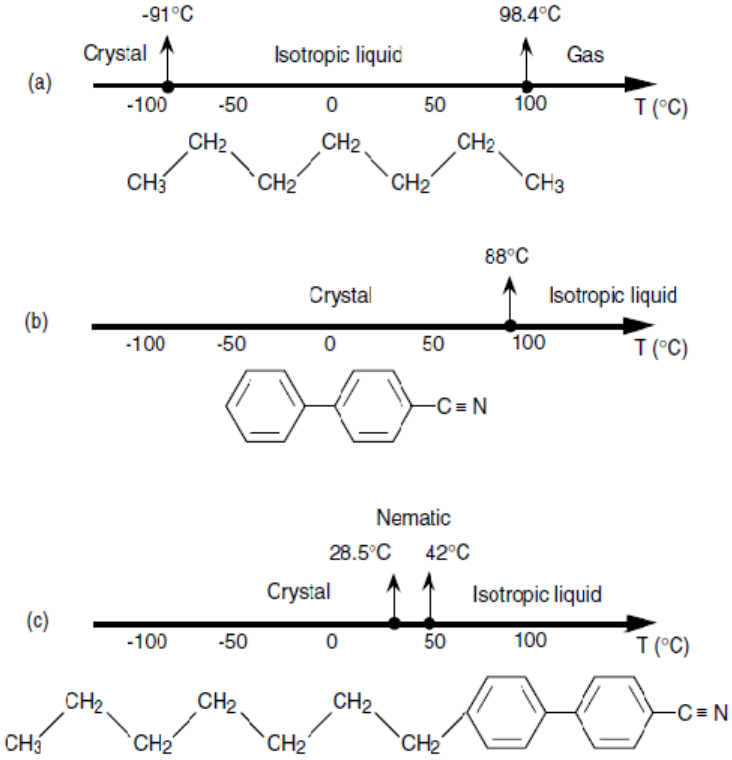

Figure 1-3: Phase sequence of three organic substances; (a) n-heptane, (b) 4-cyanobiphenyl (c) 7CB (4'-n-heptyl-4-cyano-biphenyl)

Figure 1-3 represents the phase sequence of three organic substances where the first two sequences belong to very dissimilar and non-mesogenic molecules, n-heptane (a) and 4-

cyanobiphenyl (b). The third sequence is that of the substance c (a-b) obtained by chemically bonding the first two molecules. These species were not randomly chosen; indeed, mesogenic a-b, known as 7CB, is a component of many nematic mixtures used in liquid crystal displays. In n-heptane, because the molecule bears moment dipole of dispersion forces which are weak due to the low polarizability of these molecules which have no double bond, therefore, it is not surprising that at the atmospheric pressure; heptane melts at a temperature as low as -91°C and boils at 98.4°C. On the other hand, 4-cyanobiphenyl melts at a much higher temperature, around 88°C. The height of the melting point is due to the presence of the cyano group −C≡N, which has a strong dipolar moment, and to the high polarizability of the aromatic rings. In conclusion, the 7CB molecule consists of two parts, each of which has a classical phase sequence but with very different melting temperatures.[3]

3. Classification of Liquid Crystals:

G. Friedel named the new states of matter (nematic, smectic, and cholesteric or chiral nematic) as illustrated in figure 1-4. He drew his inspiration from the Greek language:

3.1. Nematic (νημα*, thread)* because of the linear discontinuities and the winding like threads. The nematic liquid crystals have long-range orientational order but no long-range positional order. The average orientation of all of the molecules in the nematic liquid crystals is defined as the director n (figure 1-5(a)).

3.2. Smectic (σμεγμα*, soap),* which means like soaps. Smectic liquid crystals are different from nematics in that they are formed of layers with an additional degree of positional order. Within the layers, there is a loss of positional order, while the orientational order is still preserved. There are several different categories of smectics. The two well known of these are Smectic A, in which the molecules tend to align perpendicular to the layer planes, and Smectic C, where the alignment of the molecules is at some arbitrary angle to the normal (figure 1-5(b), (c)) respectively.

3.3. Cholesteric (or chiral nematic phase) is typically composed of nematic mesogenic molecules containing chiral carbon which favors an alignment between molecules at an angle to one another as presented in figure 1-5(d). The term chiral is used to denote an asymmetric molecular structure. It is achieved by attaching the aliphatic moiety to a tetrahedral sp^3 carbon atom. Figure 1-4 gives an example of a chiral molecule. This leads to the formation of a structure that can be visualized as a stack of very thin 2-D nematic-like layers with the director in each layer twisted with respect to those above and below. In this structure, the

directors actually form a continuous helical pattern around the normal layer. The pitch, P_a, is defined as the distance it takes for the director to rotate one full turn. [2]

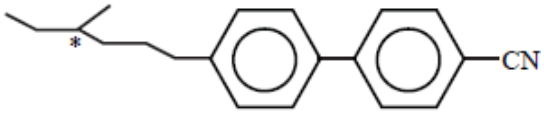

Figure 1-4: an example of cholesteric molecule: 3-methyl 4'-hexyl 4-cyanobiphenyl

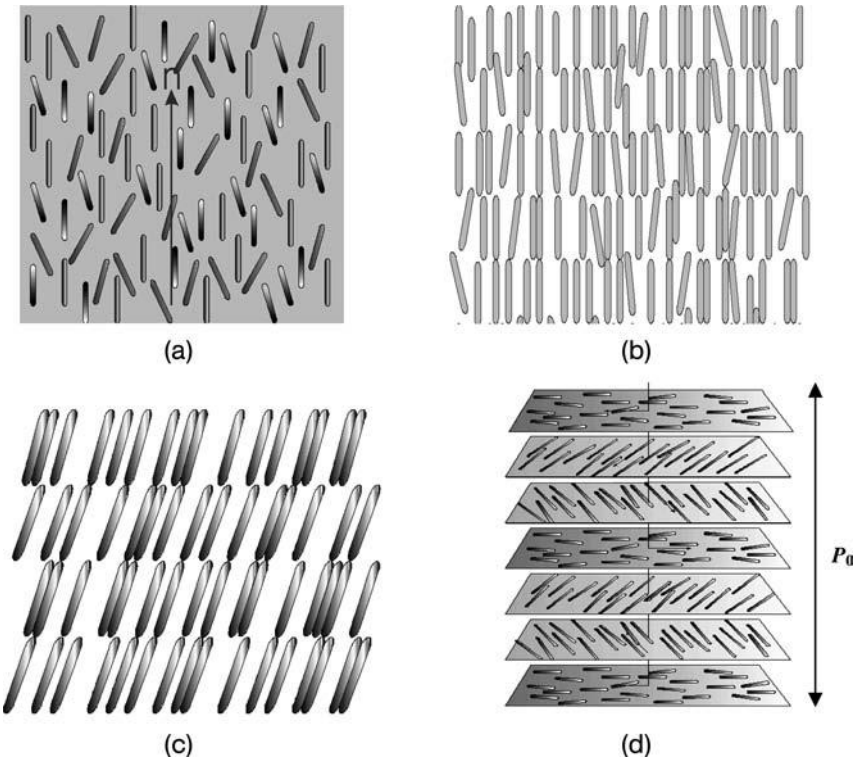

Figure I-5: Schematic description of mesogenic phases: (a) nematic, (b) smectic A, (c); smectic C, (d) cholestric.

4. Types of Liquid Crystals:

Two types of liquid crystal mesophases must be distinguished: thermotropic and lyotropic. Thermotropic liquid crystals are of interest in electro-optic displays, sensors, etc. Lyotropic liquid crystals, on the other hand, are of great biological interest and appear to play an important role in living systems. [4]

4.1. Thermotropic Liquid Crystals

The term "thermotropic" arises when transitions of mesophases are mainly affected by changing the temperature. Examples of materials showing thermotropic liquid crystal phases with molecular structures like those presented in Figure 1-6.

In general, the attraction between two organic molecules is due to:

1. Direct interaction between their permanent electric dipoles. This interaction is attractive for certain positions of the molecules.

2. Permanent dipole-induced dipole interactions. These interactions depend on the molecular polarizability.

3. Induced dipole-induced dipole interactions are among Van Der Waals forces; these interactions also depend on the molecular polarizability. [4]

In alkyl or alkoxy cyanobiphenyls, the polarity of the terminal groups frequently gives rise to very strong intermolecular attractions which result in high melting points of these compounds. The smectogenic molecules are very similar to those exhibiting nematic phases but tend to be slightly longer. This can be achieved by increasing the length of the rigid core of the molecule with the addition of more rings or by making the end groups (the aliphatic chain) longer; When the terminal groups are very short, the material melts from the solid to the nematic phase and finally to the isotropic liquid phase. As the end groups become longer, the sequence of the phase transition changes; the material melts first from the solid to a smectic phase, then to a nematic phase and ultimately to an isotropic phase. With even longer terminal groups the sequence of transition goes from solid to smectic to isotropic liquid. This discussion is recapitulated in table 1-1. [4]

Table 1-1 Transition temperatures of the alkyl cyanobiphenyls nCB

Chain length	Abbreviation	Transitions
$n = 5$	(5CB)	$\mathrm{N} \leftrightarrow 35^{\circ}\mathrm{C} \leftrightarrow \mathrm{I}$
$n = 6$	(6CB)	$\mathrm{N} \leftrightarrow 38^{\circ}\mathrm{C} \leftrightarrow \mathrm{I}$
$n = 7$	(7CB)	$\mathrm{N} \leftrightarrow 42^{\circ}\mathrm{C} \leftrightarrow \mathrm{I}$
$n = 8$	(8CB)	$\mathrm{SmA} \leftrightarrow 33.3^{\circ}\mathrm{C} \leftrightarrow \mathrm{N} \leftrightarrow 38^{\circ}\mathrm{C} \leftrightarrow \mathrm{I}$
$n = 9$	(9CB)	$\mathrm{SmA} \leftrightarrow 48.3^{\circ}\mathrm{C} \leftrightarrow \mathrm{N} \leftrightarrow 49.7^{\circ}\mathrm{C} \leftrightarrow \mathrm{I}$
$n = 10$	(10CB)	$\mathrm{SmA} \leftrightarrow 50.7^{\circ}\mathrm{C} \leftrightarrow \mathrm{I}$
$n = 11$	(11CB)	$\mathrm{SmA} \leftrightarrow 52.7^{\circ}\mathrm{C} \leftrightarrow \mathrm{I}$
$n = 12$	(12CB)	$\mathrm{SmA} \leftrightarrow 56.9^{\circ}\mathrm{C} \leftrightarrow \mathrm{I}$

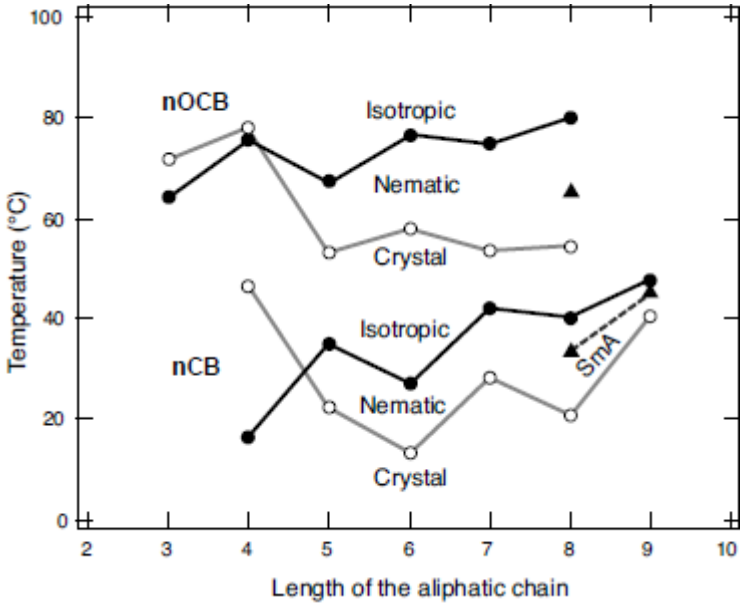

Figure 1-6: Polymorphisms of the corresponding series nCB and nOCB

4.2. Lyotropic Liquid Crystals

The most commonly encountered liquid crystals in nature are lyotropic liquid crystals, which are driven to change their phase of the matter by concentration rather than temperature. There are many examples of these materials including surfactants and soaps, the cell membranes in our bodies, the deoxyribonucleic acid (DNA), certain viruses, and many synthetic polypeptides when dissolved in an appropriate solvent (usually water) in suitable concentration form lyotropic mesophases. Therefore, life itself depends on this ubiquitous phase. [3,4]

For example, the phospholipids, which are the main component of the cell membrane, part of the molecule is hydrophobic while the another part is hydrophilic, the lyotropic liquid crystal phase forms from the dissolution of the phospholipids in water as illustrated in Figure 1-7 where (a) is a phospholipid with one saturated chain, 10 to 16 carbon atoms long, (b) a double-chained phospholipid, the R_1 chain is saturated while R_2 contains a double bond, the chains contain 12 carbon atoms, (c) sodium dodecyl sulphate(SDS), an anionic detergent, (d) a non-ionic surfactant of the C_mEO_n series, and $C_{12}EO_6$ is the hexa-ethylene glycol mono-n-dodecyl ether.

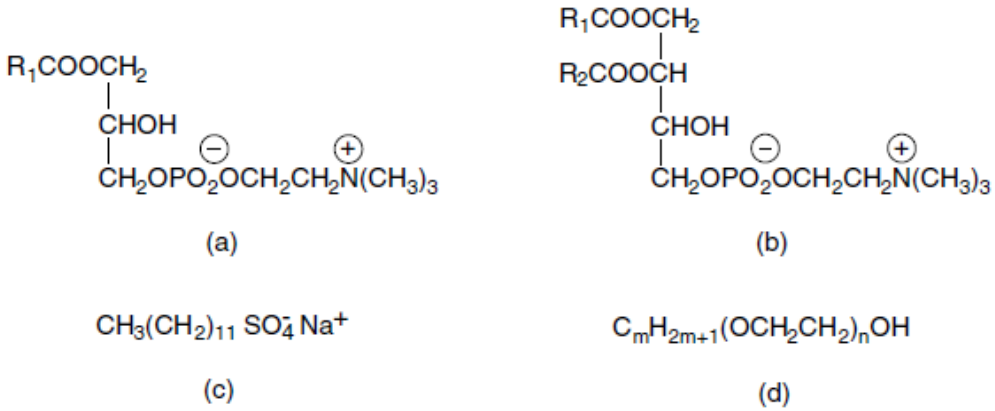

Figure 1-7: Examples of some amphiphilic phospholipid molecules.

5. Eutectic Mixtures of Liquid Crystals

In general, liquid crystal devices in automobile applications tend to be subjected to a wide range of environmental conditions where the operational temperature is in the range of less than −20◦C to more than +100◦C. Some applications are very demanding like the case of aircraft and aerospace display devices.

It is evident that the pure substances of type nCB, nOCB or nCT cannot be directly used alone in liquid crystal displays since the temperature range of the nematic phase $\Delta T_N = T_{N/I} - T_{Cr/N}$ is either too narrow or at too high temperature. For example, the liquid crystal compound 4'-n-pentyl-4-cyano-biphenyl (5CB) has a crystal/nematic transition temperature of 24°C and a nematic/isotropic transition temperature of 35°C. This small temperature window is not sufficient for most vehicular and industrial applications and the very high nematic/isotropic transition of 240°C, as in the case of 5CT (4'-n-pentyl 4-cyanotriphenyl), which is too high for such applications. For most cases, no single liquid crystal compound can satisfy all of the necessary requirements for a given practical device. [3]

It is well known that binary mixtures of liquid crystals have a melting point less than those of the two constituent materials; blending the different products in proportions corresponding to a eutectic point in which the melting point of the mixture reaches a minimum as clearly indicated in figure 1-8.

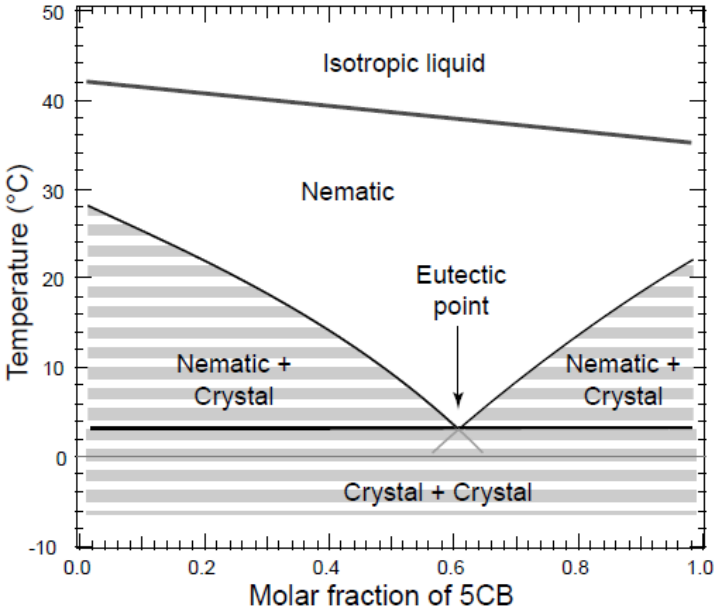

Figure 1-8: Theoretical phase diagram for the 5CB/7CB blend computed from the Schroder-van Laar law.[3]

The proportions at the eutectic point of the mixtures 5CB/7CB (figure I-8), can be easily determined by The Schroder-van Laar law:

$$\ln x_i = \frac{\Delta H_i}{R}\left(\frac{1}{T_i} - \frac{1}{T_e}\right) \qquad (1)$$

Where ΔH_i is the latent heat at the crystal/nematic transition for component *i*, ΔH_{5CB}=4.1kcal/mole and ΔH_{7CB}=6.2kcal/mole, T_i is the crystal/nematic transition temperature of component *i*, x_i is the molar fraction of component *i*, T_e is the temperature at the eutectic point and R is the ideal gas constant.

The eutectic composition is defined by the relation:

$$\sum_{i=1}^{n} x_i = 1 \qquad (2)$$

Combining equations (1) and (2)

$$\sum_i \exp\left[\left(\frac{\Delta H_i}{R}\right)\left(\frac{1}{T_i} - \frac{1}{T_e}\right)\right] - 1 = 0 \qquad (3)$$

Equation (3) can be solved by the Newton-Raphson method to allow a rapid evaluation of the eutectic point of the mixture to be around 3°C. The volume fractions are then 0.6 and 0.4 for 5CB and 7CB respectively. This type of prediction using the Schroder-van Laar law is quite useful but it can fail badly when complex mixtures of structurally different molecules are considered. [5]

The relationship between clearing temperature of a nematic mixture and the NI temperatures of its components is closely represented by equation (4):

$$NI_{mixture} = \sum_i x_i NI_i \quad (4)$$

Where NI is the nematic/isotropic transition temperature in °C and x_i represents the mole fraction of component *i*. There have been occasional observations of significance deviations from this relationship, but they are relatively few. Consequently, for the eutectic composition, the nematic/isotropic transition temperature of 5CB/7CB is around 37.8°C. [4]

To further extend the temperature range of the nematic phase, more than two components have to be mixed. For instance, in a blend **E7** containing 51% 5CB, 25% 7CB, 16% 8OCB and 8% 5CT, the nematic phase is ranging from - 60°C to T_{NI}=61°C. [6]

6. Properties of Nematic Liquid Crystals:

6.1. Order Parameter:

Nematic liquid crystals are usually uniaxial and are the most widely used liquid crystals in electro-optical applications. The director determines the direction of the preferred orientation of the molecules but it does not represent the degree of the orientational order. The order parameter S, proposed by Tsvetkov [7], provides a measure of the long-range orientational order

$$S = \frac{\langle 3\cos^2\theta - 1 \rangle}{2} \quad (5)$$

Where θ is the angle between the axis of a molecule and the director of the liquid crystal (Figure I-9); the angular brackets indicate an average over the complete system. For a perfect crystal S = 1 and for the isotropic phase S = 0.

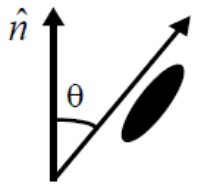

Figure 1-9: Definition of θ used in equation (5).

For nematic liquid crystals, S has a value between 0 and 1, varying with the temperature. The critical temperature at the nematic to isotropic transition point is defined as T_0 (Figure I-10). [8]

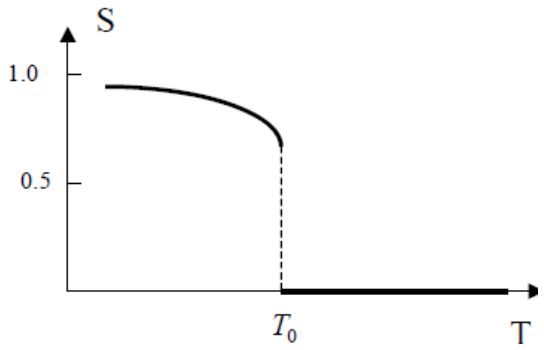

Figure 1-10: Variation of the order parameter S with temperature T.

6.2. Optical Anisotropy or Birefringence:

It is quite evident that the constituent molecules of liquid crystal mesophases are structurally very anisotropic. Because of this shape anisotropy, all the molecular response functions, such as the electronic polarizability, are anisotropic. The long range order in the liquid crystal phases prevents this molecular anisotropy from being completely averaged to zero. Such a liquid crystal exhibits a uniaxial optical symmetry with two principal refractive indices (i.e., birefringence). The ordinary refractive index, n_o, is experienced by light with polarization perpendicular to the long molecular axis and the extraordinary refractive index, n_e, is experienced by light with polarization parallel to the long molecular axis, as illustrated in Figure 1-11 [1]. The birefringence or optical anisotropy is defined as:

$$\Delta n = n_e - n_o \tag{6}$$

If o$n_e > n_o$, the liquid crystal is said to have a positive birefringence; whereas, if $ne < no$, the liquid crystal is said to have a negative birefringence.

For polarized light impinging on a liquid crystal compound at some angle to the long molecular axis, θ, the birefringence is given by:

$$n(\theta) = \left[\frac{\cos^2\theta}{n_e^2} + \frac{\sin^2\theta}{n_o^2} \right]^{1/2} \tag{7}$$

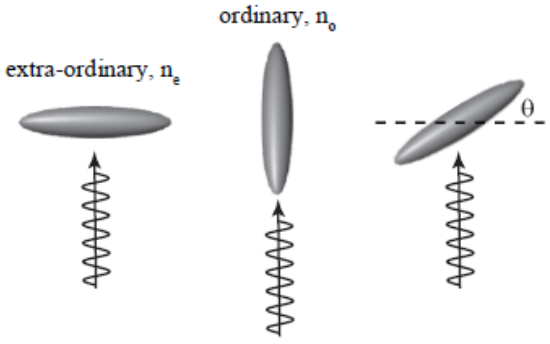

Figure 1-11: A graphical illustration of optical anisotropy or birefringence.

Values of birefringence for calamitic liquid crystals fall in the range of 0.05–0.3 for most commercial liquid crystal mixtures. The birefringence also depends on temperature and goes to zero ($\Delta n \rightarrow 0$) in the isotropic phase. The average refractive index constant in the isotropic phase is given by:

$$\left\langle n^2 \right\rangle = \frac{n_e^2 + 2n_o^2}{3} \tag{8}$$

A good experimental example of birefringence is obtained by shining a nonpolarized laser beam of λ=632.8 nm through a prism (Figure 1-12). The prism is, in fact, a wedge-shaped container filled with the nematic (E7) at 20°C. The container walls are treated by rubbing them to align the nematic molecules parallel to the wedge. [1]

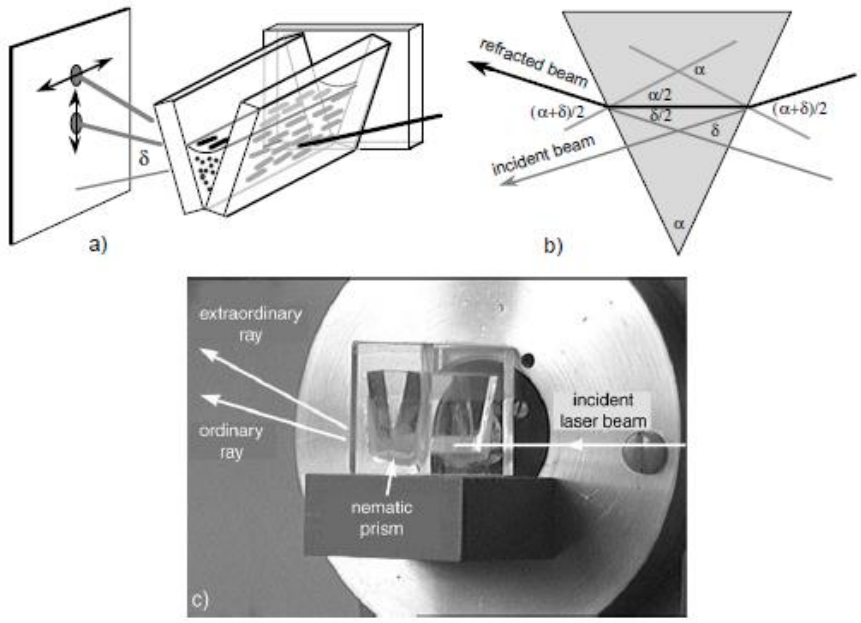

Figure 1-12: a) Experimental evidence for nematic phase birefringence; two rays linearly polarized with a 90° difference exit the prism; b) measuring the angle of least deviation; c) photograph of the experimental setup.

Two refracted rays exit the prism, both linearly polarized, but one is normal to the refraction plane, and the another one is on the plane. If the prism angle is α=20°, the angles of least deviation are δ_e=13.5° for the first beam and δ_o=9.1° for the second. With these data, one can compute the two refraction indices of E7 using the formula (see Figure I-12):

$$n_{e,o} = \frac{\sin\left(\frac{\alpha + \delta_{e,o}}{2}\right)}{\sin\left(\frac{\alpha}{2}\right)} \tag{9}$$

For E7, n_o=1.5183; n_e=1.7378, lead to a birefringence of: $\Delta n = n_e - n_o$=0.2195. [9-11]

6.3. Dielectric Anisotropy:

The shape anisotropy of calamitic liquid crystals manifests itself in two often very important properties: (1) dielectric anisotropy and (2) birefringence. Because of the ordering of calamitic molecules, liquid crystals are uniaxially symmetric (i.e., the axis of symmetry is parallel to the axis of the molecules, the director **n**). As a consequence of this uniaxial symmetry, the dielectric constants differ in magnitude along the long axis ($\varepsilon_{\parallel}$) and perpendicular to it ($\varepsilon_{\perp}$). This dielectric anisotropy ($\Delta\varepsilon$) is defined as:

$$\Delta\varepsilon = \varepsilon_{\parallel} - \varepsilon_{\perp} \qquad (10)$$

The sign of $\Delta\varepsilon$ is of the utmost importance in liquid crystal device applications. The LC molecules can align parallel or perpendicular to applied fields depending on the sign of their dielectric anisotropy, as illustrated in Figure 1-13. Most commonly, compounds exhibit a positive dielectric anisotropy ($\Delta\varepsilon > 0$) that aligns them parallel to applied electric fields, but the inverse is also possible ($\Delta\varepsilon < 0$).

It is also established in the classical dielectric theory that the macroscopic dielectric constant is proportional to the molecular polarizability. In calamitic liquid crystals, the polarizability along the long axis is often greater than that perpendicular to it. For polar calamitic liquid crystals (polar groups are placed between the two aromatic rings), the permanent dipole moment can result in a decrease in $\Delta\varepsilon$; making possible a liquid crystal system with $\Delta\varepsilon < 0$, which is also shown in Figure I-13. The dielectric anisotropy is typically $\Delta\varepsilon \sim 5$–15 for most liquid crystal materials used in device applications. The LC E7 has $\Delta\varepsilon$=13.8 with $\varepsilon_{\parallel}$=19.0 at a frequency of 1 kHz [9]

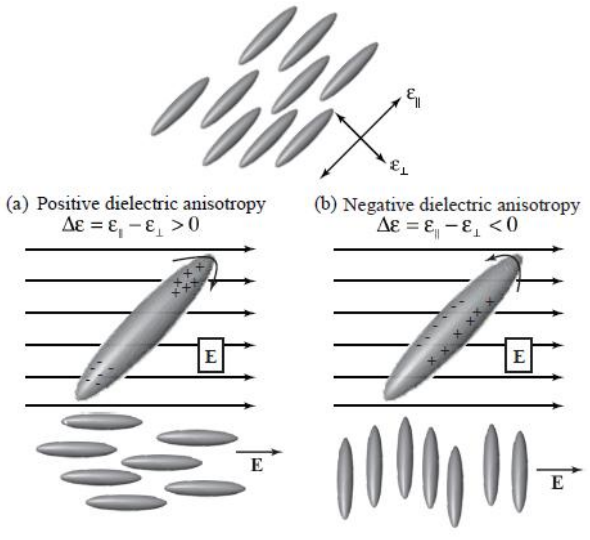

Figure 1-13: A graphical illustration of (a) positive and (b) negative dielectric anisotropy.

6.4. Elasticity:

The elastic properties of liquid crystals are one of their most notable features. Analogous to most liquids and solids, liquid crystals exhibit a so-called curvature elasticity, which is characterized by a set of elastic constants, graphically illustrated in Figure 1-14. These elastic deformations determine the static equilibrium configuration and the restoring torques that arise when the system is perturbed away from its equilibrium configuration. The elastic theory is used to predict stable configurations and electric field-induced elastic deformations of the liquid crystal material, which is a balance between the elastic and electric field torques. [1]

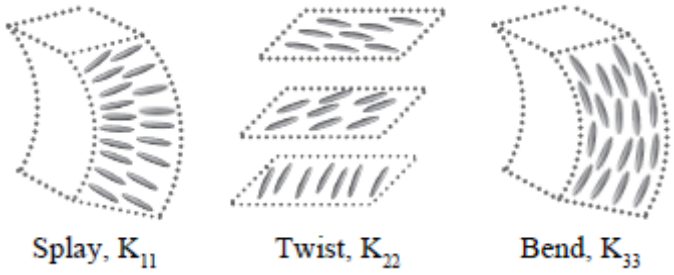

Figure 1-14: Splay, twist, and bend elastic constants.

The elastic theory expression is often written in the following form:

$$f = \frac{1}{2}\left\{K_{11}(\nabla \cdot n)^2 + K_{22}(n \cdot \nabla \times n)^2 + K_{33}(n \times \nabla \times n)^2 - \varepsilon_0 \Delta\varepsilon (E \cdot n)^2\right\} \quad (11)$$

where f is the free energy density, **n** is the nematic director, **E** is the applied electric field; K_{11}, K_{22}, and K_{33} are known as the splay, twist, and bend elastic constants as depicted in Figure I-14, respectively; and $\Delta\varepsilon$ is the dielectric anisotropy. The elastic constants are typical of the order of $K \sim 10^{-11}$ N for most liquid crystal materials used in device applications. For the LC E7, the elastic constants are $K_{11}=K_{22}=K_{33}=13\text{x}10^{-12}$ N. [9]

7. Phase Diagrams of Liquid Crystal/Polymer Blends

The phase properties of mixtures of polymers and liquid crystals (LCs) have been investigated particularly due to their importance for numerous applications. For example, Polymer Dispersed Liquid Crystals (PDLCs) that are used for light control devices like optical shutters. PDLC films can be electrically switched from a cloudy light scattering off state to an activated transparent on-state. They consist commonly of micron-sized dispersions of low molecular weight LC (LMWLC) within a solid polymer matrix. The electro-optical characteristics of these materials are governed by the thermodynamical properties and therefore, it is important to understand their phase behavior. [12-14]

Many studies on the phase behavior of polymer/liquid crystal blends have been reported in recent years. Kronberg and Patterson [15,16] developed a simple theory for the nematic–

isotropic equilibrium in the region of high LC concentration. The theory was tested with EBBA (LC-p-ethoxy benzylidene-p-n-butylaniline) blended with polystyrene and poly(ethylene oxide). Ballauff and Orendi [17,18] used the extended Flory lattice theory to describe the phase behavior of polymer–LC blends, including liquid–liquid phase separation in the isotropic phase. Kelkar and Manohar [19] and Shen and Kyu [20] extended the Flory–Huggins (FH) lattice theory [21,22] of regular solution to describe mixtures of nematic liquid crystals with polymeric solutes. The nematic phase was described in terms of the Maier–Saupe (MS) approximation [23,24]. The combined FH/MS theory predicted a complex phase diagram that consists of isotropic, isotropic–isotropic, isotropic–nematic and pure nematic regions. The theoretical calculation accorded well with the experimental phase diagram of poly(benzyl methacrylate) and PMMA of various molecular weights with nematic mixture E7 and PS with 7CB [25] and E7 [26], respectively.

In the combined FH/MS theory the total free energy g for polymer/nematic liquid crystal blends is described in terms of a simple addition of free energy of mixing of isotropic liquids g^i and free energy of nematic ordering of liquid crystals g^n:

$$g = g^i + g^n \tag{12}$$

For isotropic mixing, as in binary polymer blends, free energy is expressed in terms of the FH theory

$$g^i = \frac{G^i}{nkT} = \frac{\phi_1}{r_1}\ln\phi_1 + \frac{\phi_2}{r_2}\ln\phi_2 + \chi\phi_1\phi_2 \tag{13}$$

Where k is the Boltzmann constant; T, the absolute temperature; r_1, number of sites occupied in a lattice by liquid crystal molecule which is equal to unity; r_2, number of sites occupied by a polymer chain (each statistical segment is assumed to occupy one lattice site); ϕ_1 and ϕ_2, volume fractions of components 1 and 2

$$\phi_1 + \phi_2 = 1 \tag{14}$$

n is the total number of sites. $n = n_1r_1 + n_2r_2$; where n_1 and n_2 are the number of liquid crystal and polymer molecules, respectively, and χ is the FH interaction (between LC and polymer), a parameter which is generally assumed to be a function of reciprocal temperature

$$\chi = C + \frac{D}{T} \tag{15}$$

Where C and D are constants.

The contribution of nematic ordering to the total free energy is generally given by the MS mean field theory

$$g^n = \frac{G^n}{nkT} = -\sum(S)\phi - \frac{1}{2}\nu S^2\phi^2 \quad (16)$$

Where $\sum(S)$ is the decrease in entropy due to the alignment of individual LC molecule; ν, the nematic interaction parameter (between LC molecules)

$$\nu = 4.54\frac{T_{I-N}}{T} \quad (17)$$

S, the orientational order parameter

$$S = \frac{3\langle\cos^2\theta\rangle - 1}{2} \quad (18)$$

Where θ is the angle between a reference axis and the director of a liquid crystal molecule and $T_{I–N}$ is the isotropic–nematic transition temperature. Thus, g should be written as follows

$$g = \phi\ln\phi + \frac{1-\phi}{r}\ln(1-\phi) + \chi\phi(1-\phi) - \phi\sum(S) - \frac{1}{2}\nu\phi^2S^2 \quad (19)$$

Where ϕ is the volume fraction of LC and r is the number of lattice sites occupied by a single polymer chain. Phase diagram of polymer/LC blend including the boundaries for I–I (Isotropic–isotropic phases), I–N (isotropic–nematic phases) and I–I–N (two isotropic–nematic phases) equilibria can be predicted [25].

The study of phase separation in binary systems is important for understanding the formation of the final morphology of polymer/liquid crystal blends. In the case of PDLC the phase separation phenomena control the formation of sample morphology. Crosslinked PDLCs are formed by the two-step process:

1. A low molecular weight LC and a polymer precursor are initially mixed together to form a uniform solution. The phase diagram of the system is characterized usually with an upper critical solution temperature (UCST). The temperature of the mixture should be higher than the mixing temperature T_{mix} above which the UCST components are co-dissolved. If $T<T_{mix}$, phase separation leads to the formation of LC regions of various sizes LC. In this case, non-uniform optical properties of PDLC are observed. Calorimetry, light scattering and optical microscopy allow phase diagrams to be formed for the LC/polymer precursor binary system [27–33].

2. The demixing of the liquid crystal from the polymer matrix should occur during the curing reaction. Calorimetry and time-resolved light scattering have been applied to study demixing during cure. The curing process is important in controlling the size and number density of LC microdomains. Calorimetric studies of phase separation process, effects of the concentration and state of cure on mixing and phase separation of the binary system of low-molecular

weight liquid crystal and polymer matrix were determined for the first time by Smith [34]. Such experiments were made for a mixture of LC(E7, 5CB) with NOA65 (Norland ultraviolet curable optical adhesive 65 with photoinitiator).

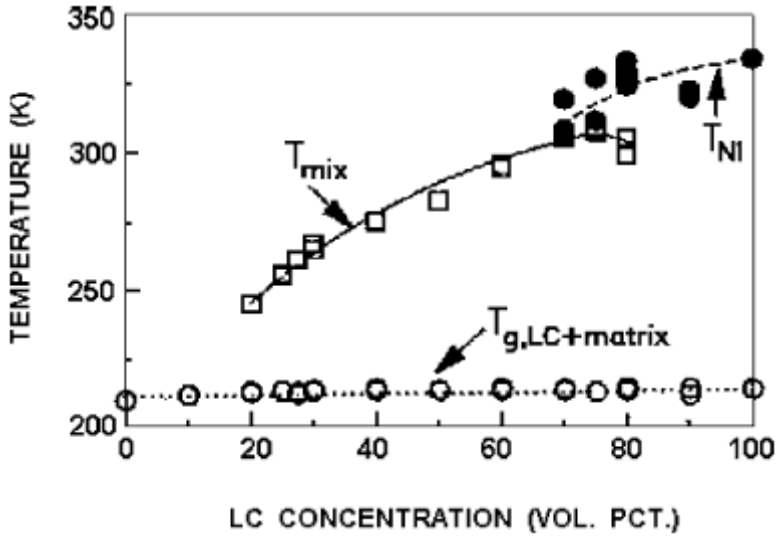

Figure 1-15: Phase diagram for uncured E7/NOA65 mixtures[12]

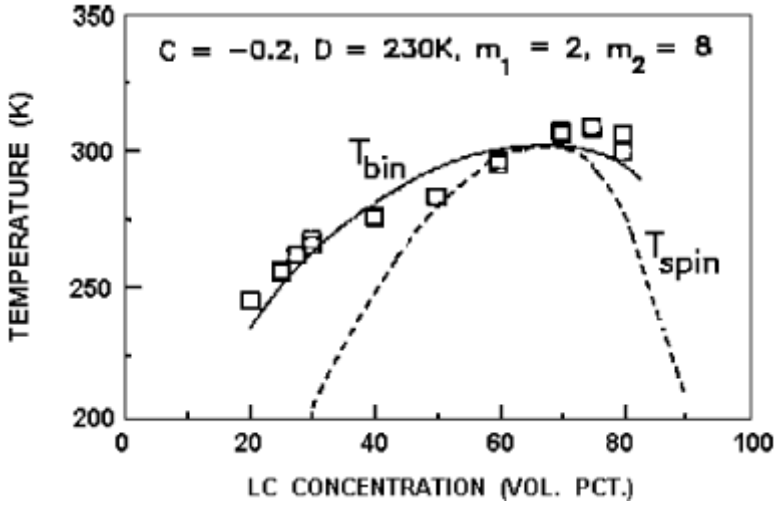

Figure 1-16: Measured and calculated mixing temperatures for the uncured E7/NOA65 system. Points are Tmix values from Figure 1-15. The solid line is FH binodal curves; dashed line is a corresponding spinodal curve. C, D: parameters of Eq. (3), m1, m2: number of sites occupied by LC and polymer segment (in Eq. (2), respectively, r1 and r2).[12]

Figures 1-15 and 1-16 show the phase diagrams for that uncured system, measured and calculated with FH theory according to Nishi [35] prediction for a critical temperature given by:

$$T_c = (-D/C)\{1| - (1/2C)[r_1^{-0.5} + r_2^{-0.5}]^2\}^{-1} \quad (20)$$

Where D, C are the constants of Eq. (15).

References

[1] G. P. Crawford, and S. J. Woltman, Liquid crystals: A unique phase of matter, Ch. 1 in, liquid crystals frontiers in biomedical applications, edit. by S. J. Woltman, G. P. Crawford and G. D. Jay, World Scientific, Singapore, **2007**.

[2] D. K. Yang, and S. T. Wu, Fundamentals of liquid crystal devices, John Wiley & Sons, West Sussex, England, **2006**.

[3] P. Oswald, and P. Pieranski, Nematic, and cholesteric liquid crystals concepts and physical properties, transl. by D. Constantin**,** Taylor & Francis CRC Press, New York, **2005**.

[4] E. B. Priestley, Liquid crystal mesophases, Ch. 1 in, Introduction to liquid crystals, edit. By E. B. Priestley, and P. J. Wojtowicz, P. Sheng, Plenum Press, New York, **1974**.

[5] V. S. Pasechnik, V. G. Chigrinov, and D. V. Shmeliova, Liquid Crystals Viscous and Elastic Properties Wiley-VCH Verlag, Weinheim, Germany, **2009**.

[6] A. W. Levine, Structure- property relationships in thermotropic organic liquid crystals Ch.2 in, Introduction to liquid crystals, edit. By E. B. Priestley, P. J. Wojtowicz, and P. Sheng, Plenum Press, New York, **1974**.

[7] V. Tsvetkov, Acta Physicochim. (USSR) 16, 132, **1942**.

[8] H. Zhang, Wavelength tunable devices based on holographic polymer dispersed liquid crystals, PhD thesis, Kent State University, USA, **2008**.

[9] Merck Product Information. Merck liquid crystals. Licrilite Brochure. Poole: Merck House, **1994**.

[10] J. Li, C. H. Wen, S. Gauza, R. Lu, and S. T. Wu, Refractive indices of liquid crystals for display applications. J. Display Technol.; 1: 51–61, **2005**.

[11] H. A. Tarry. The refractive indices of cyanobiphenyl liquid crystals. Poole, Great Britain: Merck Ltd., **1967**.

[12] J. W. Doane Polymer Dispersed Liquid Crystal Displays. In: Bahadur B (ed) Liquid Crystals: Their Applications and Uses. World Scientific, Singapore, **1990**.

[13] P. S. Drzaic, Liquid Crystal Dispersions. World Scientific, Singapore, **1995**.

[14] M. Mucha, Polymer as an important component of blends and composites with liquid crystals, Prog. Polym. Sci.; 28: 837–873, **2003.**

[15] B. Kronberg, and D. J. Patterson, Application of the Flory–Huggins theory to nematic–isotropic phase equilibria, Chem. Soc. Faraday Trans.; 72: 1686–94, **1976**.

[16] B. Kronberg, I. Bassignana, and D. J. Patterson, Phase diagrams of liquid crystals/polymer systems. Phys. Chem.; 82: 1714–22, **1978**.

[17] M. Ballauff, Phase diagrams of mixtures of liquid crystals polymers: nematic–isotropic phase equilibria versus liquid–liquid demixing. Mol. Cryst. Liq. Cryst. Lett.; 4: 15–22, **1986**.

[18] H. Orendi, and M. Ballauff, Complete phase diagrams of mixtures of a nematic liquid crystal with n-alkanes. Liq. Cryst.; 6: 497–500, **1989.**

[19] V. K. Kelkar, and C. Manohar. Mol. Cryst. Liq. Cryst. Lett.; 133: 267–71, **1986**.

[20] C. Shen, and T. J. Kyu, Spinodals in a polymer dispersed liquid crystal, Chem. Phys.; 102: 556–9, **1995.**

[21] P. J. Flory, Principles of polymer chemistry, Cornell University Press, Ithaca, NY, **1953**.

[22] M. L. Huggins, Theory of solutions of high polymers, J. Am. Chem. Soc.; 64: 1712–9, **1942.**

[23] W. Maier, and A. Saupe, Eine einfache molecular-statistische theorie der nematischen tristallinflussigen phase, Teil I. Z Naturforsch; 14a: 882, **1959.**

[24] W. Maier, and A. Saupe, Eine einfache molecular-statistische theorie der nematischen kristallinflussigen phase, Teil II. Z Naturforsch; 15a: 287, **1960**.

[25] C. C. Riccardi, J. Borrajo, and R. J. Williams, Multiple phase equilibria in polydisperse polymer/liquid crystal blends. Macromolecules; 31: 1124–32, **1998.**

[26] Z. Lin, H. Zhang, and Y. Yang. Spinodal decomposition kinetics of a mixture of liquid crystals and polymers. Macromol. Chem. Phys.; 200: 943–8, **1999.**

[27] G. W. Smith, A calorimetric study of phase separation in liquid crystal/matrix systems: determination of the excess specific heat of mixing. Mol Cryst Liq Cryst; 239: 63–85, **1994**.

[28] A. M. Lapena, S. C. Glotzer, S. A. Langer, and A. J. Liu, Effect of ordering on spinodal decomposition of liquid crystal/polymer mixtures. Phys. Rev. E; 60: 29–32. **1999.**

[29] T. Kyu, C. Shen, and H. W. Chiu. Effect of molecular weight on miscibility phase diagrams in mixtures of polymer and liquid crystals, Mol. Cryst. Liq. Cryst.; 287: 27–34, **1996**.

[30] M. Mucha, E. Grosicka, Phase separation in liquid crystal/ polymer composites, Proc. SPIE—Int. Soc. Opt. Engng.; 4147: 382–7, **2000**.

[31] E Grosicka, Wpływ separacji faz na własˊciwosˊci układu polimer-ciekły kryształ (influence of phase separation on properties of polymer/liquid crystal system). PhD Thesis. Technical University of Łoˊdzˊ, **2001**.

[32] M. Mucha, Z. Kroˊlikowski, Kinetics study of phase separation in polyacrylic acid/nematic LC system by optical technique. Proc. SPIE—Int. Soc. Opt. Engng.; 4759: 473–81, **2002.**

[33] Z. Kroˊlikowski. Badania separacji faz w dwuskładnikowych układach wielkoczą steczkowych (phase separation in two component systems), PhD Thesis. Technical University of Łoˊdzˊ, **2002**.

[34] G. W. Smith. Mixing and phase separation in liquid crystal/ matrix systems, Int. J. Mod. Phys. B; 7: 4187–213, **1993.**

[35] T. Nishi. Experimental aspects of compatible polymer mixtures. J. Macromol. Sci. Phys; B17: 517–42, **1980.**

Chapter 2. Polymer Dispersed Liquid Crystals PDLC's

As it is stated in the introduction, LC's were known since the end of the 19th century but their first applications in electro-optic devices appeared in the middle of the 20th century. In such applications, the most attractive properties concern the possibility of controlling the LC optical anisotropy by means of an electric or magnetic field, while the liquid behavior is an undesired characteristic. The term 'PDLC film' usually means a solid but flexible film (the polymer matrix) containing a more or less large number of cavities (the 'droplets') filled with a Liquid Crystal. Fergason [1, 2] is generally recognized as the first scientist who marked the birth of PDLC's, even if the term PDLC was introduced a few years earlier by Doane and co-workers [3,4].

Several parameters, influencing the PDLC film behavior, must be taken into account in the choice of the preparation technique:

. *Droplet size*: Both its average value and its uniformity affect light scattering.

. *Droplet shape*: The shape of the droplet influences the LC orientation while it is more or less uniform distribution within the PDLC film may influence light scattering.

. *Film thickness*: Once the applied voltage has been fixed, the electric field across the PDLC film is proportional to its thickness, so in large area devices both its average value and its uniformity must be taken into account.

. *Film aging*: Variations with a time of the chemical and physical properties of the PDLC films are important to be considered in practical applications.

1. PDLC Preparation Techniques

1.1. Emulsion Technique

The emulsion technique was introduced by Fergason [1,2]. This type of PDLC is obtained by the rapid stirring of a Liquid Crystal in an aqueous solution of a water-soluble polymer which is Poly(vinylalcohol) (PVA) and letting the solvent evaporate. Droplet size is determined by the characteristics of the emulsification processes (i.e. stirring speed and duration). Due to volume change during solvent evaporation, spherical droplets within the emulsion result in elliptical droplets, with major axes being in the plane of the film. The LC used generally has very low solubility with water and in the water-soluble polymer so that it is possible to assume that no phase contamination occurs during PDLC preparation. On the contrary, water-soluble polymers are hygroscopic and this can sensibly reduce the lifetime of the PDLC film.

1.2. Phase Separation Technique

The phase separation technique was introduced by Doane and co-workers [3, 4] and marks the start of the use of the term PDLC. In the phase separation technique, the PDLC is obtained starting with a homogeneous, liquid, single-phase mixture containing both the LC and the polymer (or monomer, or prepolymer). During polymer solidification, almost all LC molecules are 'expelled' from the polymer and aggregate in droplets which remain embedded in the polymeric film.

The phase separation can be induced in several ways; namely: solvent induced phase separation (SIPS), temperature-induced phase separation (TIPS), and polymerization-induced phase separation (PIPS)

1.2.1. Solvent-Induced Phase Separation

A solution is prepared by dissolving a thermoplastic polymer, a solvent and a required amount of LC which is only soluble in the solvent, and then the homogeneous mixture is placed over a single transparent conducting electrode. After the solvent has evaporated, thus inducing the phase separation of the liquid crystal into droplets, a second transparent conducting electrode is placed over the PDLC film.

1.2.2. Temperature-Induced Phase Separation

The LC is mixed with a molten thermoplastic polymer at high temperature, then placed between two transparent conducting electrodes and phase separation is induced by polymer solidification, obtained by cooling the sample at a controlled rate.

1.2.3. Polymerization-Induced Phase Separation

The monomer or prepolymer is mixed with the required amount of LC in a single-phase liquid. The liquid is placed between two transparent conducting electrodes and the polymerization process is started, by heating (thermally initiated PIPS, or T-PIPS) when an initiator is added to the mixture or illuminating (photo-initiated PIPS) in the presence of a photoinitiator or exposing the mixture to accelerated electron beams EB without any initiator.

Both PIPS and TIPS techniques allow the PDLC film to be prepared directly between the two required transparent electrodes and this has two advantages. The first is that there is a good adhesion of the PDLC film to both electrodes so that the final device is mechanically more robust than emulsion-type PDLC's. The second advantage is that it is possible to obtain a more uniform and controlled PDLC film thickness just by adding a small amount of 'spacers' (often glass spheres or cylinders) to the liquid single-phase mixture. For small PDLC samples, known thickness PET films are used as spacers. [5]

1.2.3.1. Photopolymerization

Radiation curing presents a number of advantages, particularly, ambient temperature operation, solvent-free formulations, low energy consumption and the production of polymer materials having tailor-made properties. It has found a large number of applications in various industrial sectors, especially in flexible displays, privacy windows, projection displays, sensors, etc. UV curing is also commonly used to perform the ultrafast drying of protective coatings, varnishes, printing inks and adhesives, and to produce the high-definition images required in the manufacture of microcircuits and printing plates, in addition to its great speed and spatial resolution.

Acrylate-based resins, which polymerize by a radical mechanism, have been thoroughly investigated as they are, by far, the most widely used UV-curable systems, because of their great reactivity. This feature, together with the remarkable chemical, optical and mechanical properties of the polymers obtained, account for the great commercial success of acrylate-based UV-curable resins. It also explains why the photoinitiated polymerization of multifunctional acrylate monomers and prepolymers has been so thoroughly investigated, mainly from the kinetic and mechanistic points of view.[]

Photoinitiated polymerizations occur when radicals are produced by ultraviolet UV light radiation of a homogeneous reaction system containing a monomer or a mixture of monomers or telechelic oligomers or prepolymer, a liquid crystal, and a photoinitiator. During the polymerization, the LC becomes less miscible with the growing polymer and consequently separates into fine droplets containing the confined LC molecules.

The photoinitiator undergoes excitation by energy absorption and subsequent decomposition into radicals as shown in figure II-1.

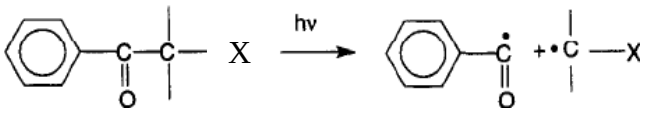

Figure 2-1: The decomposition of 2-hydroxy-2-methyl-1-phenyl-propane- 1-one (Darocur 1173), X is an OH group.

The benzoyl radical (primary radical) is found to be the major initiating species, while the other radical fragment (secondary radical) may also contribute to the initiation reaction.

For diacrylate monomer irradiated in the presence of a photocleavable aromatic ketone, the basic crosslinking polymerization process can be represented in figure 2-2.

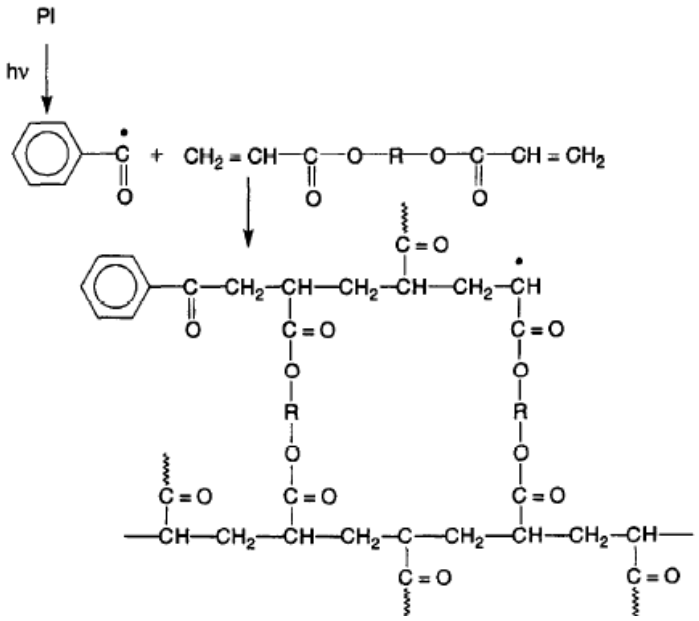

Figure 2-2: Photoinitiated crosslinking polymerisation of a diacrylate monomer. PI is an abbreviation for the photoinitiator

Different types of structures (R) can be used such as polyurethanes, polyesters, polyethers and polysiloxanes (Figure 2-2). The final properties of UV-cured acrylate polymers depend primarily on the chemical structure of the functionalized (telechelic) oligomer. The great reactivity of acrylate monomers, together with the large choice of acrylate functionalized oligomers, have afforded these radical-type systems a leading position in UV-curing applications. The high viscosity of the prepolymers often necessitates the addition of low molecular weight monomers, which will act as reactive diluents. Because of their high crosslink densities, such photocured polymers show well-designed physical properties depending on the length and chemical structure of the crosslink segments. [6]

The bulk polymerization of multifunctional monomers is a complex process that exhibits a number of anomalous behaviors with respect to the reaction kinetics and which are:

- An autoacceleration occurs at the very beginning of the irradiation because of the great number of adjacently formed radicals.
- An auto deceleration, generally observed in the later stage when the propagation reaction also becomes diffusion controlled. The decreased mobility of the propagating radical and that of the functional groups leads to a slowing down of the polymerisation, which ultimately stops before completion due to vitrification. The UV-cured polymer will, therefore, contain a certain number of functional groups that have not polymerized, as well as trapped radicals.

- A termination process controlled by reaction-diffusion**,** and not by segmental diffusion as in linear polymerization. In crosslinking polymerisation, most polymeric radicals are bound to the 3D network and have a limited mobility so that the radical site will move mainly by reacting with neighboring functional groups until it combines with another radical. When these conditions are reached, the termination rate constant becomes proportional to the propagation rate constant.
- The formation of structural heterogeneities leads to microgels which are resulting from the fast polymerization of the pendant double bonds which are in turn in large concentrations in the vicinity of the radical site.
- The physical effect of volume shrinkage on the polymerisation kinetics leads to higher final degrees of conversion at large reaction rates. At the high initiation rate provided by UV irradiation, the polymerizing system cannot maintain its volume equilibrium, as volume shrinkage occurs on a much longer timescale than the chemical reaction. The time lag between conversion and shrinkage generates a temporary excess of free volume that increases the mobility of unreacted double bonds, thus allowing higher degrees of conversion to be reached than in volume equilibrium systems. [6-11]

a. Steady State Kinetics of Linear Photopolymerization [12]

In linear photopolymerization, the rate of photochemical initiation, propagation and termination are given below

Initiation: $R_i = 2\phi I_a$ (1)

Propagation : $R_p = k_p[M^\bullet][M]$ (2)

Termination: $R_t = 2k_t[M^\bullet]^2$

(3)

Where I_a is the intensity of absorbed light in moles of light quanta per liter-second and ϕ is the number of propagating chains initiated per light photon absorbed. ϕ is referred to as the quantum yield for initiation. The factor of 2 in Eq. 1 is used to indicate that two radicals are produced per photoinitiator molecule undergoing photolysis. The factor of 2 is not used for those initiating systems that yield only one radical instead of two. ϕ is synonymous with f in that both describe the efficiency of radicals in initiating polymerization.

k_p is the constant of propagation rate, $[M^\bullet]$ is the concentration of propagating radicals and $[M]$ is the concentration of the monomer at time t.

k_t is the constant of termination rate, The use of the factor of 2 in the termination rate equation follows the generally accepted convention for reactions destroying radicals in pairs.

From the steady state conditions, $R_i = R_t$, we get: $[M^\bullet] = \sqrt{\frac{\phi I_a}{k_t}}$ and the rate of propagation becomes

$$R_p = k_p[M]\left(\frac{\phi I_a}{k_t}\right)^{1/2} \tag{4}$$

The absorbed light intensity I_a is obtained from a consideration of the Beer–Lambert law in the form

$$I_a^{'} = I_0 - I_0 e^{-\alpha[A]D} \tag{5}$$

Where I_0 is the incident light intensity at the outer surface of the reaction system and $I_a^{'}$ is the the intensity of absorbed light on a layer at a distance D (cm) into the reaction system. $I_a^{'}$ is not the same as the quantity I_a in Eq. 4. I_a is the volumetric light intensity in mol cm^{-3} s^{-1} or, more often, mol L^{-1} s^{-1}). $I_a^{'}$ and I_0 are surface area intensities in mol $cm^{-2}s^{-1}$. [A] is the molar concentration of photoinitiator. α is the absorption coefficient of photoinitiator and varies with wavelength and temperature. α has units of L mol^{-1} cm^{-1}. The molar absorptivity э, formerly called the extinction coefficient, is often used instead of α. α and э are related by the relation: α=э ln10=2.3э

I_a and, therefore, R_p vary with depth of penetration D into the reaction system. The variation of I_a with D is obtained as the differential of $I_a^{'}$ with respect to D

$$I_a = \frac{dI_a^{'}}{dD} = \alpha[A]I_0 10^3 e^{-\alpha[A]D} \tag{6}$$

The term 10^3 is obtained by converting I_a from mol cm^{-3} s^{-1} to mol L^{-1} s^{-1}. Combining Eqs. 4 and 6 yield the polymerization rate as a function of D:

$$R_p = k_p[M]\left(\frac{\phi\alpha[A]I_0 10^3 e^{-\alpha[A]D}}{k_t}\right)^{1/2} \tag{7}$$

R_p is the ‘‘local’’ polymerization rate—the rate at located distance D from the surface of the reaction system. Since R_p varies with the depth of penetration, it is useful to calculate the average polymerization rate for a thickness D of the reaction system. It is obtained by integrating the local rate over the layer thickness D and dividing by D to give:

$$\overline{R_p} = 2k_p[M]\left(\frac{\phi I_0 10^3}{\alpha[A]k_t}\right)^{1/2}\left(\frac{1-e^{-\alpha[A]D/2}}{D}\right) \quad (8)$$

b. Kinetics of Crosslinking Photopolymerization:

The polymerization of multifunctional monomers leads to highly crosslinked insoluble polymers with infinite molecular weights. The three steps of the curing process, mentioned above, become more apparent when the rate of polymerization $(R_p)_{t1}$ is plotted as a function of the exposure time (Figure 2-3). The value of R_p is easily calculated at any time from the slope of the RTIR (Real-Time Infrared spectroscopy) curve (dx/dt) (conversion Vs exposure time) and the initial acrylate double bond concentration $[M]_0$

$$(R_p)_{t1} = [M]_0 \times dx/dt \quad (9)$$

Where $[M]_0$ is the initial acrylate double bond concentration and x is the conversion.

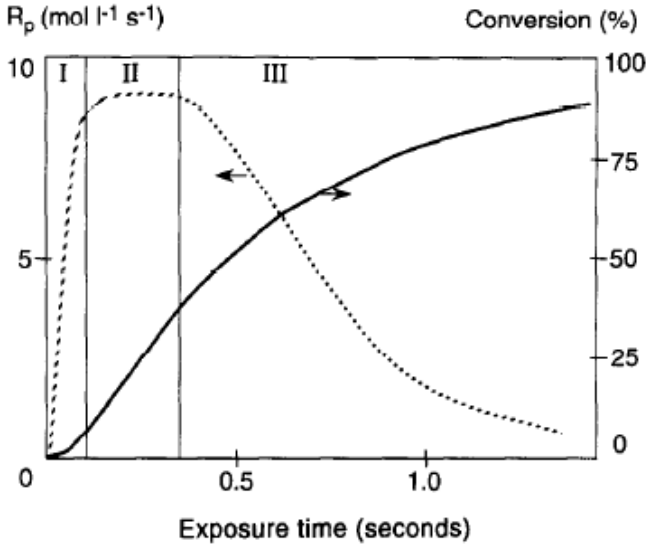

Figure 2-3: Conversion Vs exposure time (solid line) and Rp Vs exposure time (dashed line) recorded by RTIR upon UV curing of a polyurethane acrylate at light intensity: 30 mW cm^{-2}.[6]

An autoacceleration occurs at the very beginning of the irradiation because of the rapid increase in viscosity until about 5% conversion when the reaction reaches its maximum value ***(R_p)max.*** It is followed by a period where the polymerization develops at a sustained pace during 0.3 s (about 30% conversion), the time after which auto deceleration starts to take place when propagation becomes diffusion controlled. Ultimately, vitrification leads to a complete stop of the curing process at about 90% conversion. There remains in the crosslinked polymer a certain amount of unreacted acrylate double bonds, which may ultimately affect the long-term properties of the UV-cured material.

Under continuous illumination, the rate of polymerization after a given exposure, (Rp)i, is assumed to obey the following equation, once steady-state conditions are reached:

$$\left(R_p\right)_i = \frac{k_p}{\left(2k_t\right)^{0.5}}\left(\phi_i I_a\right)^{0.5}\left[M\right]_i \tag{10}$$

The ratio $\frac{k_p}{\left(2k_t\right)^{0.5}}$ can thus be easily evaluated from measurements of $(Rp)_i$ and of the remaining monomer concentration $[M]_i$, both quantities being determined from the RTIR profile.

Once the light has been switched off, the polymerization will continue to proceed for some time at a steadily decreasing rate. Under those conditions, the polymer radicals ($P^\bullet$) are expected to disappear by bimolecular reactions, and their concentration will decrease according to a hyperbolic law:

$$-\frac{d\left[P^\bullet\right]}{dt} = 2k_t\left[P^\bullet\right]^2 \quad \text{or} \tag{11}$$

$$\frac{1}{\left[P^\bullet\right]} = 2k_t \times t + \frac{1}{\left[P^\bullet\right]_i} \tag{12}$$

Where $\left[P^\bullet\right]_i$ is the radical concentration at the end of exposure. Replacing $[P^\bullet]$ by the expression $(R_p)_t/k_p[M]_t$, leads to the following rate equation for the dark reaction:

$$\frac{\left[M\right]_t}{\left(R_p\right)_t} = \frac{2k_t}{k_p} \times t + \frac{\left[M\right]_i}{\left(R_p\right)_i} \tag{13}$$

The monomer concentration $[M]_t$ and the rate of polymerization $(R_p)_t$ after a given exposure and storage in the dark at time t are directly accessible from the RTIR profile recorded after the UV exposure. A plot of the ratio $[M]_t/(R_p)_t$ versus t yields a straight line, which permits one to calculate from its slope the ratio $2k_t/k_p$ **,** and, together with the $\frac{k_p}{\left(2k_t\right)^{0.5}}$ ratio, to determine individual values of k_p, and k_t.[6-7]

1.2.3.2. Polymerization by Accelerated Electron Beams

Radiation-initiated polymerization has achieved some commercial success. The most frequently used irradiation is by electrons; this technology is called electron-beam (EB) technology. Electron Beams have a significant advantage over UV radiations which is the fact that the depth of penetration is much greater than for UV. There are several areas of application for EB technology. Coatings and other thin reaction systems, involving mostly crosslinking polymerization, are an area of application where EB competes directly against UV light. EB is not used to the same extent as UV because of the higher overall equipment costs and the perception that working with ionizing radiations is risky from a health–safety viewpoint. Other EB uses include the crosslinking of wire and cable insulation and packaging films. EB is the technology of choice in microelectronics industry. [12]

The interactions of these radiations with matter are complex. The chemical effects of the radiation are qualitatively the same, although there are quantitative differences. Molecular excitation may occur with the subsequent formation of radicals in the same manner as in photolysis, but ionization of a compound C (monomer) by ejection of an electron is more probable because of the higher energies of these radiations compared to visible or ultraviolet light energy:

$$C + \text{radiation} \longrightarrow C^{+\bullet} + e^{-}$$

Ionizing radiations have particle or photon energies in the range 10 keV–100 MeV compared to 1–6 eV for visible–ultraviolet photons. For this reason, such radiations are termed ionizing radiations. The radical–cation $\mathbf{C}^{+\cdot}$ is formed by the loss of a π-electron, it can propagate at the radical and cationic centers depending on reaction conditions. It can also dissociate to form separate radical and cationic species as follows:

$$C^{+\bullet} \longrightarrow A\bullet + B^{+}$$

The initially ejected electron may be attracted to the cation $\mathbf{B}^{+}$ with the formation of another radical:

$$B^{+} + e^{-} \longrightarrow B\bullet$$

Radicals may also be produced by a sequence of reactions initiated by the capture of an ejected electron by C:

$$C + e^{-} \longrightarrow C^{-}$$

$$C^{-} \longrightarrow B\bullet + A^{-}$$

$$A^{-} \longrightarrow A\bullet + e^{-}$$

Where C^- may or may not be an excited species depending on the energy of the electrons. The radiation of olefinic monomers results in the formation of cations, anions, and free radicals as described above. It is then possible for these species to initiate chain polymerizations. Whether a polymerization is initiated by the radicals, cations, or anions depends on the monomer and reaction conditions. Most ionizing radiation polymerizations are radical polymerizations, especially at higher temperatures where ionic species are not stable and dissociate to yield radicals. [12-20]

1.2.3.3. Comparing EB to UV

Electron beam curing of coatings requires an inert atmosphere to prevent oxygen inhibition. Inertization is achieved by nitrogen. Another advantage of using an inert atmosphere is to prevent the formation of ozone, which is formed in the presence of air. EB process has the advantage of offering the possibility of curing much thicker coats and pigmented formulations at much higher speeds than UV radiation. There is no need to use photoinitiator systems, which are often expensive and sometimes discolor the finished film. EB-cured coatings frequently have better adhesion to substrate because of the penetration of the electrons. However, these advantages are offset by the much higher capital cost of the EB equipment. Another issue is to have enough production to sufficiently utilize the highly productive EB equipment. In some cases, a technological or economical advantage can be realized by combining UV and EB processes.

It is well known that electron beam processors generate two types of ionizing radiation: their primary product is high-energy electrons and a secondary product, x-rays resulting from their interaction with matter. The ionizing radiation is damaging because of its ability to penetrate into the human body. X-rays can cause cell damage that can lead to cancer formation or genetic mutations. Even at low dosage, x-ray exposure can also cause skin burning and general radiation syndrome. Manufacturers of EB equipment provide adequate shielding. The thickness of the shielding and the material used for it depends on the accelerating voltage. Typically, 1 in. (25 mm)-thick lead shielding is capable of stopping any x-rays generated by a 300 keV accelerator. Most lower-voltage EB processors are self-shielded, which means that the electron and x-ray sources are completely enclosed by shielding. Removable parts of the shielding must be equipped by safety interlocks so that the high voltage of the accelerator is turned off when the shielding is opened. EB units are provided with a radiation detector that automatically shuts down the power if an alarm setting is exceeded.

Ultraviolet energy is a non-ionizing form of electromagnetic radiation. The energy level is not high enough to penetrate into the human body and interact with the tissues to cause cell damage, as do other forms of radiation. However, a direct exposure to UV light can have effects on both skin and eyes.

The curing equipment should be properly shielded to prevent the escape of UV light into the workplace. Personnel working in the UV curing area should wear special protective eyewear. Another potential hazard is exposure to ozone, which is generated by most UV lamps, particularly at wavelengths below 200 nm. This colorless gas has a characteristic strong smell and can, therefore, be detected at concentrations below its acceptable workplace limit of 0.1 ppm. It will cause biological effects such as a headache, fatigue, dryness of upper respiratory tract and pulmonary irritation, and may also contribute to respiratory infections. The majority of UV lamps generate an appreciable amount of heat, therefore, there is a risk of getting burned when touching the lamps or certain parts of the equipment. This hazard can be minimized by proper equipment design and by adequate air or water cooling of reflectors, lamp housings, and shutters, and by placing aluminum plate heat sinks below the lamp and the substrate. Because most UV equipment operates at voltages well above the main level, it is important to prevent exposure to a high voltage by proper installation. [21]

2. Properties of PDLC's

2.1. Electro-optical Properties of PDLC's:

The best choice of monomers or prepolymers with known refractive indices and an LC with a positive dielectric constant is crucial to get a well prepared PDLC film which is sandwiched between two transparent ITO electrodes. During polymerization, no ordering is induced in the PDLC film, the droplets nor LC molecules orientation. The obtained droplets are almost spherical in shape, and randomly and uniformly distributed within the polymer matrix. The droplet size is comparable with the wavelength of visible light; the size is controlled by the rate of polymerization, the relative concentrations of materials, the types of liquid crystal and monomer or prepolymers used, and by such physical parameters as viscosity, rate of diffusion, and solubility of the liquid crystal in the growing polymer network. The refractive index of the isotropic polymeric matrix n_p matches with the ordinary one n_o of the LC. Because of the difference between the refractive index of the polymeric film and that of the LC inside droplets, light passing through a PDLC film in the OFF-state is highly scattered so that the film appears opalescent (milky). (Figure 2-3 left)

The application of a low-frequency electric field orthogonally to the film surface aligns the LC molecules (with positive dielectric anisotropy) to the direction of the field. As a result, the refractive index of the isotropic polymeric matrix n_p matches with the ordinary one n_o of the LC and the film becomes highly transparent at ON-state. (Figure III-1 right)

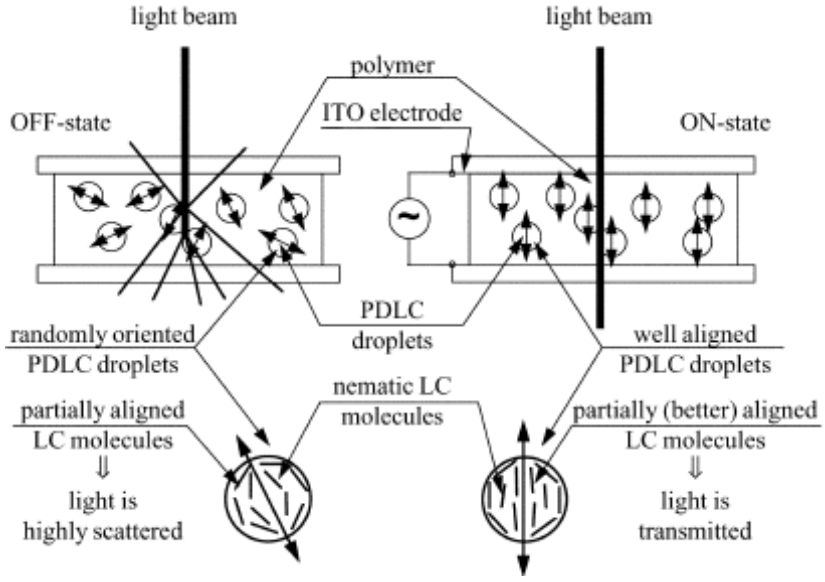

Figure 2-4: Schematic representation of a PDLC light shutter in the OFF-state (left) and when a low-frequency electric field is applied across it (ON-state, right). Double arrows are a schematic representation of the droplet director.

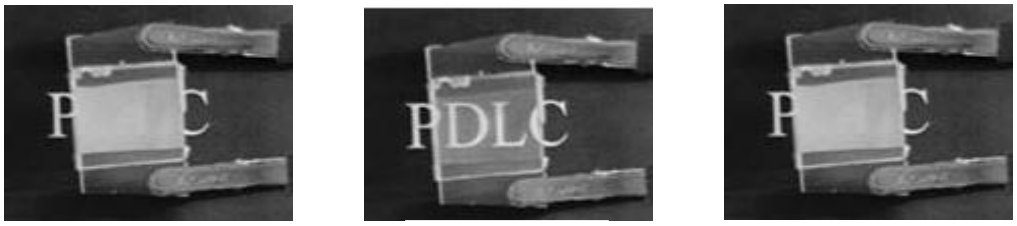

a) OFF-state b) ON-state c) Field is removed

Figure 2-5: a typical PDLC film: a) at the OFF-state, b) at the ON-state, c) when electric field is removed

When the electric field is removed the LC molecules recover their initial orientations and the PDLC film returns to its highly scattering behavior due to the elastic character of the LC (figure III-2).

The amount of scattered light is related to a large number of parameters concerning the light beam : wavelength, incidence angle, polarization state, the operating conditions : temperature, value and waveform of the applied electric or magnetic field, the component characteristics: polymer and LC refractive indices and dielectric constants and LC elastic constants, the PDLC configuration :droplet shape, size, uniformity and distribution. [6,22-30]

Some parameters, useful to characterize PDLC devices in terms of their electro-optical behavior, are defined as follows: [6]

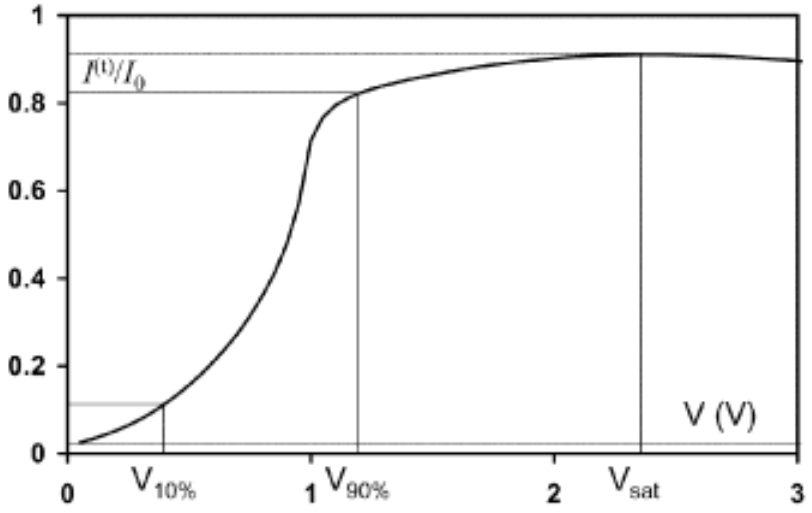

Figure 2-6: Typical behavior of the light intensity transmitted by a PDLC film.

The contrast ratio is generally defined as the ratio of T_{ON}/T_{OFF} between the maximum and minimum transmittance at normal incidence. To increase the ON-state transmittance, the polymer refractive index, n_p, must be matched to the droplet ordinary refractive index, n_o. To reduce the OFF-state transmittance the LC optical anisotropy, i.e. the difference between LC extraordinary and ordinary refractive indices $\Delta\mathbf{n=n_e-n_o}$, must be as large as possible. Note that PDLC light transmittance is angle dependent and, for off-axis incidence, it is polarization dependent. Moreover light scattering, and therefore contrast ratio is wavelength dependent. The contrast ratio is a very important parameter in all applications, but it must be used with care since often, in normal operation conditions, light does not impinge orthogonally to PDLC film surface.

Driving voltage is generally defined as the lowest voltage, V_{sat}, at which the transmitted light reaches its maximum value I_{max}. Sometimes the two values $V_{90\%}$(the voltage at 90% of the range T_{ON} - T_{OFF}) and $V_{10\%}$ (threshold voltage) are used instead of V_{sat} (figure 2-5). A low-frequency alternative current voltage (frequency order of magnitude 10^1–10^3 Hz) is usually used to avoid conductivity effects.

Response (rise and decay) times, rise time is usually defined as the time needed for transmitted intensity to reach 90% of the saturation value, when the driving voltage is applied. Similarly, decay time is defined as the time needed for transmitted intensity to fall to 10% of the saturation value when the driving voltage is removed. It has been reported that response time orders of magnitude are typically 1–10 ms for the rise and 10–100 ms for decay times. A low-frequency electric field is used to switch ON the PDLC film, while a high-frequency

electric field is used to rotate LC molecules away from aligned direction. It has also been found that a small amount of cholesteric dopant sensibly reduces the decay time.

Hysteresis is usually defined as the difference between the voltages required to reach half light transmission intensity ($I_{50\%}$) during switching ON ($V^{+}_{50\%}$) and switching OFF ($V^{-}_{50\%}$) $\Delta V_{50\%} = V^{+}_{50\%} - V^{-}_{50\%}$. It has been generally observed that alignment is better achieved by decreasing than for increasing values of the electric or magnetic fields. It has been suggested that hysteresis is due to the difference in response time of bulk and surface LC layer.

Haze is defined as the fraction of light scattered out of a cone of 58 of full aperture, with respect to the total transmitted light. This is an important parameter since in a PDLC film non-transmitted light is scattered and not absorbed. When observing an object through an ON-state PDLC film some scattered light seems to come from dark areas thus producing a hazy image. Moreover, it must be taken into account that an ON-state PDLC film has an anisotropic behavior. Since such an off-axis haze effect is polarization dependent, it can be reduced (at the cost of reducing the overall transmission ratio) by introducing a polarizing sheet.

Phase contamination may constitute a problem since it affects the refractive index of the droplets and of the surrounding medium and changes the clearing point: it has been shown that the clearing point of E7 (a eutectic mixture by Merck) is lowered by 3–7 °C with respect to the temperature of the nematic-to-isotropic (N–I) transition of pure LC. Moreover, the LC molecules trapped in the polymer do not contribute to the droplet formation altering the LC/polymer volume fraction while the monomer trapped in the droplets may polymerize during use, thus altering PDLC characteristics.

Droplet configuration and size, the droplet configuration affects light scattering of the LC droplet, the type of anchoring and consequently the electro-optical behavior of a PDLC film. The formation of uniform liquid crystal droplets in a polymer matrix may be achieved by homogeneous polymerization throughout the PDLC film thickness.

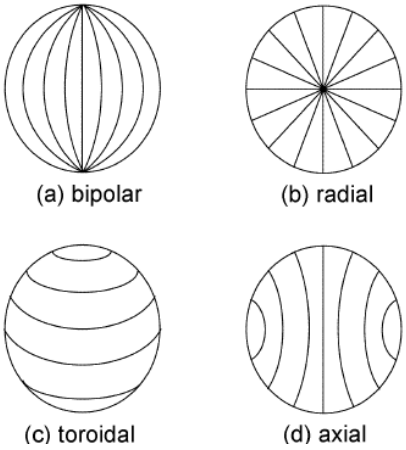

Figure 2.7: Common nematic director configurations: (a) bipolar, (b) radial, (c) toroidal, (d) axial.

Surface anchoring Surface interactions at the droplet wall return the LC molecules in the droplets to the original orientation upon the field removal to yield a scattering or opaque state. A competition between the applied field and the elastic and viscous torques of the liquid crystal governs the response times and switching voltages of such PDLC's. Two types of surface anchoring can be distinguished, homeotropic and planner anchoring (figure 2-8):

. Homeotropic anchoring, where the ax of LC molecules is perpendicular to the droplet surface. Radial and axial configurations permit the homeotropic anchoring.

. Planar anchoring, where the LC molecules are parallel to the interface of the droplet surface. Bipolar and troidial permit the planner anchoring. Planar orientation is produced by a mechanical rubbing of the surface of the glass with paper or cloth. Rubbing creates a micro-relief in the electrode coating or glass in the form of ridges and troughs, which promotes the orientation of the molecules along these formations. [31]

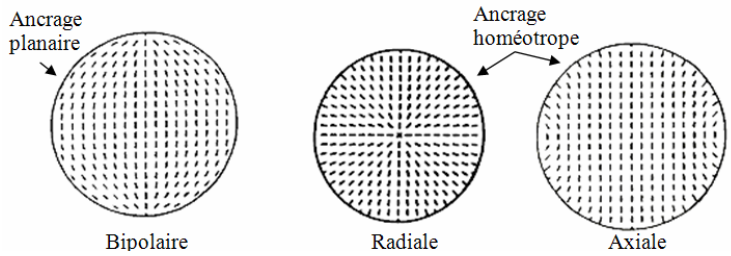

Figure 2-8: Types of anchoring inside droplets

3. Applications of PDLC's

PDLCs have a wide variety of applications due to their peculiar electro-optical and mechanical properties. Such properties allow their use in situations where other LC devices cannot be used. Summarizing some PDLC characteristics useful in one or more applications is important, before describing the application of smart windows in more detail in the following section:

. PDLC's do not require rigid boundaries (glass plates) so they can be easily produced in large, flexible films.

. The amount of LC's in a PDLC film is lower than in other LC-based devices, with economic advantages since an LC is an expensive material.

. Changes in the light transmission ratio are obtained by changing the light scattering cross-section within the PDLC film. The absence of polarizing sheets in PDLC devices has two related advantages: the whole light from the source is used by the device and only a moderate heating of the device occurs even under high light flux.

. PDLC films switch to a transparent state when heated to the N/I nematic/isotropic transition temperature since the isotropic LC refractive index value $n^{(I)}=n_e/3+2n_o/3$ is similar to the ordinary refractive index of nematic LC n_o, which is matched to the polymer refractive index n_p. Such 'thermal switching effect' is often undesired, but can be used in some applications. [6]

3.1. Smart Windows:

This is one of the first and the most popular PDLC application. This is realized by placing a PDLC film between two glass planes with conducting surface treatment. It is possible to switch the window between a transparent and an opalescent state by applying a low-frequency voltage across the conducting electrodes. Since LC droplets are anisotropic, the scattering effect is both polarization and angle-dependent.

Smart windows are obtained by using a 'positive LC', i.e. an LC having positive dielectric anisotropy ($\Delta\varepsilon=\varepsilon_{\parallel}-\varepsilon_{\perp}>0$), and are transparent only when a voltage is applied (i.e. in the ON-state). However, in several situations such as car windows which are required to be transparent in the OFF-state and opaque in the ON-state, several types of 'reverse mode' PDLC's have been developed:

. Negative anisotropy PDLC: by using a polymer that induces homeotropic anchoring and a negative LC. If the refractive index of the polymer matrix is close to that of the droplets

($n_p=n_o$), the OFF-state is transparent. Since the applied electric field aligns the negative LC molecules parallel to the PDLC film surface, the ON-state is opalescent.

. Dual-frequency addressable PDLCs: by using an LC whose dielectric anisotropy is positive at low frequencies and negative at high frequencies. Applying a low-frequency field during polymerization, the LC droplets are aligned to give a transparent film in the OFF-state. Application of a high-frequency electric field aligns LC molecules in a direction orthogonal to the applied field so that the film becomes opalescent in the ON-state.[6,32-33]

Conclusions:

In this theoretical background, one can find the basic definition of liquid crystals, their classifications, and types, the idea behind the eutectic mixtures of LC's and the effect of the chemical composition on the physical properties and the different aspects of the phase diagrams of mixtures of LC in the first chapter. In the second chapter, the different ways to get PDLC's, the factors affecting their electrooptical properties and their most important application in smart windows.

References:

[1] J. L. Fergason, Encapsulated liquid crystal, and methods, US Patent 4, 435, 047, **1984**.

[2] J. L. Fergason, Polymer encapsulated liquid crystals for display and light control applications, Tech. Digest. SID Int. Symp.; 85: 68-70, **1985**.

[3] J. W. Doane, N. A. Vaz, B. G. Wu and S. Zumer, Field controlled light scattering from nematic-nematic microdroplets, Appl. Phys. Lett.; 48: 269-271, **1986**.

[4] J. W. Doane, G. Chidichimo and N. A. Vaz, US Patent 4, 688, 900, **1987**.

[5] F Bloisi and L Vicari, Polymer-dispersed liquid crystals, ch. 4 in , Optical applications of liquid crystals, Edit. by L Vicari, Institute of Physics Publishing, Bristol, UK, 185-210, **2003**.

[6] C. Decker, Photoinitiated crosslinking polymerisation. Prog. Polym. Sci.; 21: 593–650, **1996**.

[7] C. Decker, and B. Elzaouk, Photopolymérisation de monomères multifonctionnels—VII. Evaluation des constantes de vitesse de propagation et de terminaison. Eur. Polym. J.; 31: 1155–1163, **1995**.

[8] T. Scherzer, and U. Decker, Kinetic investigations on UV-induced photopolymerization reactions by real-time FTIR-ATR spectroscopy: the efficiency of photoinitiators at 313 and 222 nm, Nuclear Instruments and Methods in Physics Research; B 15: 306-312, **1999**.

[9] E. Andrzejewska. Photopolymerization kinetics of multifunctional monomers. Prog Polym Sci.; 26: 605–665, **2001**.

[10] P. J. Flory, Principles of Polymer Chemistry, Ch. 4, Cornell Univ. Press, New York, **1953**.

[11] K. S. Anseth, C. M. Wang, and C. N. Bowman, Kinetic evidence of reaction-diffusion during the polymerization of multi(meth)acrylate monomers, Macromolecules; 27: 650–655, **1994**.

[12] G. Odian, Principles of polymerization, 4th Edit., John Wiley & Sons, New Jersey, **2004**.

[13] A. Chapiro, Radiation Chemistry of Polymer Systems, Chap. 4, Wiley-Interscience, New York, **1962**.

[14] J. E. Wilson., Radiation Chemistry of Monomers, Polymers, and Plastics, Chaps. 1–5, Marcel Dekker, New York, **1974**.

[15] B. Defoort, D. Defoort, and X. Coqueret, Electron-beam initiated polymerization of acrylate compositions, 2. Simulation of thermal effects in thin films, Macromol. Theory Simul.; 9: 725–734, **2000**.

[16] C. Patacz, B. Defoort, and X. Coqueret, Electron-beam initiated polymerization of acrylate compositions 1: FTIR monitoring of incremental irradiation, Rad. Phys. Chem.; 59: 329–337, **2000**.

[17] C. Patacz, X. Coqueret, and C. Decker. Electron-beam initiated polymerization of acrylate compositions 3: compared reactivity of hexanediol and tripropyleneglycol diacrylates under UV or EB initiation. Rad. Phys. Chem.; 62: 403–410. **2001**.

[18] U. Maschke, X. Coqueret, and C. Loucheux, Electron beam processing for polymerization induced phase separation: preparation of polymer dispersed liquid crystal films. Nucl. Instr. Meth. Phys. Res. Sec. B: Beam Interact with Mater Atoms; 105: 262–266, **1995**.

[19] W. Knolle, and R. Mehnert, Primary reactions in the electron-induced polymerization of acrylates, Nucl. Instr. Meth. Phys. Res. Sec. B: Beam Interact. Mater. Atoms; 105: 154–158, **1995**.

[20] A. Chapiro, Radiation effects in polymers, Encyclopedia of Materials: Science and Technology: 1-8, **2004**.

[21]J. G. Drobny, Radiation technology for polymers, CRC Press, New York, **2003**.

[22] U. Maschke, N. Gogibus, A. Traisnel, and X. Coqueret, Preliminary communication. Electron beam cured liquid crystal-polymer composite materials: electrooptical enhancement effect, Liq. Cryst., vol. 23, pp. 457–461, **1997**.

[23] U. Maschke, A. Traisnel, J. D. Turgis, and X. Coqueret, Influence of liquid crystal concentration on the electro-optical behavior of polymer dispersed liquid crystal films

prepared by electron beam processing, Mol. Cryst. Liq. Cryst. Sci. Tech. Sec. A Mol. Cryst. Liq. Cryst., vol. 299 pp. 371- 378, **1997**.

[24] F. Z. Abdoune, L. Benkhaled, L. Méchernène, and U. Maschke, Investigation of the electro-optical behavior of UV cured polymer/liquid crystal systems. Phys. Procedia; 2: 643–648, **2009**.

[25] M. Kashima, H. Cao, Q. Meng, H. Liu, D. Wang, F. Li, and H. Yang, The influence of crosslinking agents on the morphology and electro-optical performances of PDLC films, J. Appl. Polym. Sci.; 117: 3434–40, **2010**.

[26] Z. Yang, D. Li, C. Pan, and Y. Wang, Effects of hyperbranched prepolymers prepared from butyl acrylate and butyl methacrylate on the electro-optical properties of polymer dispersed liquid crystal, Polym. Adv. Technol.; 23: 1321–27, **2012**.

[27] J. He, B. Yan, B. Yu, S. Wang, Y. Zeng, and Y. Wang, The effect of molecular weight of polymer matrix on properties of polymer-dispersed liquid crystals, Eur. Polym. J.; 43: 2745–49, **2007**.

[28] J. H. Ryu, S. G. Lee, J. B. Nam, and K. D. Suh, Influence of SMA content on the electro-optical properties of polymer-dispersed liquid crystal prepared by monodisperse poly(MMA-co-SMA)/LC microcapsules, Eur. Polym. J.; 43: 2127-34, **2007**.

[29] M. M. Dzhons, S. A. Bulgakova, I. A. Pantyukhina, and I. A. Kazantzeva. Effects of chemical structure and composition of the polymer matrix on the morphology and electro-optical performance of polymer-dispersed liquid crystal films. Liq. Cryst.; 38: 1263–68, **2011**.

[30] P. Malik, and K. K. Raina, Droplet orientation and optical properties of polymer dispersed liquid crystal composite films, Opt. Mat.; 27: 613–17, **2004**.

[31] G. Barbero, and L. R. Evangelista, Adsorption phenomena and anchoring energy in nematic liquid crystals, Taylor & Francis Group CRC press, Boca Raton, USA, **2006**.

[32] G. P. Crawford and S. J. Woltman, Liquid crystals: A unique phase of matter, Ch. 1 in, liquid crystals frontiers in biomedical applications, edit. by S. J. Woltman, G. P. Crawford and G. D. Jay, World Scientific, Singapore, **2007**.

[33] P. S. Drzaik, Liquid crystal dispersion, Series on liquid crystals, World scientific, Singapore, **1995**.

Experimental Work

Chapter.3: Experimental work

1. Raw Materials

Tripropyleneglycoldiacrylate (TPGDA) with a molecular weight Mn = 300 g/mol (n=3, corresponding to three propyleneglycol repeating units) and poly(propyleneglycoldiacrylate) PPGDA800 with Mn = 800 g/mol (n=12) were purchased from Sigma-Aldrich.

The liquid crystal used E7 is an eutectic mixture (Merck, Japan) containing four cyanoparabiphenylene derivatives, namely 51 wt % 4-cyano-4'-pentyl-biphenyl (5CB), 25 wt % 4-cyano-4'-heptyl-biphenyl (7CB), 16 wt % 4-cyano-4'-octyloxy-biphenyl (8OCB) and 8 wt % 4-cyano-4'-pentyl-p-terphenyl (5CT). It exhibits a nematic-isotropic transition temperature at T_{NI}=61°C and a positive dielectric anisotropy $\Delta\varepsilon$=13.8 ($\varepsilon_{\parallel}$=19.0) at a frequency of 1 kHz, where $\varepsilon_{\parallel}$ represents the parallel dielectric constant. The refractive indices of E7 at T=20°C are given as n_o=1.5183; n_e=1.7378 (λ=632.8 nm), leading to a birefringence of $\Delta n=n_e-n_o$=0.2195, Franck elastic constants associated to splay, twist and bend were taken from literature as $K_{11}=K_{22}=K_{33}=13x10^{-12}$ N.[1–3]. The chemical structures of the E7 components are shown in Figure 3-1(b).

Darocur 1173 (2-hydroxy-2-methyl-1-phenyl-propane-1-one) from Ciba (Italy) was used as a photoinitiator. All chemicals were used as received without any purification. For UV curing, 2 wt % (compared to the diacrylate) of Darocur 1173, the LC E7, and the monomer were weighed and let for mixing overnight before use. For EB curing, no photoinitiator was needed. Samples for all kinds of studies were prepared by sandwiching the initial reactive mixture between two glass substrates, allowing a uniform penetration of the applied dose in the depth of the sample. The indium tin oxide (ITO)-coated poly(ethylene terephthalate) (PET) foils of thicknesses 50 and 100 μm were donated by Renker (Germany), and 13μm-thick PET foils were purchased from the Good fellow. ITO coated glasses used for electro-optical measurements were purchased from AWAT/Poland. The film thickness was measured by a micrometer caliper (Mitutoyo; certainty: ±1μm). No temperature control during the irradiation processes was performed.

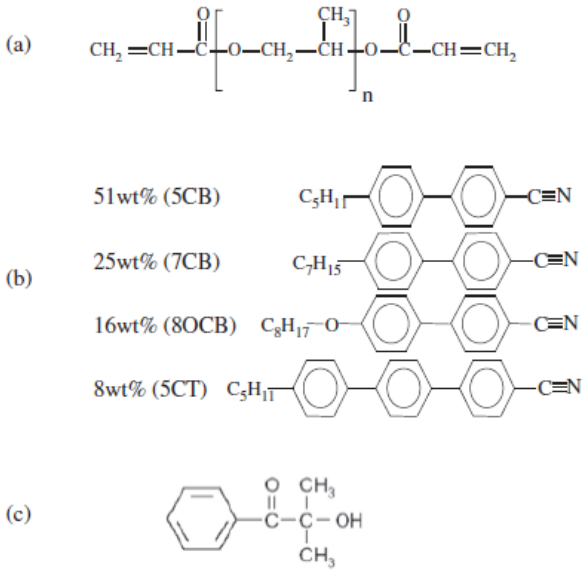

Figure 3-1: Chemical structures of (a) polypropyleneglycoldiacrylate (PPGDA) monomers, (b) nematic LC E7 mixture and (c) photoinitiator: 2-hydroxy-2-methyl-1-phenyl-propane-1-one (Darocur 1173).

2. Sample Preparation

2.1. Elaboration Techniques

2.1.1. UV Lamps

Two parallel UV curing lamps, type TL08 (Philips) with an output power of 18 W each, were employed as a static low-power UV light source fixed inside a wooden box and separated from each other by around 10 cm as clearly indicated in figure 3-2. They have a maximum output at a wavelength of λ=365 nm, and a dose rate of 0.5 mJ/cm^2.s (figure 3-2).

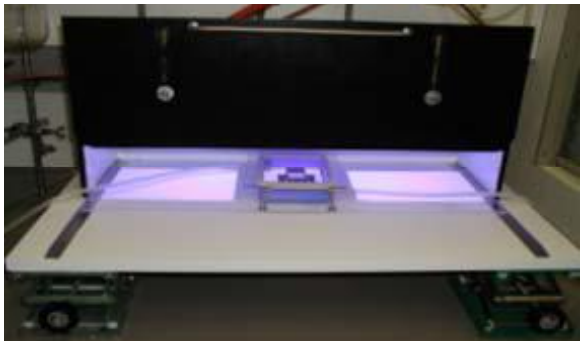

Figure 3-2: The UV light source TL08 used

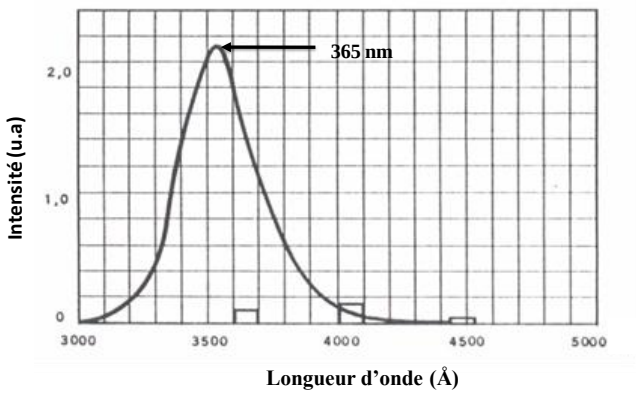

Figure 3-3: the lamp Philips TL08 spectrum

The exposure times ranged from a few seconds up to several minutes depending on monomer reactivity. This UV equipment was chosen deliberately to lead to relatively slow photopolymerization and phase separation reactions. Exposure to UV irradiation was conducted at room temperature. The dose received by the sample was recorded by a dosimeter (UV integrator)

Figure 3-4: Photo of the dosimeter used

Moreover, a second light source was applied, a Dr. Hönle system (Dr. Hönle AG, UV-Technologie, Germany), equipped with a UVH medium-pressure mercury arc lamp (UVH lamps are mercury vapour medium pressure lamps of high specific power and an optimized UVC yield) rated at minimum 240 W/cm similar to the Electron Beams process. The Dr. Hönle UV lamp provides fast curing processes with an output power of around 10 kW that can be regulated from 20% to 100%. The irradiation process parameters resemble to be close to that from EB processing in terms of the exposure time to irradiation using a conveyor belt. In this study, the power was set at 70% to obtain a dose rate of 100 mJ/cm^2.s and allows better control of the photopolymerization and phase separation kinetics. The maximum residence time under the UV source did not exceed 3 s. This equipment was deliberately used to have

very fast processes of both the photopolymerization and phase separation (figure 3-5). The dose received by the sample was recorded by the same dosimeter presented in figure 3-4.

Figure 3-5: Photo of the Dr. Hönle UV lamp (UVH medium-pressure mercury arc lamp)

2.1.2. EB Machine

The generator used in these experiments was an Electrocurtain Model CB 150 (Energy Sciences Inc.) with an operating high voltage up to 175 kV used for electron acceleration to reach a penetration depth of 100 µm (figure 3-6). The samples were covered by 50-µm-thick PET films and placed on a tray, which passed under the electrocurtain by means of a conveyor belt. This thickness of PET films was chosen deliberately to have a homogeneous polymerization throughout the film thickness; the maximum electron beam penetration was around 100 µm at the voltage of 175 kV. The received dose can be controlled by adjusting the intensity of the beam current (from 0.2-8 mA) which determines the number of released electrons (1 mA= 6.25×10^{15} electrons per second) and the speed of the conveyor belt (2.04–31.25 cm/s). The maximum exposure time during one pass was around 2.45 s.

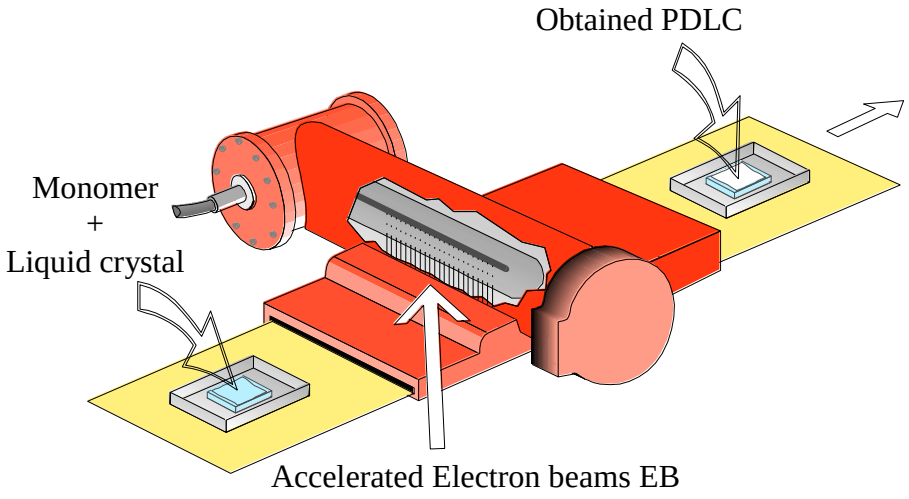

Figure 3-6: Scheme of Electron Beam EB process

3. Characterization Methods:

3.1. Optical Methods:

3.1.1. Polarized Optical Microscope

The polarizing optical microscope (POM) used was an Olympus BX-41 model, equipped with a heating/cooling stage Linkam LTS 350, a Linkam TMS 94 temperature control unit and a digital camera that can record images with high resolution, conjugated with a computer (figure 3-7). A small drop of the monomer/E7 mixture was placed on a glass plate inside an oven set at a temperature of around 50°C so that the mixture became isotropic. Then the sample was placed under the POM on the heating/cooling stage, which was set at 60°C. Next an upper glass plate was put on the drop and heated for about 5 min, before cooling the sample down at a rate of 0.5° C/min with the help of liquid nitrogen, in order to detect the transition from the isotropic to the (nematic + isotropic) state.

For the morphologies of the obtained polymer/LC blends, the samples prepared for the electro-optical measurements were analyzed by POM at room temperature. For the case of the nematic-isotropic transition of neat E7, it was detected easily without the help of the rapid cooling using liquid nitrogen.

Figure 3-7: The Olympus BX-41 model; polarizing optical microscope POM.

3.1.2.. Scanning Electron Microscope

The scanning electron microscope SEM forms an image by scanning a probe and , a focused electron beam, across the specimen. The probe interacts with a thin surface layer of the specimen, a few micrometers thick at most. SEM (HITACHI S4700 Field emission gun) (figure 3-8) was used in this morphological study. The PDLC samples were prepared by

sandwiching the reactive mixture (monomer, LC, and photoinitiator) between two pieces of glass and irradiated for 05min under UV-TL08 and then the pieces of glass were separated in such a way that the PDLC film stuck to only one glass. The stuck PDLC film was immersed in n-hexane for about 5 min in order to extract the LC E7 then dried in vacuum oven for about three days. After drying, the sample was coated with a thin layer of carbon. This sample preparation technique leads to the appearance of dark holes that were once filled with LC. An acceleration voltage of 10kV was used in this experiment.

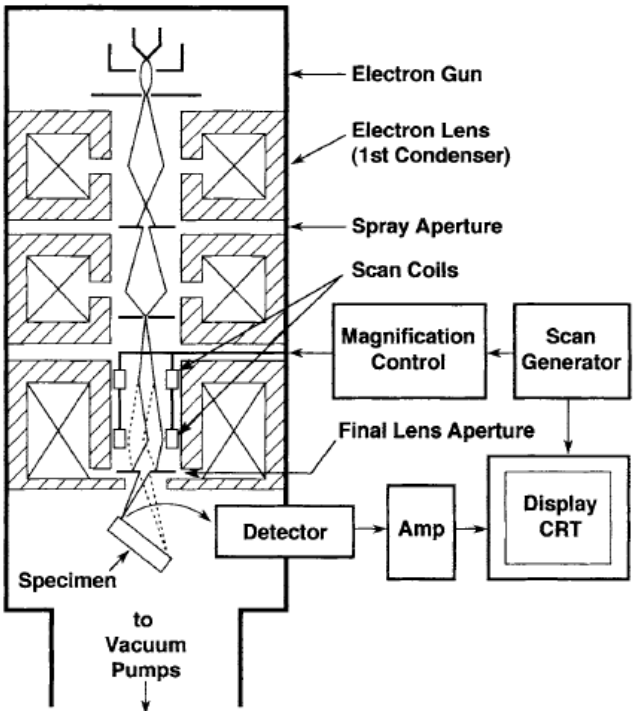

Figure 3-8: Schematic diagram of a scanning electron microscope.

Two pairs of scan coils are shown in the SEM column. This double deflection allows the scanning beam to pass through the final aperture. Four pairs are actually used, for double deflection in both X and Y directions. [4]

3.2. Spectroscopic Methods

3.2.1. Fourier Transform Infrared Spectroscopy

The Fourier Transform Infrared spectroscopy (FTIR) is a powerful method used for both qualitative and quantitative analysis of the functional groups in chemical substances. In this study, the FTIR spectra of thin films (less than 10 μm) were recorded in the transmission and absorbance modes using a Perkin Elmer 2000 model with a spectral resolution of 4 cm^{-1} over 16 scans. A small drop of the reactive mixture on a NaCl plate was covered by PET films with

thicknesses of 100 µm and 50 µm for UV and EB curing respectively as shown in figure 3-9. Small cumulated doses were applied for all methods of elaboration. The interval of time between the end of exposure and the infrared analysis was kept constant at around one minute. The experiments were repeated three times to check the reproducibility of the results. The conversion was calculated from the difference between the peak heights, at 810 cm^{-1} for the neat monomers and at around 1637 cm^{-1} for the mixtures monomer/Liquid crystal E7, from summit to the baseline at 0 sec and Dose D at time t by the following formula: (figure 3-10)

$$\text{Conversion (\%)} = 100 \times \frac{(A_{810})_{(D=0)} - (A_{810})_{(D)}}{(A_{810})_{(D=0)}} \qquad (1)$$

For the case of raw materials, the FTIR spectra were obtained just by sandwiching and squeezing the samples between two NaCl plates.

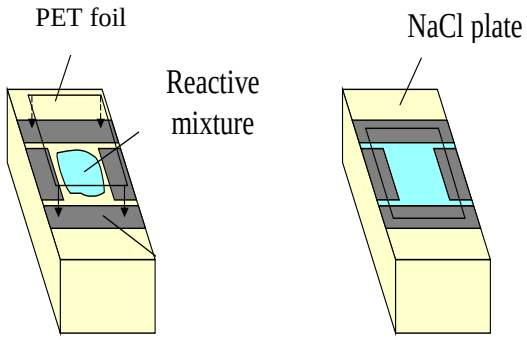

Figure 3-9: Sample preparation for the polymerization

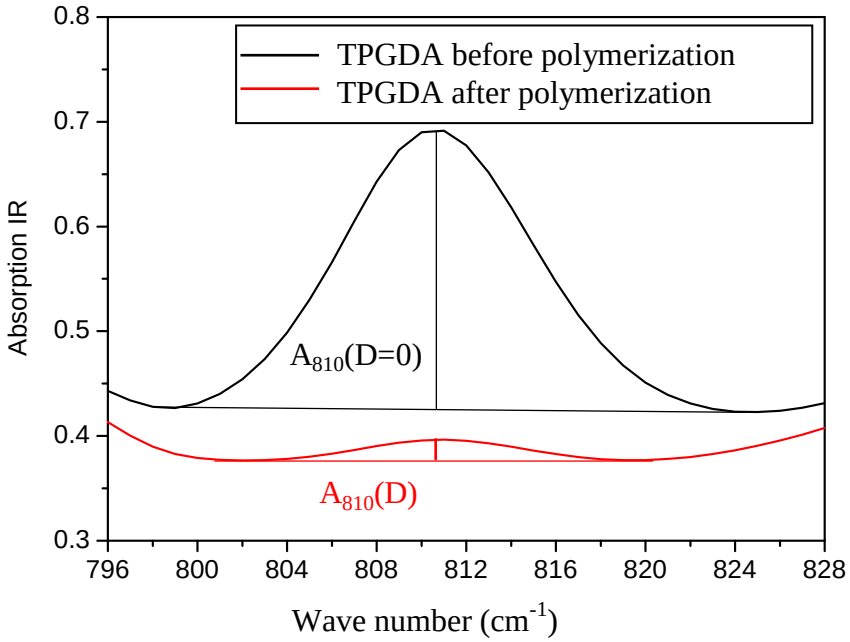

Figure 3-10: Double bond absorbance before and after polymerization

3.2.2.. Nuclear Magnetic Resonance Spectroscopy:

Nuclear Magnetic Resonance (NMR) spectroscopy is a very powerful technique used to determine the chemical composition of substances, the stereochemistry of polymers and the crosslink density of polymer networks. [5]

The proton ^{1}HNMR experiment was carried out by using a Brucker AC300 apparatus (figure 3-11 (a)) at room temperature. About 8 mg of the sample was weighed and dissolved in 01 ml of deuterated chloroform $CDCl_3$, the resulting solution was poured into an NMR tube (figure 3-11 (b)) which was placed in the apparatus and tested at a frequency of about 300 MHz.

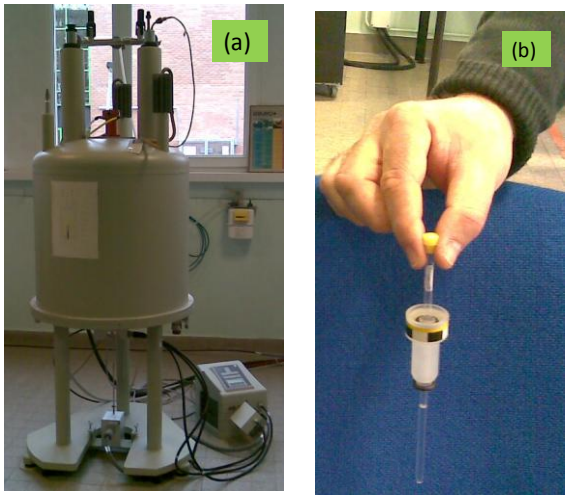

Figure 3-11: (a): NMR Bruker AC300, (b): NMR tube

3.3. Thermal Methods

3.3.1. Thermo Gravimetric Analysis

Thermogravimetric analysis (TGA) was used to investigate the thermal stability of both monomers and the obtained PDLC's. TGA measures the weight loss during heating at a controlled rate and atmosphere. The weight loss in monomers and polymers is due to the presence of moisture or some volatile impurities and the thermal decomposition (degradation) or oxidation in the presence of oxygen as the atmospheric medium.[6] TGA made by Perkin Elmer company was employed in this study were about 8 mg of the sample was weighed and put in a suspended way by the help of a crochet which was attached to a high precision balance. The heating rate was fixed at 20°C/min from room temperature to around 600°C.

3.3.2. Differential Scanning Calorimetry:

Differential Scanning Calorimetry (DSC) is a technique which is part of a group of techniques called Thermal Analysis (TA). Thermal Analysis is based upon the detection of changes in the

heat content (enthalpy) or the specific heat of a sample with temperature. As thermal energy is supplied to the sample its enthalpy increases and its temperature rises by an amount determined, for a given energy input, by the specific heat of the sample. The specific heat of a material changes slowly with temperature in a particular physical state but alters discontinuously at a change of state. As well as increasing the sample temperature, the supply of thermal energy may induce physical or chemical processes in the sample, e.g. melting or decomposition, accompanied by a change in enthalpy, the latent heat of fusion, the heat of reaction etc. Such enthalpy changes may be detected by thermal analysis and related to the processes occurring in the sample.

DSC is among the most widely used thermal analysis techniques. In this technique, the energy difference (heat enthalpy) between the sample and the reference is measured. The sample is very small (3-20mg) and is placed in a small aluminum vessel (pan). An empty pan is always used as a reference. When the sample is heated up at a constant rate, any kind of change in its calorimetric properties will cause a temperature difference between the sample and the reference. In the DSC apparatus, the measured temperature difference is controlling the electrical power to the sample and the reference in order to keep them at the same temperature. In this technique, the difference in the power supply to the sample and reference is recorded. This means that a peak area from the output recording directly corresponds to the heat consumed or produced by the sample. The typical application for DSC is a determination of important transition temperatures like Tg and Tm, the heat of fusion of a crystalline phase and the degree of crystallization, heat capacity, rate of cross-linking reactions, miscibility in polymer blends, structural relaxation like enthalpy relaxation during physical aging. [7]

The DSC is widely used to characterize the thermophysical properties of polymers, liquid crystals and PDLC's, where the difference in the amount of heat required to keep the sample and reference at the same temperature was measured during both heating and cooling cycles at a controlled rate usually fixed at 10°C/min. DSC gives an information about both primary and secondary phase transitions of polymers and the phase transitions of liquid crystals.

The DSC measurements were performed on a Perkin-Elmer DSC apparatus. About 8 mg of a sample was weighed inside an aluminium pan and then covered to avoid any leakage during the thermal treatment. After that, the pan was put inside the oven chamber which was also covered. Finally, after the heat treatment for about three cycles; each cycle comprises a heating and cooling ramp from -72°C to 100°C at a rate of 10°C/min. the glass transition temperature of the polymer matrix and that of LC E7 was calculated from the midpoint of

the endothermic shouldering in the base line of the DSC thermogram. The nematic to the isotropic transition temperature of E7 was determined from the peak summit.

3.4. Electro-optical Measurements

The electro-optical properties were determined at room temperature using the set-up described in Figure 3-12 below. In this set-up, a linearly collimated beam from unpolarized He–Ne laser light (λ = 632.8 nm) that passes perpendicularly through the sample, and the transmitted intensity was measured by a silicon photodiode. The electro-optical measurements were performed on PDLC samples sandwiched between two ITO-coated glasses or an ITO glass and a 50-µm-thick PET film for UV- and EB-cured specimen, respectively. The samples were polymerized under the optimum conditions found after studying the polymerisation kinetics. The applied alternating sinusoidal voltage at a frequency of 1 kHz was increased linearly up to a desired maximum value Vmax, and then subsequently decreased in the same way to 0 V. The entire up and down cycles lasted 120 s with an additional 60 s to allow the sample to relax as illustrated in Figure 3-12. The same procedure was repeated in the same manner for all values of the voltage applied, which ranged from 20 to more than 300 V using increments of 20 V. Transmittance measurements of PDLC films were made by comparing the transmittance of the cell containing the PDLC film with that filled with glycerol. The values obtained from the latter cell were used to define the maximum transmittance and were set at 100% transmittance.[8]

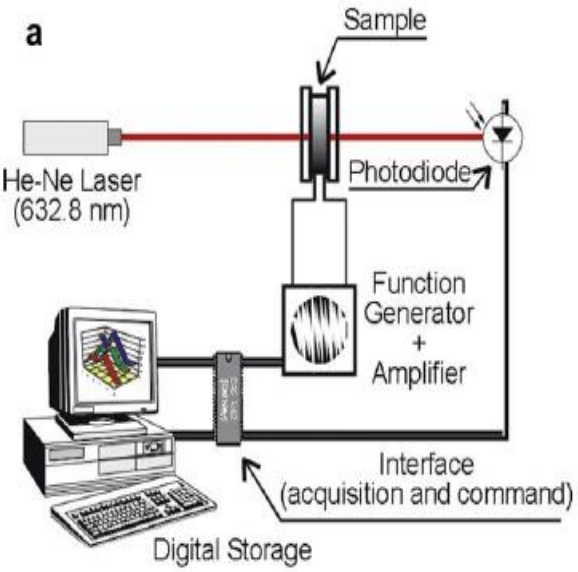

Figure 3-12: An electro-optical bench

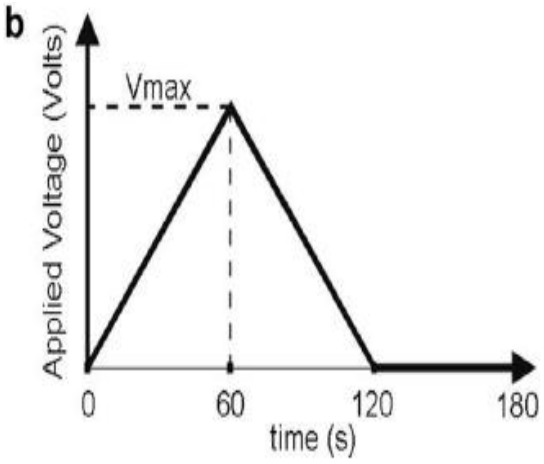

Figure 3-13: The applied voltage.

References:

[1] Merck Product Information. Merck liquid crystals. Licrilite Brochure. Poole: Merck House, **1994**.

[2] J. Li, C. H. Wen, S. Gauza, R. Lu, S. T. Wu, Refractive indices of liquid crystals for display applications. J. Display Technol.; 1: 51–61, **2005**.

[3] H. A. Tarry. The refractive indices of cyanobiphenyl liquid crystals. Poole, Great Britain: Merck Ltd, **1967**.

[4] J. L. Koenig, Spectroscopy of polymers, Elseiver Science Inc , New York, **1999**.

[5] L. C. Sawyer, D. T. Grubb, G. F. Meyers, Polymer Microscopy, 3rd Edit., Springer, New York, **2008**.

[8] L. Méchernène, L. Benkhaled, D. Benaissa, U. Maschke, Studies of optical transmission properties of electron beam cured polymer/liquid crystal systems, Opt. Mat.; 31: 632–639, **2009**.

Results and Discussion

Chapter 4. Results and Discussion

1. Raw Materials Characterization

1.1. Spectroscopic Methods

1.1.1. FTIR Analysis:

Figures 4-1, 4-2, and 4-3 present the FTIR spectra of TPGDA, TPGDA/PPGDA800, and E7 respectively . It can be noticed that both TPGDA and PPGDA800 have almost the same FTIR spectra, they have a symmetric C=C stretching at 1637cm^{-1} and =CH_2 twisting at 810cm^{-1} in which their intensity reductions can be used the calculate the conversion during the polymerization reaction.

The band designations of TPGDA and PPGDA800 and that of E7 are presented in Tables 4-1, 4-2 respectively.

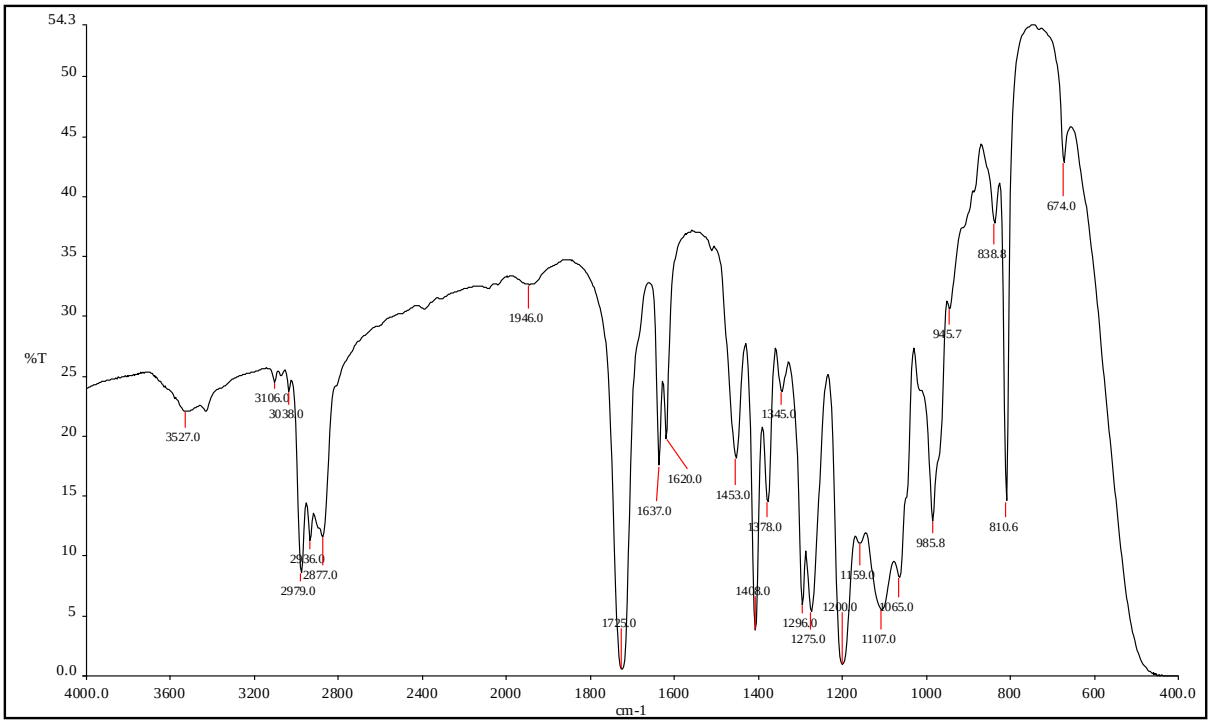

Figure 4-1: FTIR spectrum of TPGDA

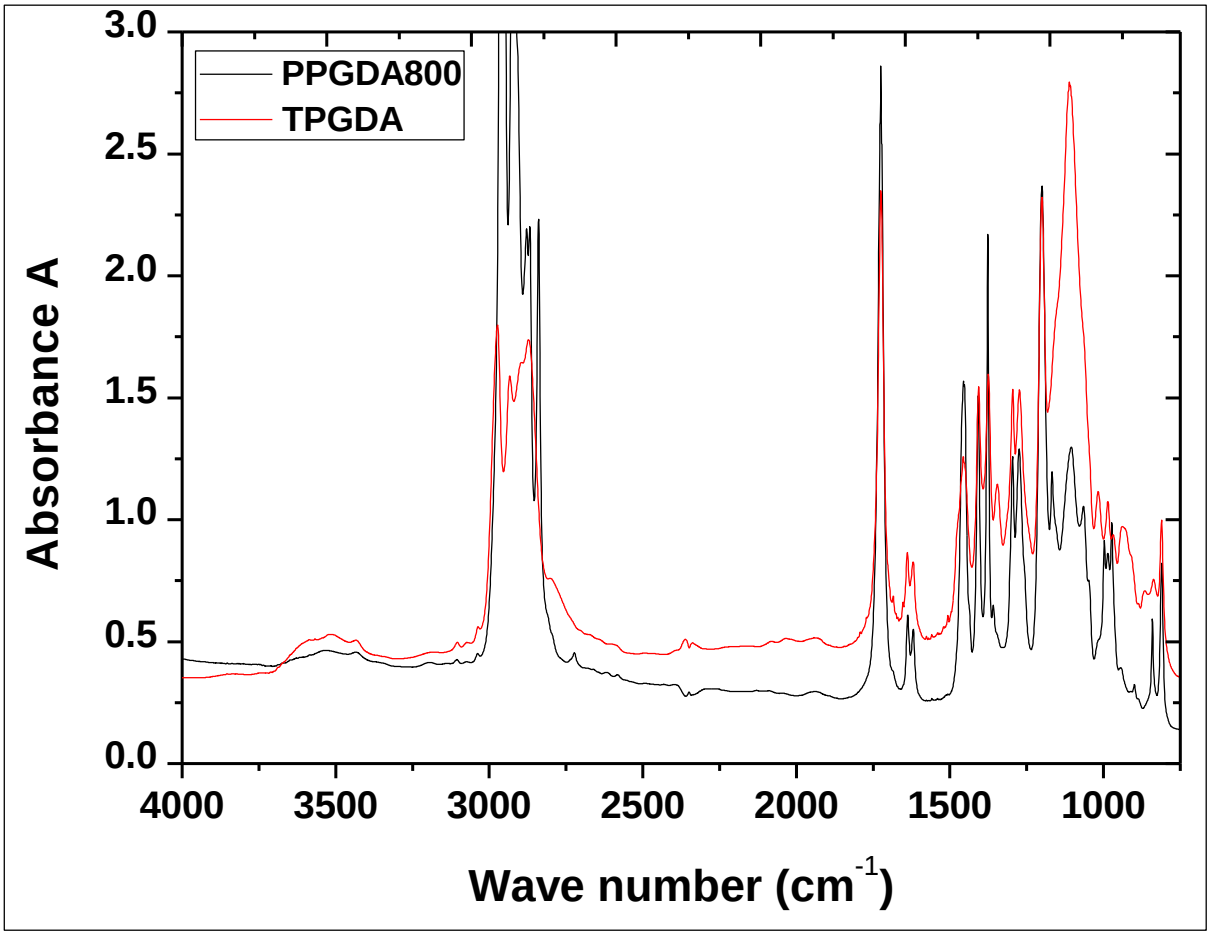

Figure 4-2: FTIR spectra of TPGDA and PPGDA800

Table 4-1: IR band designations for TPGDA and PPGDA800

ν (cm^{-1})	Band designation	ν (cm^{-1})	Band designation
2979	ν_{as} CH_3 asymmetric stretching	1378	δ CH_3 bending
2936	ν_{as} CH_2 asymmetric stretching	1296	=CH rocking
2877	ν_{s} CH_2 symmetric stretching	1275	=CH rocking
1725	ν_{s} C=O symmetric stretching	1159	ν C-O stretching
1637, 1620	ν_{s} C=C stretching	1056	$=CH_2$ rocking
1453	δ CH_2 bending	985	Trans-CH, $=CH_2$ wagging
1408	δ $=CH_2$ bending	810	$=CH_2$ twisting

The FTIR spectrum of E7 presented in figure 4-3 clearly shows that the vibration of the phenyl groups at 823cm^{-1} which would hide the $=CH_2$ twisting of the neat monomers at 810cm^{-1} ,and also the presence of an intensive absorption of C≡N at 2226cm^{-1}.

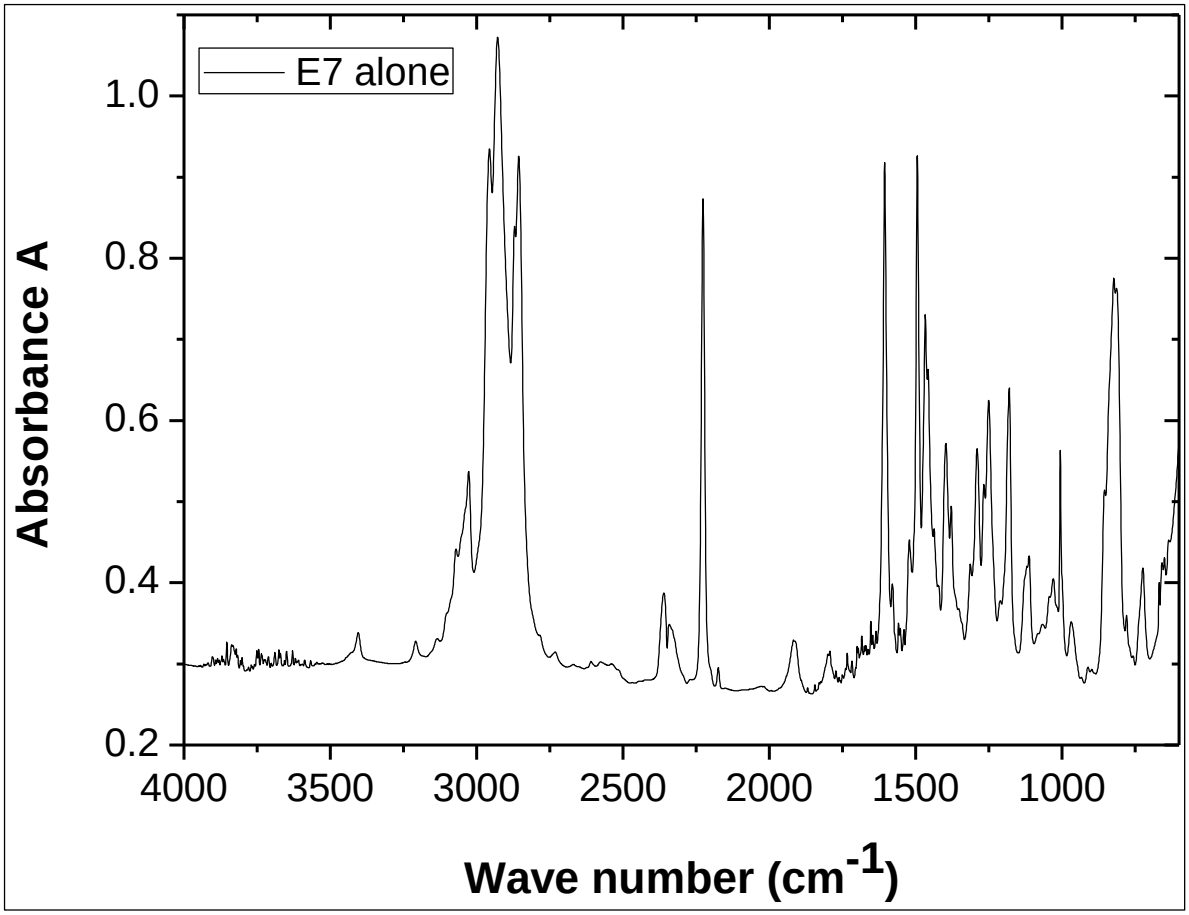

Figure 4-3: FTIR spectrum of LC E7

Table 4-2: IR band designations for E7

ν (cm^{-1})	Band designation	ν (cm^{-1})	Band designation
2856-3027	ν aromatic C-H stretching	1289	ν biphenyl C-C stretching
2226	ν C≡N stretching	1250	δ_s CH_3 symmetric deformation
1606, 1494	ν C=C stretching	1180, 1006	δ aromatic C-H in plane deform.
1466	δ_s CH_2 symmetric deform.	968	ρ dangling of terminal CH_3
1397	δ lateral C-H deformation	823	phenyl groups vibration

1.1.2. NMR Spectroscopy

The ^{1}H NMR spectra for PPGDA800 and TPGDA which are presented in Figures 4-5 and 4-6 confirm the chemical structures (shown in Figure 4-4) given by the suppliers. In Figure 4-4, Nevertheless , it was found that the TPGDA contains some impurities which contain hydrogen atoms between 4.05 and 4.15 ppm). This might be related to the presence of mono, dipropyleneglycol diacrylate, acrylic acid and tripropyleneglycol.

In the PPGDA800 spectrum, the six acrylic protons (a, b) appear between 5.5 and 6.5 ppm. The extreme proton "d_1" is located between 1 and 1.5 ppm, the two extreme protons "c_1" between 5 and 5.5 ppm and the other protons between 3 and 4 ppm. The 36 methyl protons "e" are observed between 1 and 1.5. After calculating all the protons by integrating the surfaces under the peaks, it was found that PPGDA800 and TPGDA have 12 and 3 propylene glycol repeat units between the two acrylic double bonds respectively. The results are reported the in Table 4-3:

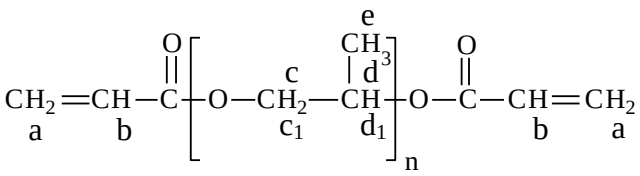

Figure 4-4: The chemical structures of TPGDA (n=3) and PPGDA800 (n=12)

Table 4-3: ^{1}H NMR results of PPGDA800

Chemical shift (ppm)	Position (i)	Type of hydrogen
5.5-6.5	a, b	Ha, Hb
3-4	c, d	Hc, Hd
5-5.5	Extreme c_1	Hc_1 extreme
1.5-2	Extreme d_1	Hd_1 extreme
1-1.5	e	He

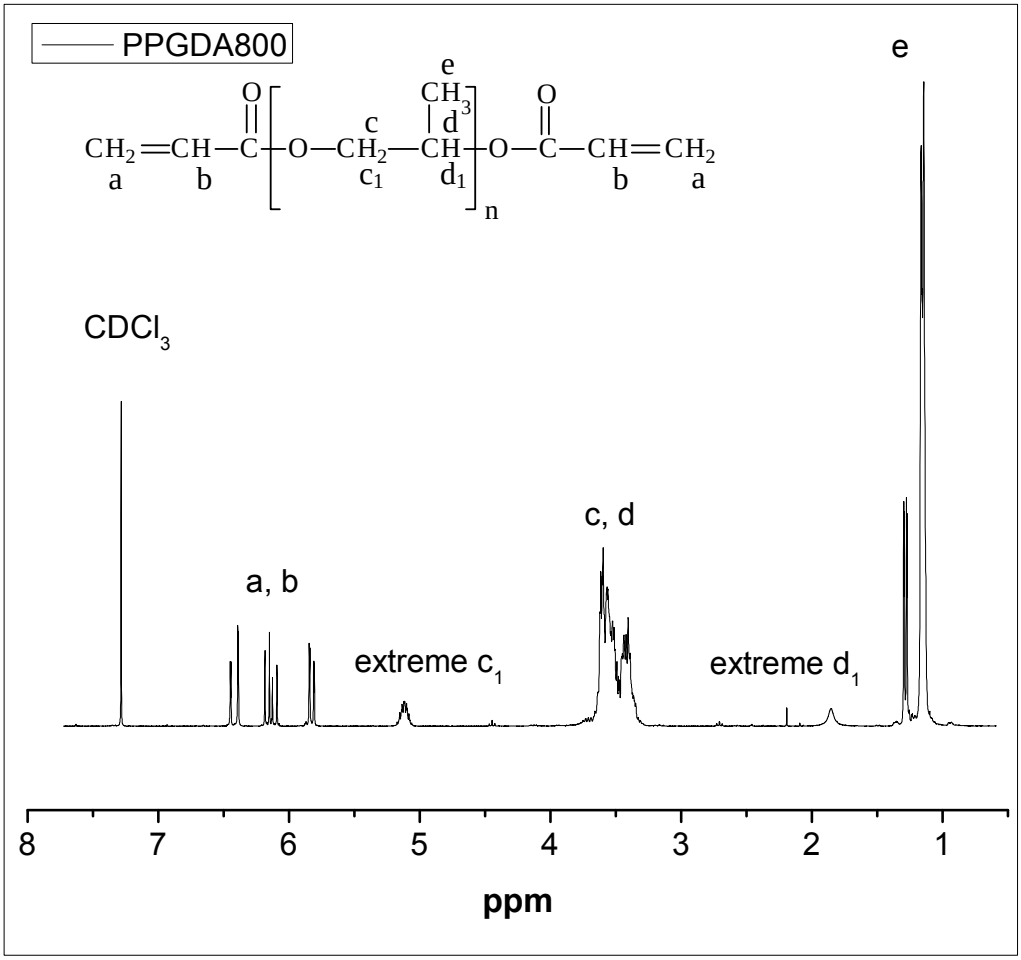

Figure 4-5: ^{1}H NMR spectrum of PPGDA800 (n=12).

Table 4-4: ^{1}H NMR results of TPGDA

Chemical shift (ppm)	Position (i)	Type of hydrogen
5.5-6.5	a, b	Ha, Hb
3-4	c, d	Hc, Hd
4.05-4.15		Impurities
5-5.5	Extreme c_1	Hc_1 extreme
1.5-2	Extreme d_1	Hd_1 extreme
1-1.5	e	He

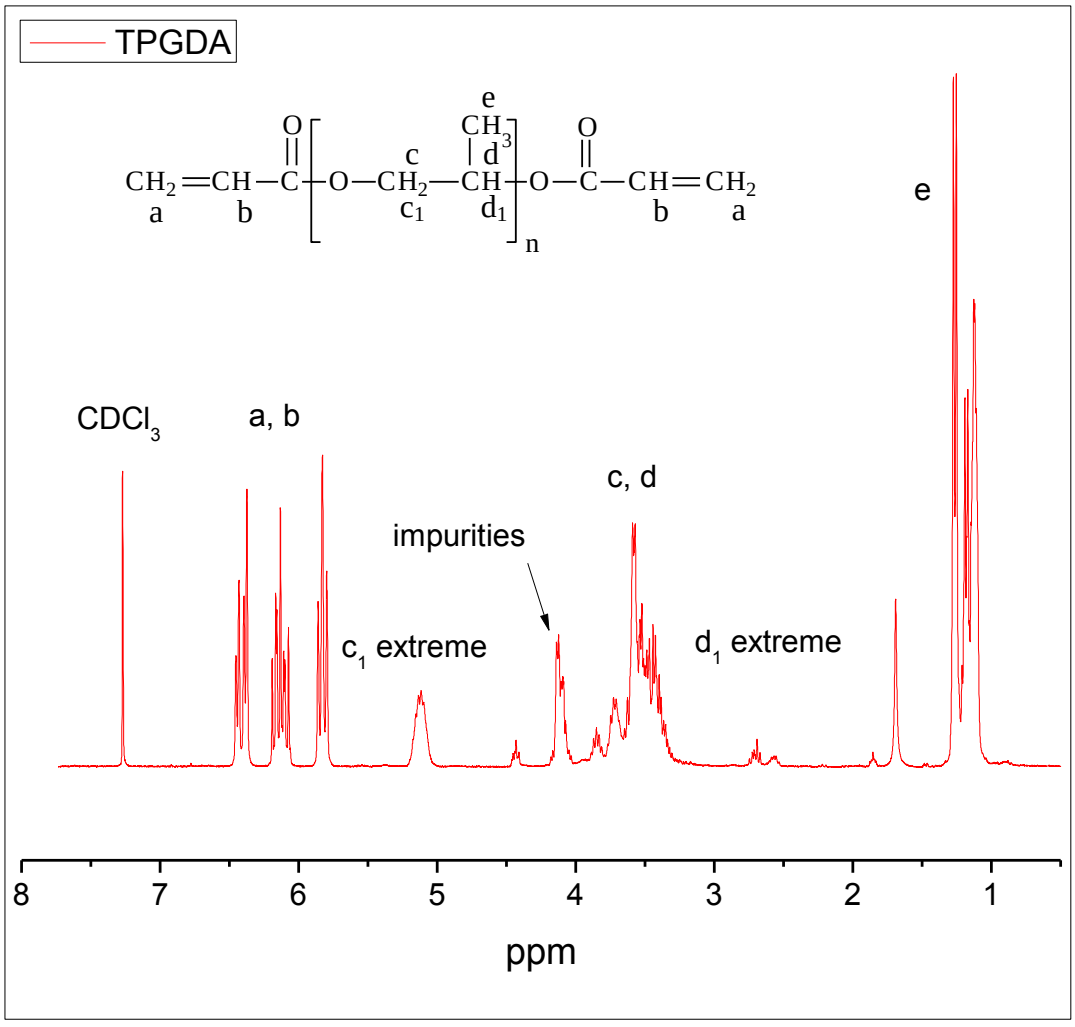

Figure 4-6: ^{1}H NMR spectrum of TPGDA (n=3).

1.2. Thermal Methods

1.2.1. Thermogravimetric Analysis TGA

Figure 4-7 illustrates the thermogravimetric analysis (TGA) thermograms of TPGDA (triangular symbols) and PPGDA800 (square symbols) under a nitrogen atmosphere. The TPGDA was decomposed more rapidly than PPGDA800. The TPGDA was decomposed in two steps. In the first step, it remained stable up to 140°C then decomposed to reach around 70% of its original weight at 200°C. At this temperature, it stayed stable at this level until 350°C. In the second step, it was completely decomposed at around 475°C. The first step of decomposition might be related to the presence of organic impurities and this was attributed to mono and dipropylene glycol diacrylates in conjunction with TPGDA. The second decomposition step was connected with the thermal decomposition of TPGDA. The TGA thermogram confirms the presence of organic impurities detected by ^{1}H NMR.

For the case of PPGDA800, it remained stable up to 350°C before it decomposed completely at 425°C. By the help of TGA analysis, one can determine the service temperature limit for the two monomers and the percentage of inorganic impurities which are higher in TPGDA (about 1%) as clearly shown in Figure 4-8.

From Figure 4-9, it was clearly demonstrated that among the 30% of impurities present in neat TPGDA, only 3% were unpolymerized. This confirms the result that the detected impurities by ^{1}H NMR were mainly mono-propylene glycol diacrylate or dipropylene glycol diacrylate. The TPGDA samples were photopolymerized under UV-TL08 for about 10 min.

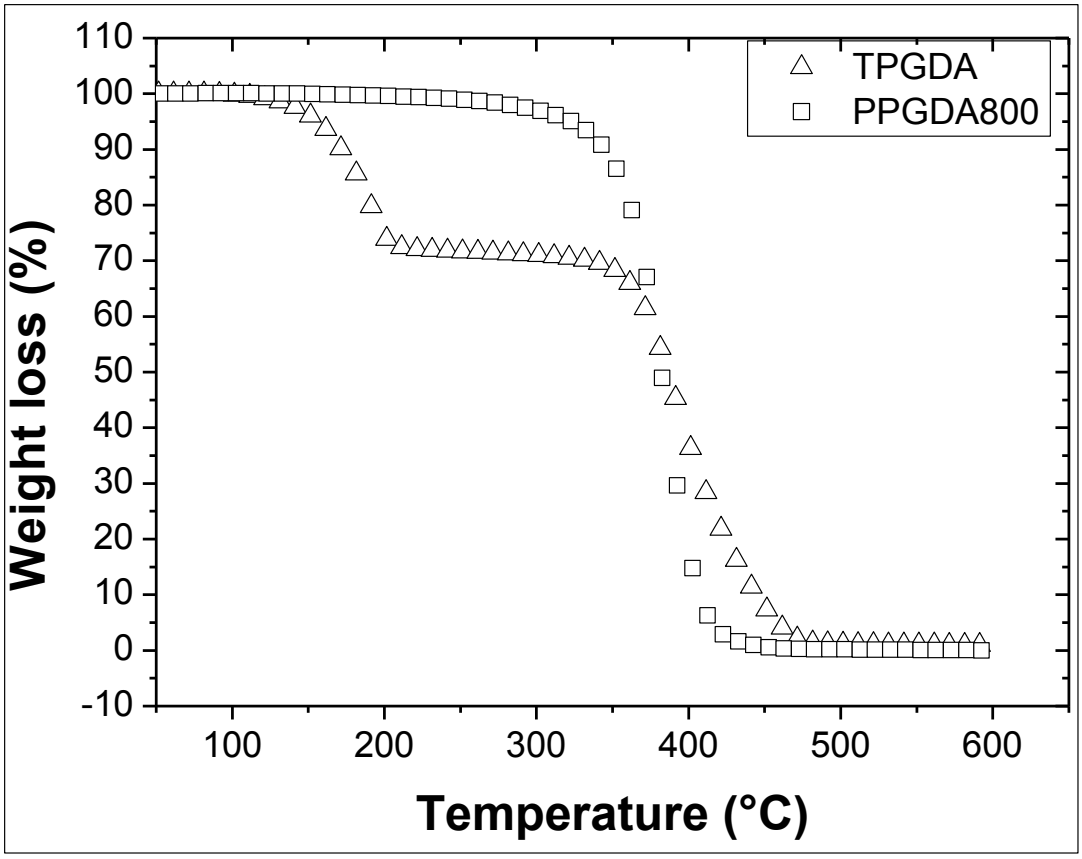

Figure 4-7: TGA thermograms of TPGDA and PPGDA800

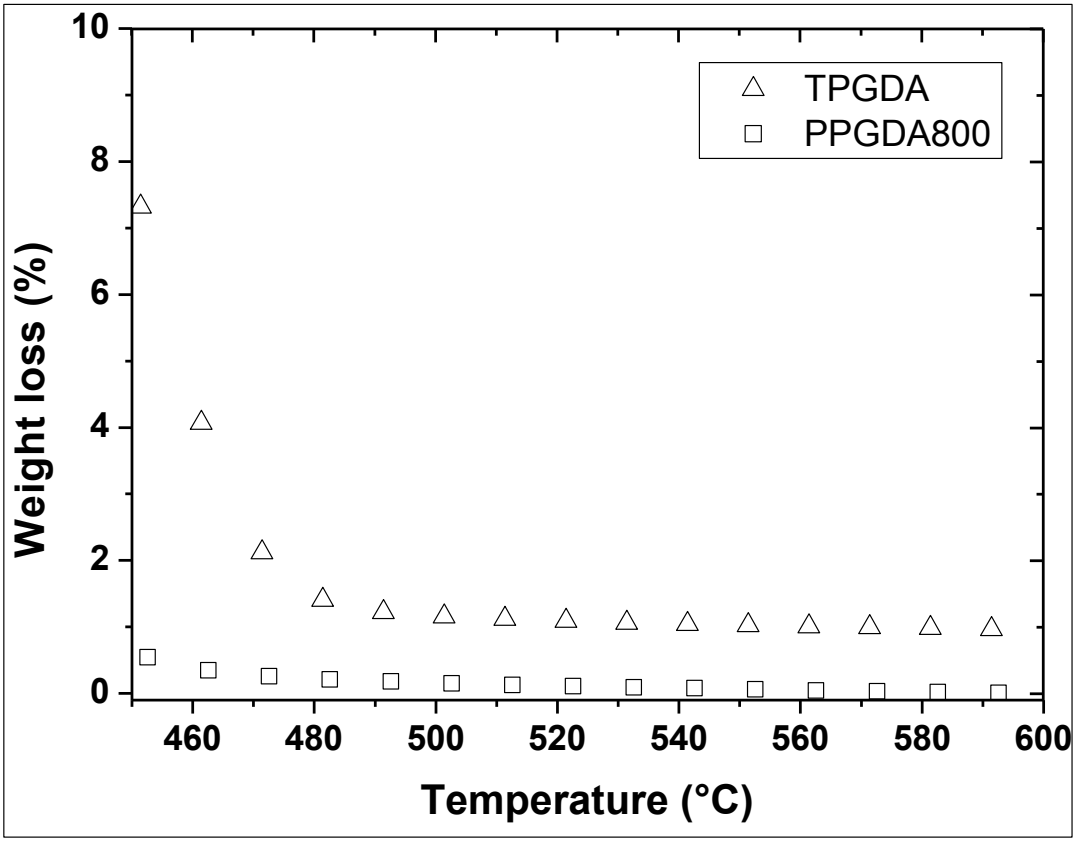

Figure 4-8: TGA thermograms of TPGDA and PPGDA800 from 450 to 600°C.

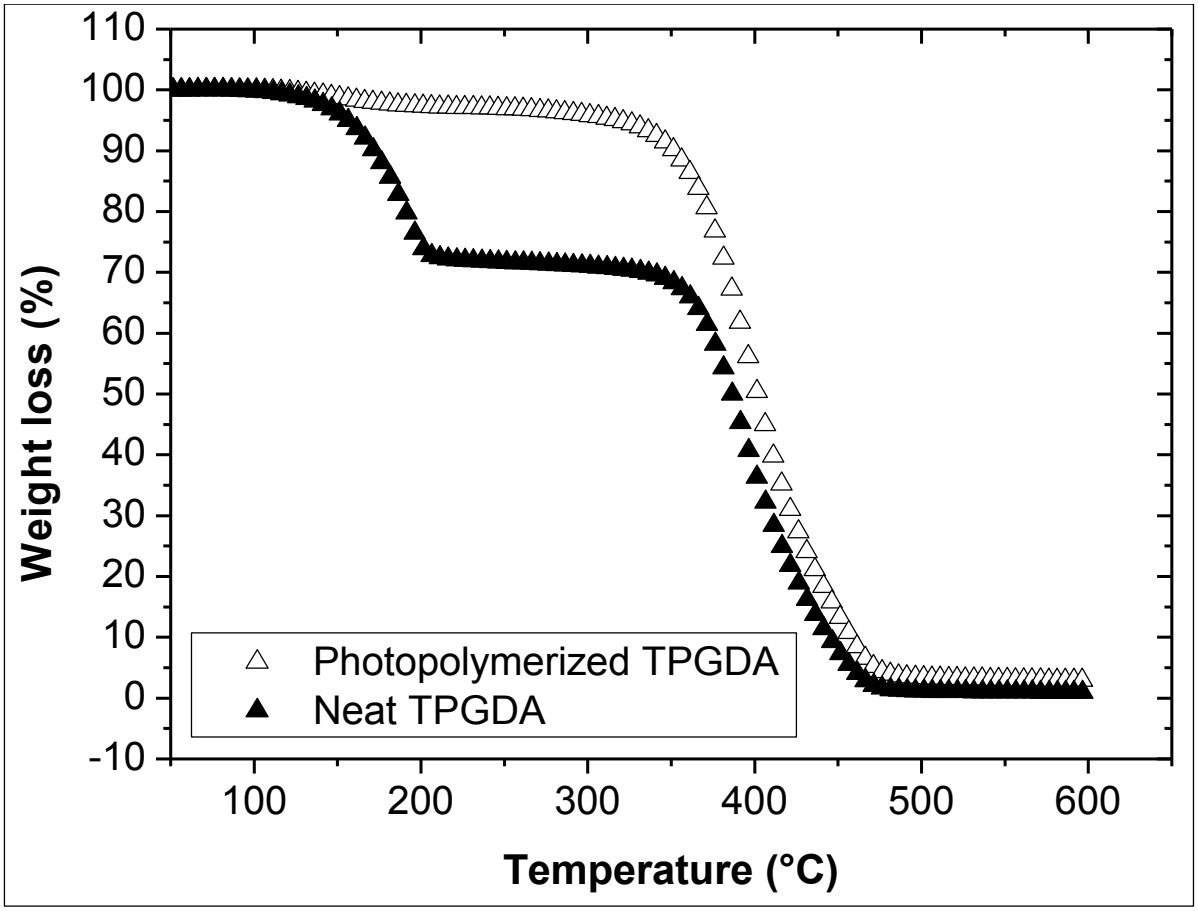

Figure 4-9: TGA thermograms of the neat TPGDA and that of photopolymerized TPGDA (under UV-TL08 for about 10min)

4.2. Analysis Monomers/LC E7 mixtures

4.2.1. Phase Diagrams

Figure 4-10 illustrates the phase diagrams by POM of the two monomeric binary mixtures TPGDA/E7 and PPGDA800/E7, determined by the polarized optical microscopy (POM). The (nematic+ isotropic)/isotropic (N + I)/(I) transition temperature ($T_{N+I/I}$) decreases upon adding the monomer to the LC E7. The depression of T_{N+I}/T_I follows a similar trend for the two monomers; they differ from each other because of the difference in the molecular weight of TPGDA and PPGDA800. POM observations were performed by varying the temperature from 60°C to −30°C, and concentration of the nematic LC E7, covering the range from 30 wt. % to 100 wt % of E7, to detect the segregated LC domains in the (N + I) – phase. For the 30 and 40wt.% E7, their T_{NI} transitions were found by the help of the DSC by applying the same conditions as stated for POM.

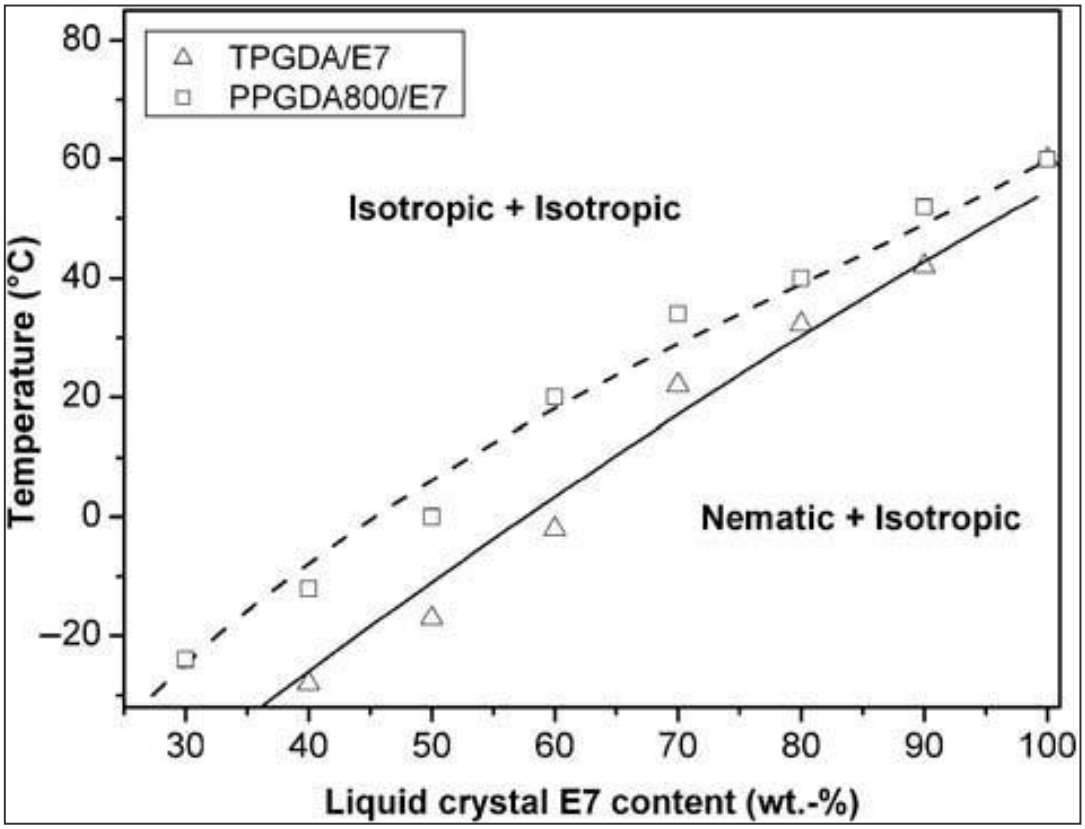

Figure 4-10: Phase diagrams of the monomeric mixtures: PPGDA800/E7 (square symbols) and TPGDA /E7 (triangular symbols).

Figure 4-11 shows the morphologies corresponding to the monomeric PPGDA800/E7 mixture at a temperature of 20°C for three different E7 concentrations. The micrographs reveal a clear variation of the LC domain sizes in the nematic state, depending on E7 concentration. The choice of the right monomeric mixture is crucial in terms of the phase separation induced by PIPS since good electro-optical results can generally be obtained if the initial reactive blend is in the homogeneous isotropic phase, close to the limit of the E7 solubility [1]. A concentration of 60 wt. % E7, which corresponds to the E7 solubility limit in PPGDA800, was chosen for all mixtures in order to carry out all investigations at the same E7 concentration.

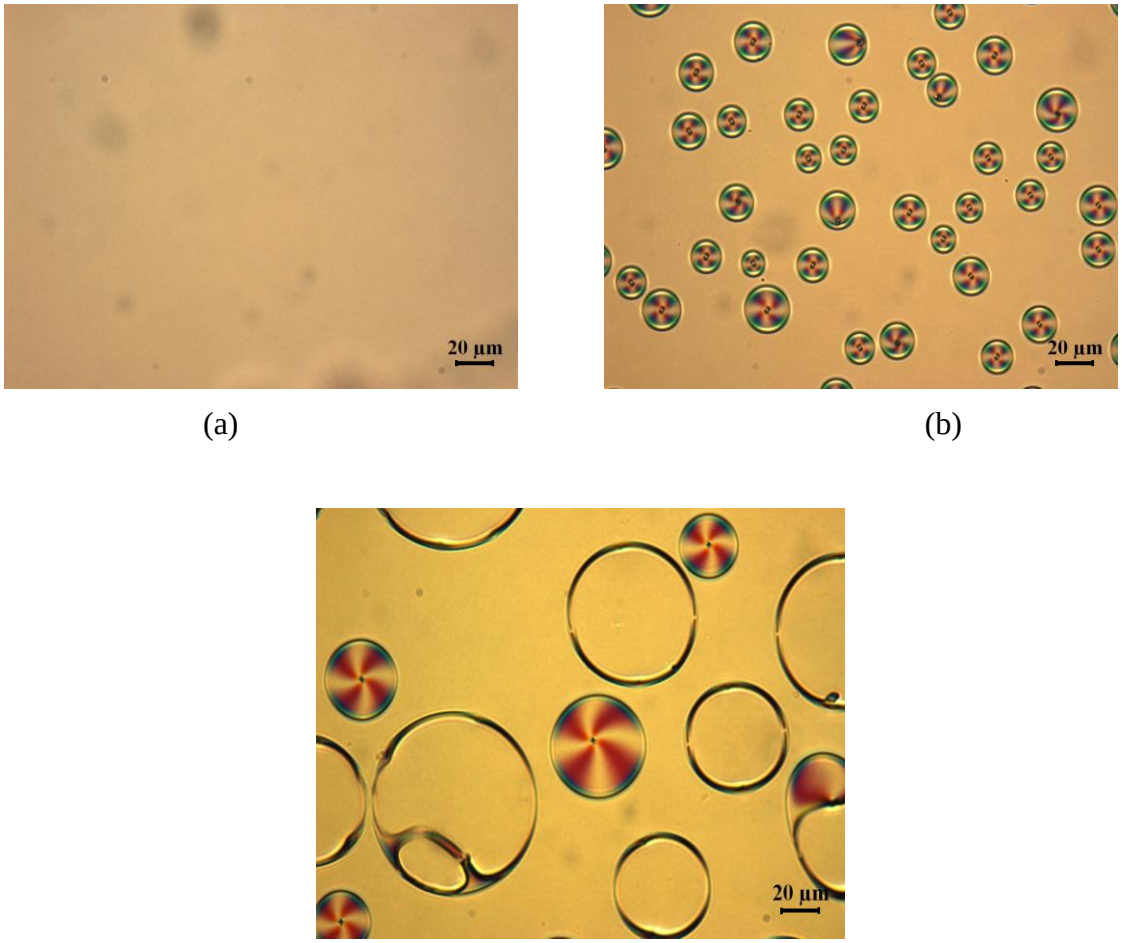

(a) (b)

(c)

Figure 4-11: Morphologies of monomeric PPGDA800/E7 mixtures obtained from POM at T = 20°C: (a) 60 wt %, (b) 70 wt % and (c) 80 wt % E7.

3. Analysis of PDLC Systems

3.1. Infrared Spectroscopy

FTIR spectroscopy is a versatile method used to investigate the extent of curing using carbon–carbon double bond consumption. The di-functional acrylate monomers lead to the formation of cross-linked polymer networks. It is evident that high monomer conversions should be reached to minimize the undesired effects of unreacted monomer molecules. Polymerisation/cross-linking and phase separation kinetics of monomer/LC mixtures govern the architecture of the obtained polymer networks. At least two absorption bands are available to monitor polymerization/cross-linking processes and to evaluate the conversion of the acrylic double bonds of TPGDA and PPGDA800. One of the most characteristic absorption bands that are quite often used in FTIR analysis of acrylates is the one corresponding to the CH_2=CH– vibration at 810cm^{-1}. However, since the LC E7 alone exhibits a strong absorption band near 810cm^{-1} originating from the vibration of the phenyl groups,[2–4] another peak that appears at 1638cm^{-1} is used for the analysis of the monomer/E7 mixtures. The calculation of the monomer conversion is made by considering the peak heights of the absorption band at 1638 cm^{-1}. The conversion ratio C is calculated using the following equation:

$$C(\%) = \frac{(A_{1638})_{(D=0)} - (A_{1638})_{(D)}}{(A_{1638})_{(D=0)}} \quad (1)$$

where $(A_{1638})_{(D=0)}$ is the height of the peak at 1638cm^{-1} (i.e. irradiation dose D is zero), and $(A_{1638})_{(D)}$ is the corresponding result for the system exposed to a dose D. Figure 4-11 presents the results of the polymerization kinetics of the two different systems based on 40 wt % monomer and 60 wt % E7 under UV-TL08, UV-Dr. Hönle system and EB. For the UV curing systems, Figure 4-11(a) shows the evolution of the acrylic double bond conversion as a function of UV light exposure time under UV-TL08. The inset of this figure is an amplification of the variations observed in the range from 0 to 70 s. It was noticed that increasing irradiation doses (exposure time) lead to an uptake of the monomer conversion during three stages. The first stage, called the induction period, is induced by the presence of traces of hydroquinone and molecular oxygen, which delayed the polymerisation of the neat monomers and an additional extra retardation time due to the presence of E7 solvent. In the second stage, the phase separation started to take place and in this case, E7 will be confined to small domains and does not act as a solvent anymore, and the reaction will then be enhanced towards higher conversions. In the third stage, an auto-deceleration process was noticed and

the reaction could reach 100% conversion in some systems and there is still high enough mobility of the reacting species. For the UV-TL08 curing process, presented in Figure 4-11(a), the TPGDA system showed slower polymerization rates, leading to lower conversion values compared to those of the PPGDA800 system even though it has a lower viscosity than that of PPGDA800. The TPGDA polymer network exhibited higher crosslink density, leading to a relatively high glass transition temperature (Tg=49°C), which exceed room temperature and thus lead to a very restricted or hindered mobility of the reacting species during the later stages of polymerization. The PPGDA800 system revealed a sharp increase in the conversion, reflecting faster photopolymerization than TPGDA. This could be explained by the enhanced mobility of the reacting species related to the strongly reduced Tg (-46°C), less than room temperature, due to the greater distance (spacing) between acrylic functional groups. Adding E7 to the mixture leads to a retardation effect at the early stages of the reaction, probably due to the solvation effect of E7. Polymerisation/cross-linking was then controlled by diffusion of the propagating species in the E7 solvent, but when phase separation began, E7 will be confined in small domains and would not act as a solvent anymore, and the reaction would then be enhanced towards completion. The phase separation of TPGDA/60 wt % E7 started 30 s later than that of the PPGDA800/60 wt % E7 system. This might be related to the fact that phase separation was mainly affected by the increase in molecular weight of the network . The starting PPGDA800/60 wt % E7 mixture was at the limit of solubility, but in the case of the TPGDA/60 wt % E7 blend, it was lower than its solubility limit, which is 70 wt % E7 at 20°C. For the UV-Dr. Hönle system, shown in Figure 4-12(b), one observes very fast processes for both photopolymerization/cross-linking and phase separation. No induction period was detected for the neat monomers due to the very rapid reactions. Similar trends were noticed for PPGDA800/60 wt % E7 and TPGDA/60 wt % E7, although these systems present different initial double-bond concentrations. By comparing UV-TL08 with the UV-Dr. Hönle system, even the process speed was found to have increased very much; PPGDA800/60 wt % E7 was still more rapid in terms of photopolymerization and phase separation kinetics, meaning that the photoinitiator radicals would have better accessibility to the double bonds of PPGDA800 than in the case of TPGDA. For the EB curing systems, Figure 4-12 (c) shows the evolution of the acrylic double bond conversion as a function of EB exposure time. The inset of this figure presents an amplification of the results in the range between 0 and 2.5 s. The TPGDA system exhibited faster polymerization rates, leading to higher conversion values compared to those of PPGDA800. This is mainly attributed to the higher number of reactive sites, which were close to each other in TPGDA than in

PPGDA800. Limited conversions were obtained at higher times of exposure due to the reduced reactive species mobility during the later stages of polymerization (glass transition effect). Adding E7 to the two systems induced the same effects as stated for UV curing. By comparing UV-TL08, UV-Dr. Hönle system and EB, one can say that not only the mobility enhanced the reaction towards completion but also the possibility that the reactive species meet with each other. Another difference between photopolymerization and accelerated EBs is that during photopolymerization, the reaction starts first around the photoinitiator radicals and forms spots of micro-networks, which might be different from one spot to another. As a result, this will induce some heterogeneity not only in the obtained networks but also in the morphologies after phase separation. On the other hand, it is to be mentioned that under EB, the electrons open directly the double bonds that are more or less homogenous in the mixture and as a result, homogeneous networks will be formed across the PDLC film.

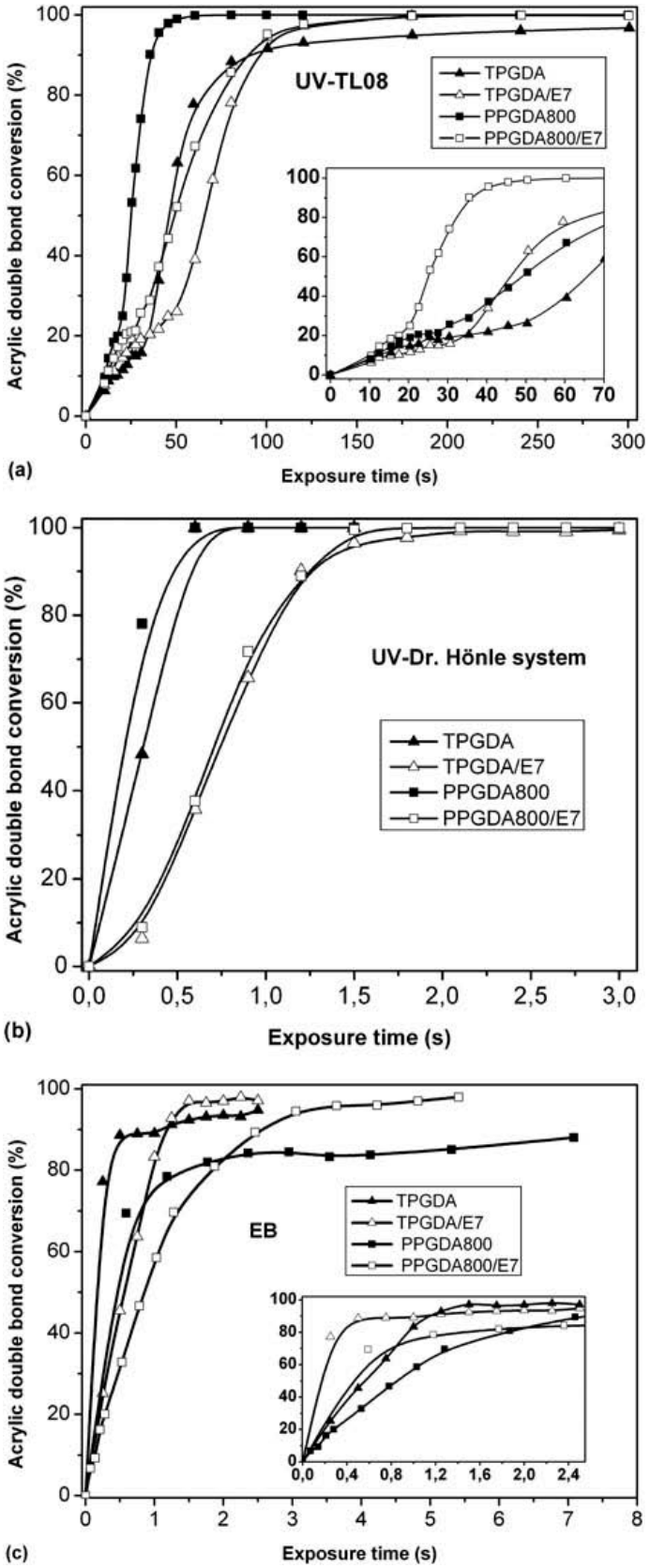

Figure 4-12: Variation of acrylic double bonds Conversion for TPGDA and PPGDA800, TPGDA/60 wt % E7 and PPGDA800/60 wt % E7as a function of exposure time, prepared by (a) UV-TL08, (b) UV-Dr. Hönle system and (c) EB curing.

3.2. Morphologies

3.2.1 Morphology by Polarized Optical Microscope

The samples for the morphology analysis by the polarized optical microscopy (POM) were prepared under the optimum conditions that were derived from the curves of conversion versus exposure time (Figure 4-13) i,e the conditions that enabled us to obtain the highest possible conversions in just one passage of the sample under the beam. All samples were analyzed by placing a small amount of the mixture between two ITO-coated glasses, spaced by 13-µm-thick PET films, and then cured under UV-TL08 at a dose of 150mJ/cm^2 for about 5 min. The UV-Dr. Hönle system samples were tested at a total dose of 240mJ/cm^2 for about 2.4 s, which was achieved by regulating the apparatus at 70% of its power capacity and the conveyor belt speed at 125 mm/s. The EB samples were analyzed by sandwiching a small droplet of the mixture between an ITO-coated glass and an ITO coated 50-µm-thick PET sheet, spaced by 13-µm-thick PET films or a double-phase adhesive tape, and exposed to a dose of 120 kGy for about 2.45 s exposure time. This was achieved by fixing the intensity at 2mA and adjusting the conveyor belt speed. No post curing was carried out on the samples before investigating the morphologies.

The micrographs are presented in Figure 4-13. It can be noticed that the chemical structure of the monomer played a great role in forming any desired morphology in the case of the slow photopolymerization process (UVTL08-18W). The bigger interconnected droplets obtained from PPGDA800/60 wt % E7, compared to TPGDA/60 wt % E7, were mainly due to the fact that the neat monomer (PPGDA800) contains bigger spacing, n = 12, between the reactive double bonds, than TPGDA (n = 3). However, when using the very rapid photopolymerization process (UV-Dr Hönle system-10kW), smaller LC domains of PPGDA800/ 60 wt % E7 were found, compared to the same system under slow photopolymerization process (TL08). This might be attributed to a lack of sufficient time to form large domains. In the case of EB samples, because of the formed slack network, polymerisation/cross-linking and thus phase separation of PPGDA800/60 wt % E7 system were not completed. For the TPGDA/60 wt % E7 system, small and regular domains were obtained, probably due to the homogeneous polymerization under EB.

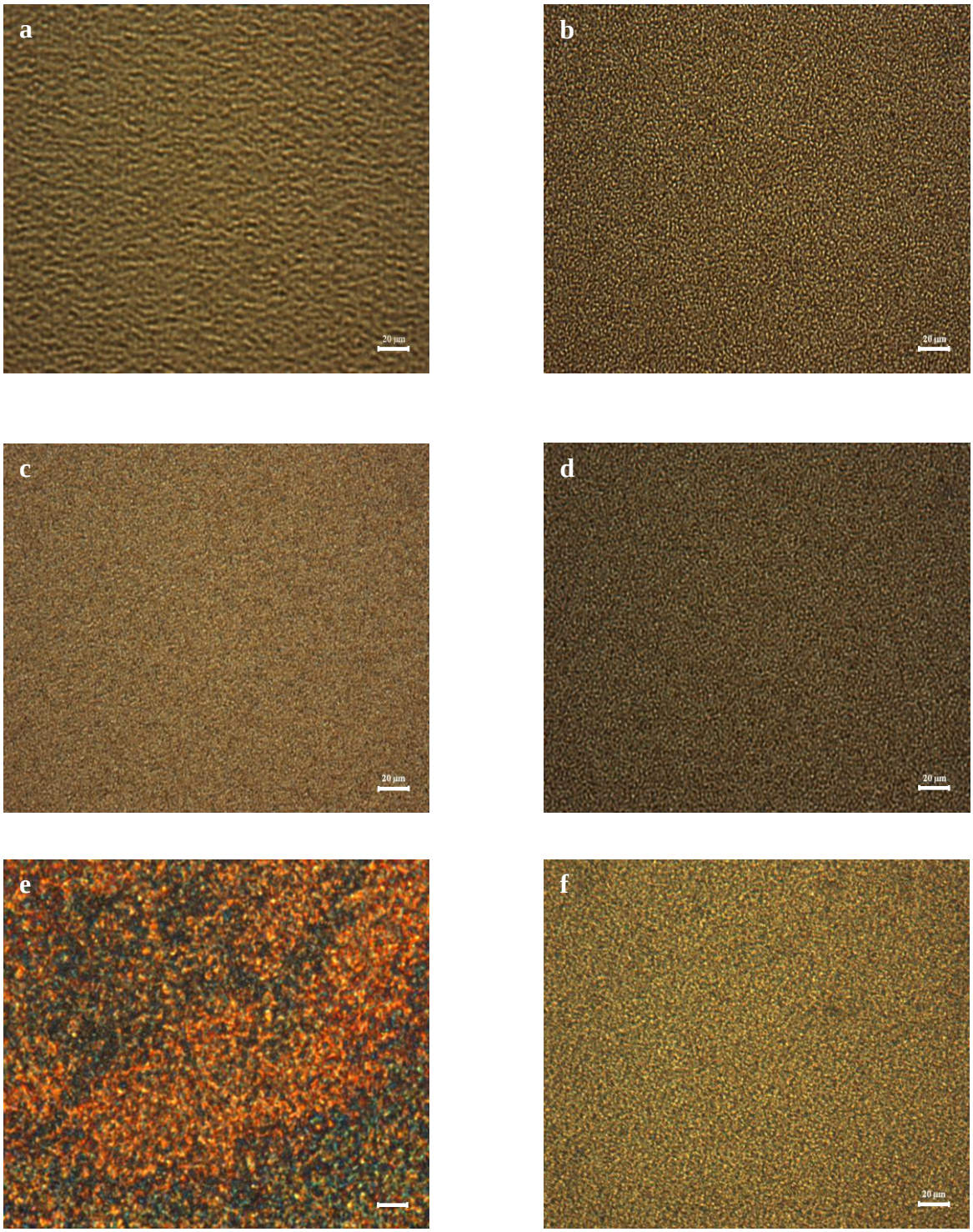

Figure 4-13: Micrographs obtained by POM; UV-TL08: (**a**) PPGDA800/60 wt % E7; (**b**) TPGDA/60 wt % E7. UV-Dr. Hönle system: (**c**) PPGDA800/60 wt % E7; (**d**) TPGDA/60 wt % E7; and EB curing: (**e**) PPGDA800/60 wt % E7; (**f**) TPGDA/60 wt % E7.

3.2.2. Morphology by Scanning Electronic Microscope

Figure 4-14 shows the scanning electron (SEM) micrographs of PPGDA800/60 wt.% E7 and TPGDA/60 wt.% E7 photopolymerized under UV-TL08 for about 05 min. For the case of PPGDA/E7 system, It can be noticed that there was LC E7 droplets collapsed during the extraction at room temperature which is well above the glass transition temperature of the PDLC. However, for TPGDA/E7, no droplet size change was noticed because of the rigidity of the obtained PDLC.

Non-regular droplet sizes and even interconnected LC domains in the TPGDA/E7 system was mainly due to the non-homogeneous nature of the photopolymerization.

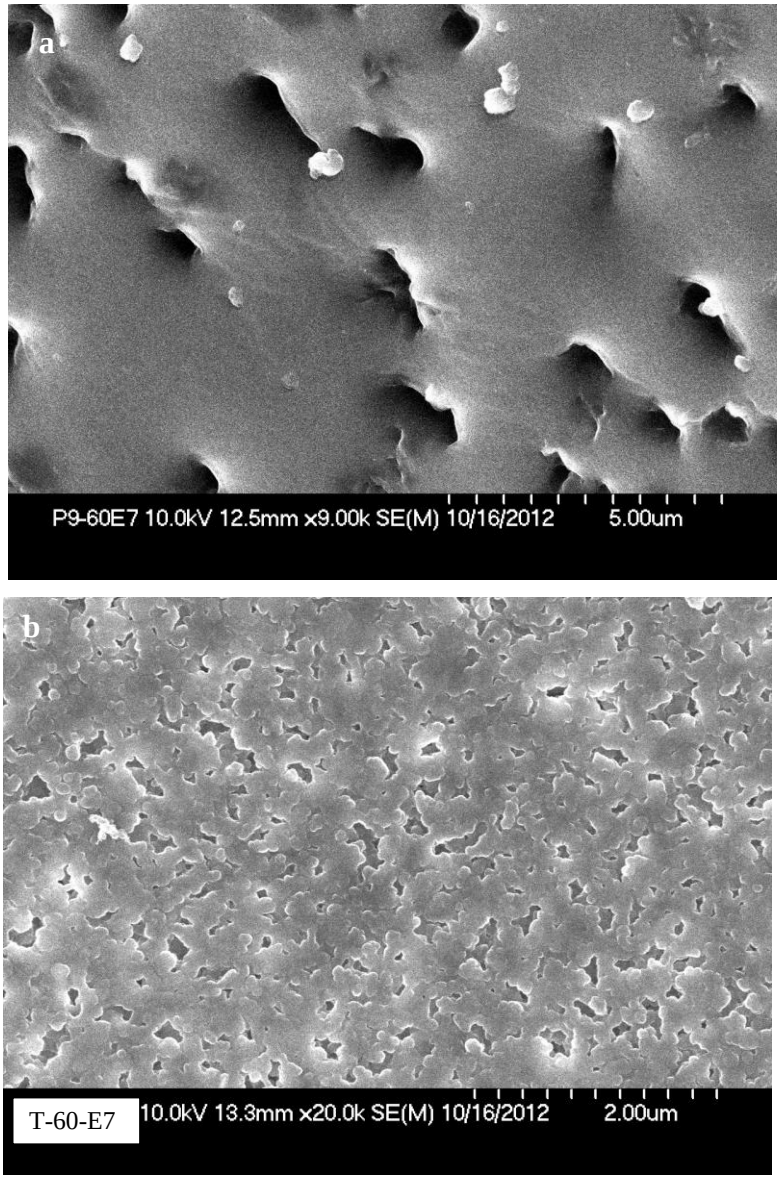

Figure 4-14: SEM microphotographs of a: PPGDA800/60 wt. % E7 and b: TPGDA/60 wt. % E7

3.3. Thermal Properties by DSC

Figure 4-15 illustrates the DSC thermograms of TPGDA and TPGDA/60wt.%E7 photopolymerized under UV-TL08. For that of TPGDA, it was very difficult to calculate the Tg because the curve did not show a real shouldering in the baseline but rather a broad peak which was present in the first heating cycle (red line curve) and disappeared in the second heating cycle (green line curve) and no peak was noticed during all cooling cycles. The confusing Tg might be related to very high crosslink density which made its detection very difficult.

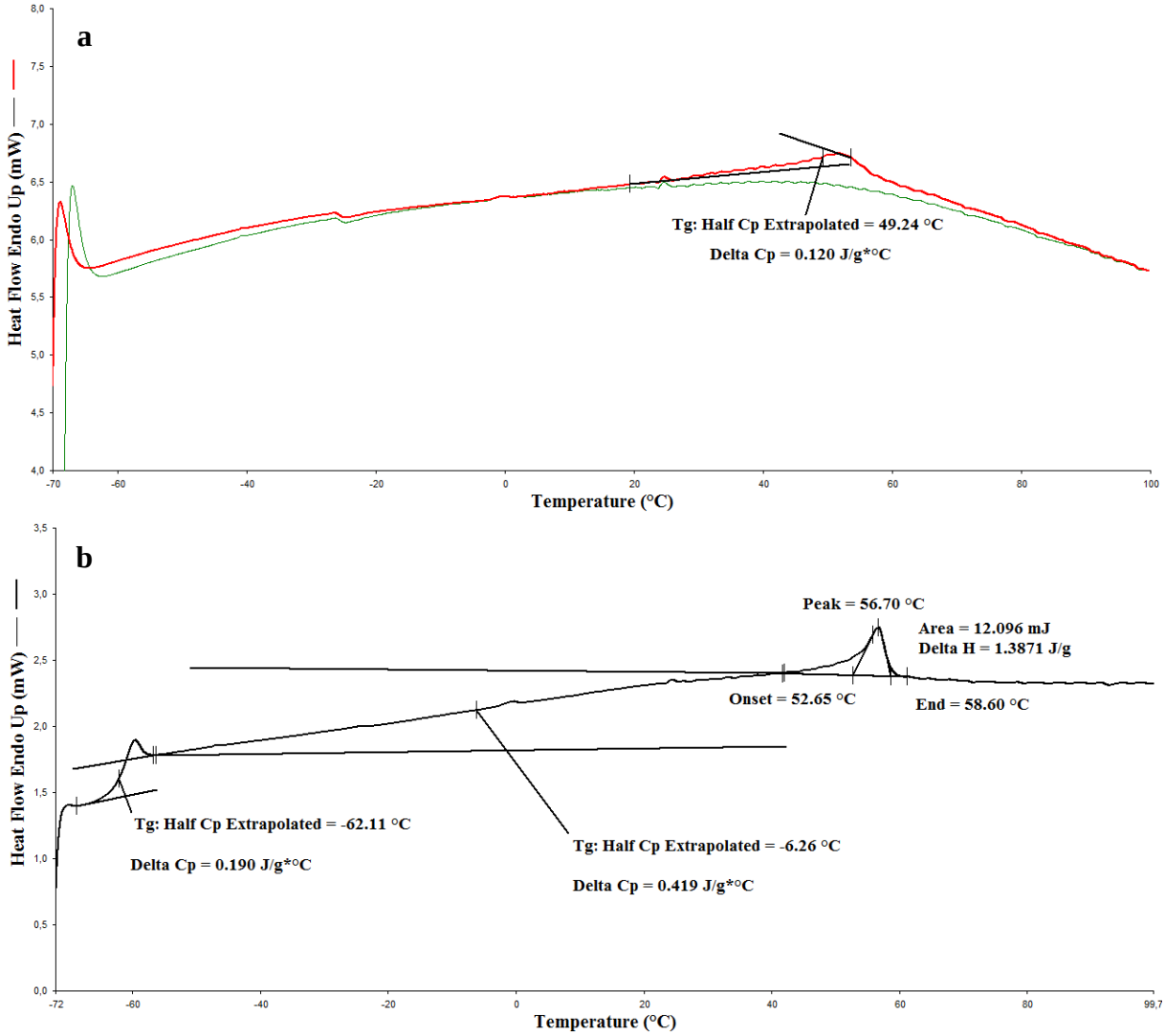

Figure 4-15: DSC thermograms of the photopolymerized samples under UV-TL08 a:TPGDA for about 10min, **b:** TPGDA/60 wt.% E7 for about 05min.

Figure 4-16 presents the DSC thermograms of the photopolymerized PPGDA800 under UV-TL08 and that of PPGDA800/60wt.% E7. It was noticed that there was a very small decrease of about 01°C in the Tg indicating thus that E7 had not any plasticizing effect for the PPGDA800.

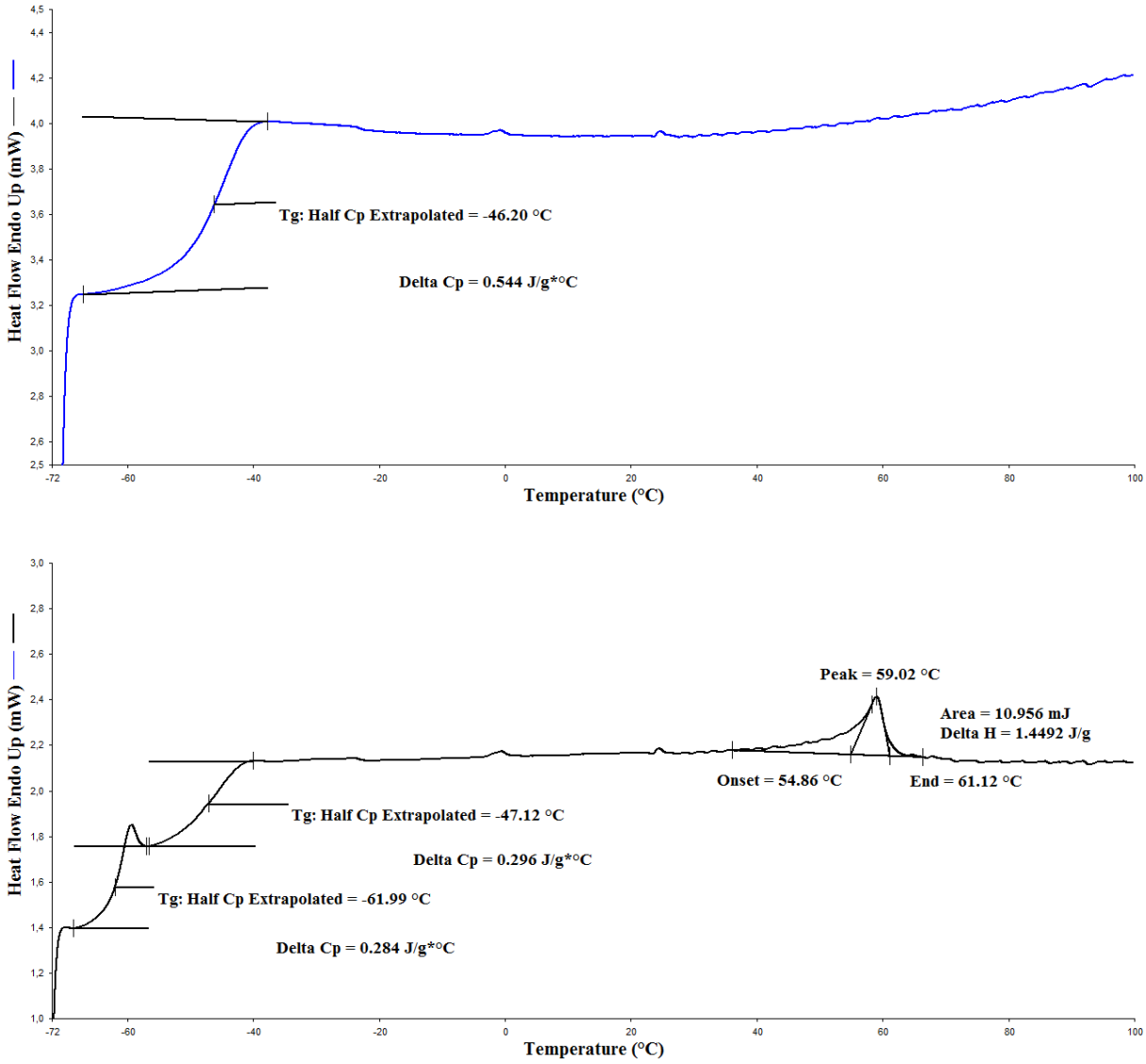

Figure 4-16: DSC thermograms of photopolymerized films under UV-TL08 of PPGDA800 for about 02min (blue line), PPGDA800/60 wt.% E7 for about 05min (black line)

Figure 4-17 shows the DSC thermogram of E7. It is to be noticed that the E7 alone showed a Tg of 62.48°C and a T_{NI} of 60.23°C at the peak summit. The slight change in The Tg with that given by the supplier [5].

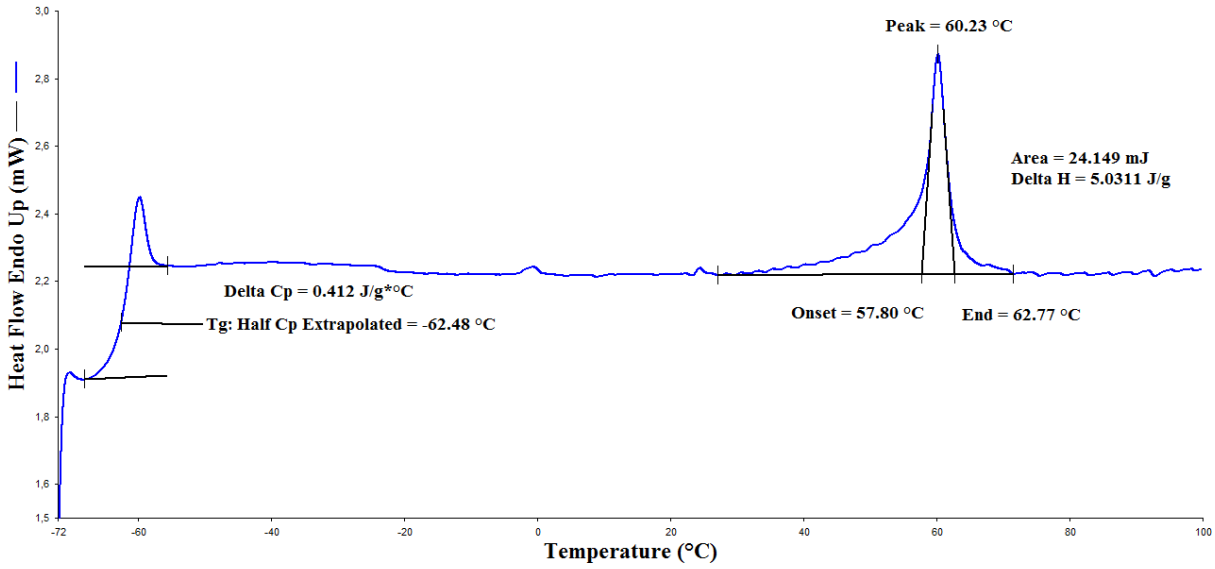

Figure 4-17: DSC thermogram of LC E7

From Table 4-4 which presents the transitions in TPGDA and PPGDA800 either neat monomers or photopolymerized polymers with or without 60wt.%E7, one can notice that both PDLC's showed a slight decrease in the $T_{N/I}$ with respect to that of E7 alone; for the TPGDA/60wt.%E7, there was a decrease of 3.54°C but for the PPGDA800/60wt%E7 only 1.21°C This could be attributed to the fact that there was no contamination of the confined LC droplets by the non-reacted PPGDA800 monomers or the growing polymer during the polymerization reaction. There was also a big decrease in the Tg of the photopolymerized TPGDA/60wt.%E7 from 49.24°C of the photopolymerized TPGDA under UV-TL08 for about 10min to -6.26°C of the photopolymerized TPGDA/60wt.%E7 under UV-TL08 for about 02min; this was mainly attributed to the fact that E7 acted as a plasticizer for TPGDA but not to the same extent as for PPGDA800.

Table 4-4: Transitions in neat and photopolymerized TPGDA and PPGDA800 with or without 60wt.%E7.

Sample	Tg* (°C)	Tg E7** (°C)	T_{NI} (°C)
E7		-62.48	60.23
TPGDA monomer [6]	-85	…….	….....
Photopolymerized TPGDA	49.24	…….	…….
Photopolymerized TPGDA/60wt.% E7	-6.26	-62.18	56.69
PPGDA800 monomer [6]	-70	…….	……..
Photopolymerized PPGDA800	-46.20	…….	…….
Photopolymerized PPGDA800/60wt.% E7	-47.12	-61.99	59.02

* The glass transition temperature Tg of monomers and matrices.

** The glass transition temperature Tg of the liquid crystal E7.

The amount of demixed liquid crystal can be quantified by the fractional amount of phase-separated LC from polymer α which can be determined from measurements of ΔC_{LC}, specific heat change at the glass transition temperature of LC and of ΔH_{NI}, the nematic–isotropic transition enthalpy. Smith [7,9] derived a simple expression for α

$$\alpha = \frac{m_{s\,LC}}{m_{LC}} = \left(1 + \frac{m_P}{m_{LC}}\right) P_{(x)} \qquad (2)$$

Where $m_{s\,LC}$ is the mass of phase-separated LC; m_{LC}, the total mass of LC; m_P, the mass of polymer; x, the LC concentration in the blend; $P_{(x)} = m_{s\,LC}/(m_P + m_{LC})$; the ratio of the mass of phase-separated LC to the total mass of the blend which can be found from nematic–isotropic transition studies

$$P_{(x)} = \frac{\Delta H_{NI\,(x)}}{\Delta H_{NI\,(LC)}} \qquad at\ T = T_{NI} \qquad (3)$$

Where $\Delta H_{NI\,(x)}$ and $\Delta H_{NI\,(LC)}$ are the nematic–isotropic transition enthalpies (per unit mass) for blend and pure LC, respectively.

At the LC glass transition temperature

$$P_{(x)} = \frac{\Delta C_{LC\,(x)}}{\Delta C_{LC\,(LC)}} \qquad at\ T = T_g \qquad (4)$$

Where $\Delta C_{LC\,(x)}$ and $\Delta C_{LC\,(LC)}$ are the incremental increase in specific heat (per unit mass) at the liquid crystal glass transition in blends and in pure LC.

For PPGDA800/60wt % E7:

From the ΔC_p measurements: P_x=0.6893 and thus α>1; that means that all LC was separated from the matrix during the photopolymerization reaction.

From ΔH_{TNI} measurements: Px= 0,2880 and thus α=0,48; the confined content of the LC E7 was about 48%.

From the above results, one can notice that about 52% of the LC E7 was bloomed out to the PDLC film surface because of big droplet sizes which are induced by the long spacing between crosslinks. E7 was not found as an effective plasticizer for the PPGDA800. As a result, it was found that 31.2 wt.% was bloomed out from the core to the PDLC surface and only 28.8wt.% E7 was confined in LC droplets.

For TPGDA/60wt. % E7:

From the ΔC_p measurements: P_x=0.4611 and thus α= 0,7686; that means that 76.86% of the LC E7 was separated from the matrix during the photopolymerization reaction and around 23.14% would act as a plasticizer for the matrix because of the great compatibility of the E7 with TPGDA as also stated by some investigators [10-14].

From ΔH_{TNI} measurement: P_x=0,2757 and α=0,4595, the confined LC content was about 45.95%. the remained 30.91% might act also as a plasticizer for the matrix. As a result, it was found that 32.43wt.% from the 60 wt.% E7 incorporated in TPGDA would act as a plasticizer for the TPGDA, the same percentage reported by L. Méchernène et. al.[14]

The confined LC content for the TPGDA/60wt. % E7 was comparable to that in PPGDA800/60wt. % E7 this might be related to faster kinetics of phase separation seen in PPGDA800/60wt.% E7 PDLC's during cure.

3.4. Electro-optical Responses

Figure 4-18 represents the electro-optical responses under UV-TL08, UV-Dr. Hönle system and EB curing of 17-μm-thick polymer/LC films. The results of TPGDA/E7 under EB, The plateau of the ON state transmission T_{ON} in the UV systems was reached at higher voltages than that in EB systems. The threshold V_{10} and saturation voltages V_{90} increased strongly in the UV systems compared to the EB systems; i.e. the UV-cured samples required higher voltages to be activated. This might be related to the different types of morphologies obtained by the three curing methods as shown in Figure 4-12. A more regular morphology would be obtained in the case of EB [15–17] . The higher crosslinking density of TPGDA/70 wt. % E7 and lower spacing between the reactive double bonds yielded smaller droplet sizes than the PPGDA800/60 wt. % E7 system. For this reason, the OFF-state light transmission was reduced while the width of the hysteresis loop was narrowed. In the case of EB-cured systems, it was found that threshold V_{10} and saturation voltage V_{90} of TPGDA/70 wt. % E7 are much lower than those of the PPGDA800/60 wt. % E7 system. T_{OFF} remained near zero before and after applying the electric field, meaning that there was nearly no memory effect. In addition, the maximum transmission T_{ON} of 90% can be achieved at a voltage as low as 17 V and the width of the hysteresis loop was also very narrow. In the case of the PPGDA800/60 wt. % E7 system, optimum conditions of the reaction were not reached to obtain better results. The results of TPGDA/E7 confirmed the conclusions made earlier by F. Gyselinck et al. [18] and L. Benkhaled et al.[19] that EB-cured PDLC films have better electro-optical responses compared to their analogous UV-cured systems even though a very fast UV curing method (UV-Dr. Hönle system) is employed. PPGDA800/60 wt. % E7 samples obtained from UV-TL08 suffered from the problem of the presence of short circuits, which might be attributed to the presence of humidity because the PPGDA800 is more hygroscopic than TPGDA as detected by the FTIR analysis . The first response seen upon the application of an external electric field was associated to the free E7 molecules at the PDLC surface. The problem of blooming out of E7 molecules from the core to the surface of PPGDA800/60 wt. % E7, due to the large domain dimensions, was greatly reduced by using the UV-Dr. Hönle technique.

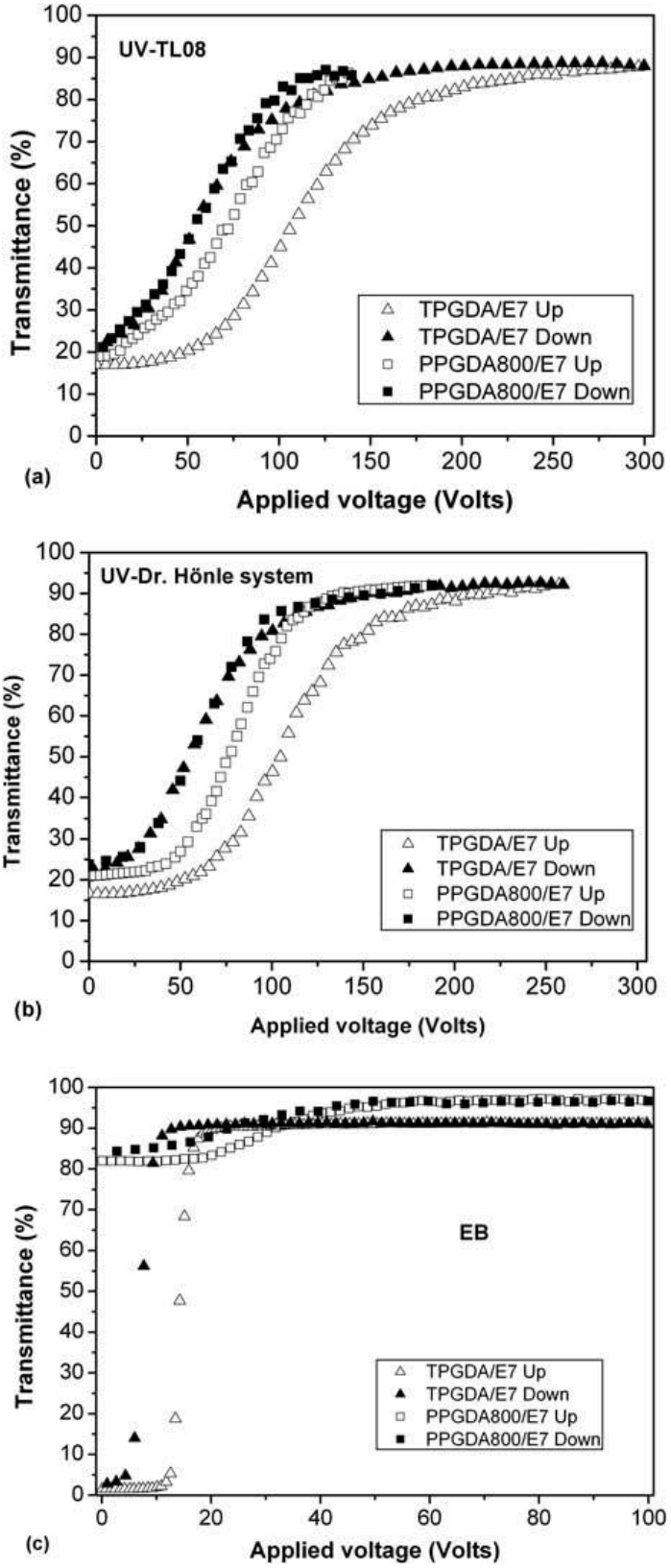

Figure 4-18. Electro-optical responses of 17µm thick samples of TPGDA/60wt.%E7 and PPGDA800/60wt.%E7 prepared by (a) UV-TL08; (b) UV-Dr Hönle system; and (c) EB curing.

Figure 4-19 presents the electro-optical responses of 17-µm-thick samples under UV-TL08 and UV-Dr. Hönle system of (a) TPGDA/60 wt % E7 and (b) PPGDA800/60 wt % E7. A slight enhancement of the electro-optical responses of TPGDA/60 wt % E7 was observed in terms of the maximum T_{ON} and V_{90}. This could be explained by the fact that when the intensity of the UV light was increased, the time necessary to get a complete reaction and the LC domain dimensions was reduced. In the case of PPGDA800/60 wt % E7, the encountered problem of short circuits was reduced but not definitively overcome by reducing the sizes of the LC domains. In addition, the maximum ON state transmission was slightly improved.

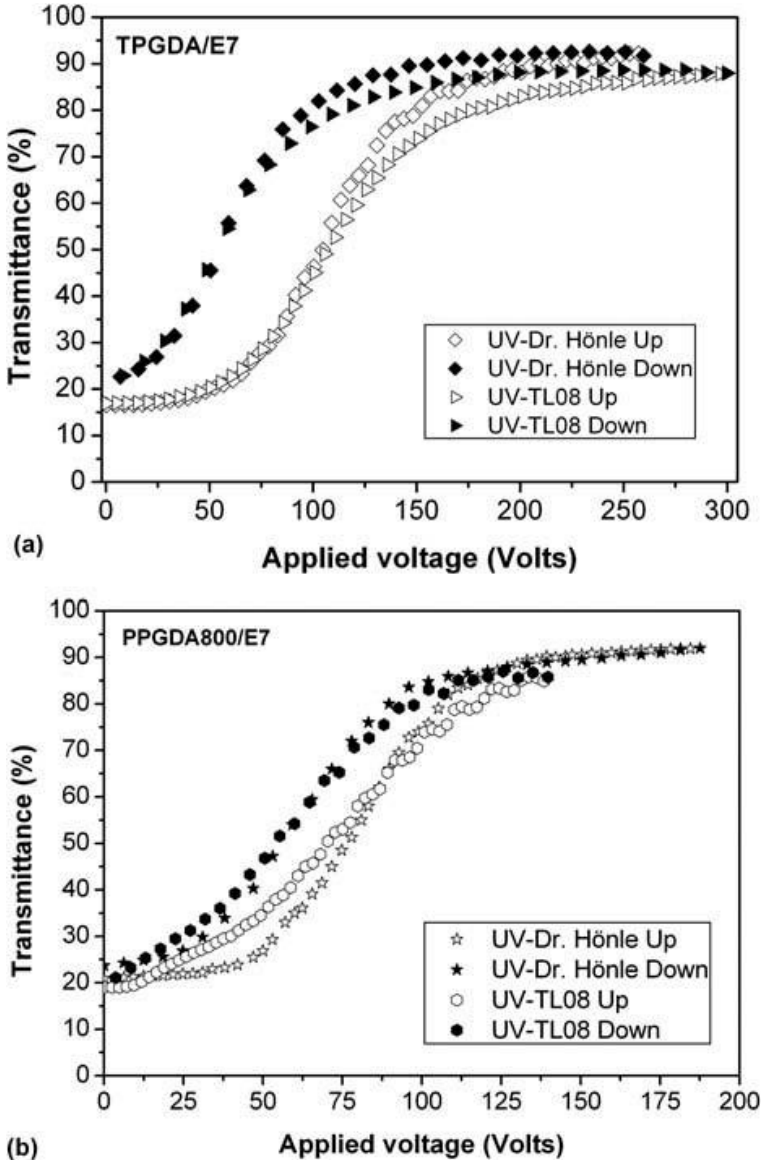

Figure 4-19: The electro-optical responses of 17-µm-thick samples elaborated by UV-Dr. Hönle system and UV-TL08; (a) TPGDA/60 wt % E7 and (b) PPGDA800/60 wt % E7.

References:

[1] K. Amundson, A. V. Blaaderen, and P. Wiltzius, Morphology and electro-optic properties of polymer dispersed liquid-crystal films. Phys. Rev. E; 55: 1646–54, **1997**.

[2] B. G. Wall, and J. L. Koenig, Studying the curing kinetics of a diacrylate by using infrared spectroscopy, Appl. Spectr.; 51: 1453–59, **1997**.

[3] Y. Derouiche, F. Dubois, R. Douali, C. Legrand, and U. Maschke, Some properties of nematic liquid crystal E7/acrylic polymer networks, Mol. Cryst. Liq. Cryst.; 541: 439–48, **2011**.

[4] T. Scherzer, and U. Decker, Kinetic investigations on UV-induced photopolymerization reactions by real-time FTIR-ATR spectroscopy: the efficiency of photoinitiators at 313 and 222 nm, Nuclear Instruments and Methods in Physics Research; B 151: 306-12, **1999**.

[5] Merck Product Information. Merck liquid crystals. Licrilite Brochure. Poole: Merck House, **1994**.

[6] Y. Derouiche, Etude spectroscopique et électrooptique de matériaux polymères-cristaux liquides, PhD thesis University of Tlemcen1, Algeria, **2013**.

[7] M. Mucha, Polymer as an important component of blends and composites with liquid crystals, Prog. Polym. Sci.; 28: 837–873, **2003.**

[8] F. Roussel, J. M. Buisine, U. Maschke, and X. Coqueret, Photopolymerization kinetics and phase behavior of acrylate based polymer dispersed liquid crystals, Liquid Crystals ; 24, 4: 555-61, **1998**.

[9] G. W. Smith, Mixing and phase separation in liquid crystal/ matrix systems. Int. J. Mod. Phys. B; 7: 4187–213, **1993**.

[10] A. Elqidra, Effet du rayonnement sur des systèmes monomère-cristal liquide, PhD thesis, University of Lille1, France, **2012**.

[11] Y. Derouiche, S. A. K. Ghefir, F. Dubois, R. Douali, C. Legrand, M. Azzaz, and U. Maschke, Preparation and characterization of selected polypropyleneglycoldiacrylate/nematic liquid crystal materials, Irephy.; 4: 188–93, **2010**.

[12] A. Berrayah, L. Zair, A. Olivier, and U. Maschke, Mechanical properties of polymer/liquid crystal systems prepared by electron-beam and ultra-violet processing: filling effect and plasticization. Phys. Procedia; 2: 1119–24, **2009**.

[13] U. Maschke, A. Traisnel, J. D. Turgis, and X. Coquret, Influence of liquid crystal concentration on the electrooptical behavior of polymer dispersed liquid crystal films prepared by electron beam processing, Mol. Cryst. Liq. Cryst.; 299: 371-73, **1997**.

[14] L. Méchernène, L. Benkhaled, Dj. Benaissa, and U. Maschke, Studies of optical transmission properties of electron beam cured polymer liquid crystal systems, Optical Materials; 31:632-39, **2009**.

[15] A. M. Lackner, J. D. Margerum, E. Ramos, and K. C. Lim, Droplet size control in polymer dispersed liquid crystal films. Spie; 1080: 53–61, **1989**.

[16] A. M. Lackner, J. D. Margerum, L. J. Miller, F. G. Yamagishi, E. Ramos, K. C. Lim, Jr. W. H. Smith, and C. I. Van Ast, Methods to obtain lower-voltage-activated polymer dispersed LCDs. Proc. SID.; 32: 173–176, **1991**.

[17] S. A. Carter, J. D. LeGrange, W. White, J. Boo, and P. Wiltzius, Dependence of the morphology of polymer dispersed liquid crystals on the UV polymerization process, J. Appl. Phys.; 81: 5992–99, **1997**.

[18] F. Gyselinck, U. Maschke, A. Traisnel, and X. Coqueret, PDLC films prepared by the electron beam and ultraviolet curing: influence of curing conditions on the electrooptical properties. Liq. Cryst.;27: 421–28, **2000**.

[19] L. Benkhaled, L. Méchernène, A. Traisnel, M. Benmouna, J. M. Gloaguen, X. Coqueret, and U. Maschke, Electrooptical properties of EB-cured PDLC systems. Mol. Cryst. Liq. Cryst.; 375: 651–58, **2002**.

General Conclusions

Conclusions

The aim of the present study is set mainly to compare Ultra-Violet (UV) to Electron Beams (EB) irradiations, when used for the elaboration of polymer dispersed liquid crystals to find out some relationships between the physical properties; namely: phase diagrams, polymerization/crosslinking, phase separation kinetics, morphology, and electro-optical responses of tripropyleneglycoldiacrylate/liquid crystal E7 (TPGDA/E7) and polypropylene glycoldiacrylate/E7 (PPGDA800/E7) PDLC systems prepared by three methods: UV-TL08 (slow photopolymerization), UV-Dr. Hönle system (rapid photopolymerization) and EB (rapid curing). The monomers used differ in their molecular weights: 300g/mole for TPGDA and 800g/mole for PPGDA800 , being different in the number of propyleneglycol units between the two acrylate double bonds.

The following results were obtained:

1_ The ^{1}H MNR spectrum of the TPGDA monomer revealed the presence of impurities which were confirmed and quantified by TGA at around 30% of polymerizable impurities. They were found to be related to polymerizable mono and di-propyleneglycol diacrylates, acrylic acid and tripropyleneglycol.

2_ The studies of phase diagrams of the mixtures: monomers/E7, by the polarized optical microscopy, indicated that 60 wt % E7 was the limit of solubility for the mixture PPGDA800/E7. This concentration was then consequently chosen for the TPGDA/E7 mixture although it was far away from its limit of solubility which is 70wt. % E7.

3_The polymerization kinetics was performed by FTIR spectroscopy, it can be noticed that:

- In the case of UV-TL08 (slow photopolymerization), the longer the spacing between two double bonds in the neat monomer, the higher will be the mobility of reactive species, and the higher will be the rate of photopolymerization/crosslinking reactions.
- In the case of UV-Dr. Hönle, more rapid photopolymerization was observed compared to UV-TL08 for both monomers. The photopolymerization of PPGDA800 was slightly more rapid than TPGDA. The PPGDA800/E7 and TPGDA/E7 were found to follow the same trends.
- In the case of the EB curing system, the shorter the spacing between the two double bonds in the monomer, the higher the number of reactive sites, which are close to each other, and the higher the rate of polymerization/cross-linking reactions.

- The LC E7 was found to act as a solvent for the reaction at the early stages of polymerization, but during the phase, separation E7 would be confined in small domains and would not act as a solvent anymore, and the reaction would then be enhanced towards higher conversions for all curing methods.

4_ Bigger LC-droplet dimensions were obtained for the PPGDA800/E7 PDLC films under the slow UV-TL08 than TPGDA/E7, however, comparable LC droplet dimensions were obtained under the more rapid UV-Dr. Hönle. In the case of the EB curing, the homogeneous polymerization reaction would lead to more regular morphologies obtained for the TPGDA/60 wt % E7 system. The non-complete polymerization reaction and phase separation of PPGDA800/60 wt % E7 might be related to the limited maximum available exposure time under EB and the slack network formed.
Concerning the SEM micrographs of PPGDA800/60wt.% E7 PDLC samples, photopolymerized under UV-TL08, the LC droplet collapsing was found to be related to the slack network that was formed because of the lower glass transition temperature Tg of the matrix , but no droplet collapsing was observed for TPGDA/60wt.% E7 but rather irregular LC droplet sizes out of the heterogeneity of the photopolymerization reaction.

5_ The DSC thermograms of PPGDA800/60wt.% E7, photopolymerized under UV-TL08, showed that the LC E7 did not act as a plasticizer for the matrix as reported in the literature for TPGDA/E7 PDLC films having comparable confined liquid crystal contents for both systems, however, some part of the E7 bloomed out to the PDLC surface of PPGDA800/60wt.% E7 because of the big droplets sizes.

6_The electro-optical responses of the two systems TPGDA/60 wt % E7 and PPGDA800/60 wt % E7, those elaborated by the UV-Dr. Hönle system showed a slight improvement of the response compared to UV-TL08 but did not lead to the steep responses seen under EB. This was mainly due to the non-homogeneous photopolymerization reaction. In the case of EB curing, the shorter the spacing between the double bonds, the more homogenous was the polymerization reaction, leading to a more regular morphology and better and steeper electro-optical responses.

Recommendations

Recommendations

For an eventual continuation of this work, it is recommended to:

- Carry out the solid state NMR at different temperatures to determine the crosslink densities.
- Complete the investigation of the thermal properties of the other methods of elaboration EB and UV-Dr. honle.
- Complete the morphological studies by SEM for the other methods of elaboration EB and UV-Dr. honle.
- Explore the use of other non-hygroscopic monomers.